91602
new 82-10

LEGAL NOTICE

This report was prepared by Ontario Hydro and, while effort has been made to assure the accuracy and applicability of the material contained herein, neither Ontario Hydro nor any person acting on its behalf:

(a) makes any warranty, express or implied with respect to the use of any information, apparatus, method or process disclosed in this report or that such use may not infringe privately owned rights; or

(b) assumes any liabilities with respect to the use of, or for damages resulting from the use of, any information, apparatus, method or process disclosed in this report.

ontario hydro
research division

COMPLIMENTARY COPY

Please Credit Ontario Hydro Research if Reproduced in Whole or in Part

TEST PROGRAM OF THE PROTOTYPE OF THE TWPP CONTAINER PART 3 - DETAILED STRESS ANALYSIS AND COMPARISON WITH TEST RESULTS

Report No 87-296-K

B. Teper
Engineer
Applied Mechanics Section
Mechanical Research Department

ABSTRACT

The Thin-Walled, Particulate-Packed (TWPP) container was developed for immobilization and disposal of used fuel bundles from CANDU Nuclear Power Stations. A test program on a full scale prototype demonstrated its adequate structural performance under the postulated loads. This part of the report deals with the detailed stress analysis of the prototype, aimed at showing that a finite element model can satisfactorily approximate the hydrostatic test results and that this approach is a viable method for analyzing the container. The analysis provided similar general pattern of deformations and strains as obtained in the hydrostatic test program. A comparison of analytical and experimental results for lifting loads is made. The analysis was extended to estimate the container behaviour under several other loading conditions: internal pressure, reduced wall thickness, and thermal expansion. Both linear-elastic and elastic-plastic methods of analysis were used.

job	file	date	report no.
21-152	825.123	July 15, 1988	87-296-K

91602
new 82-10

ontario hydro
research division

EXECUTIVE SUMMARY

TEST PROGRAM OF THE PROTOTYPE OF THE TWPP CONTAINER PART 3 - DETAILED STRESS ANALYSIS AND COMPARISON WITH TEST RESULTS

B. Teper
Applied Mechanics Section
Mechanical Research Dept

The Thin-Walled, Particulate-Packed (TWPP) container was designed for the immobilization and disposal of used fuel from CANDU Nuclear Power Stations. To demonstrate our ability to assemble the container and to show that the container can perform satisfactorily under an external pressure of 10 MPa, a prototype of the container was constructed and tested.

In spite of certain manufacturing flaws in the as-constructed container, the prototype test program was completed successfully. The performance of the container during packing and hydrostatic tests was described in Part 1 of a comprehensive report on the testing and analysis of the test prototype. Part 2 deals with the tests and inspections that were conducted following the hydrostatic test program. This report shows that finite element analyses can be used to simulate the test results with adequate accuracy, including the analysis of the effect of voids.

The analysis was extended to the evaluation of several other conditions that were not included in the prototype test program. Settlement of particulate over a 500-year period was estimated based on the preliminary tests of creep in glass beads. Its effect was analysed and shown to be small. An overpressure of 13 MPa was considered and shown not to overstress the container. The effect of a void, which could form due to incomplete packing, was evaluated. If only two millimetres of titanium shell remained after 500-year corrosion, the strain in the shell was shown to be acceptably low, provided that good initial packing was obtained. Stresses in the titanium shell during lifting were analysed and compared with the test results.

The container represents a structurally viable option for the disposal of used fuel from CANDU reactors if specific constraints are met, as described in this report.

JC

job	file	date	report no.
21-152	825.123	July 15, 1988	87-296-K

TABLE OF CONTENTS

	Page
LIST OF TABLES	iv
LIST OF FIGURES	v
NOMENCLATURE	viii
LAYOUT OF REPORT	ix
1.0 INTRODUCTION	1
2.0 PAST ACTIVITIES	2
3.0 PROPERTIES OF PARTICULATE	4
3.1 Strength	4
3.2 Creep Properties	4
4.0 PROPERTIES OF TITANIUM	5
5.0 CONTAINER UNDER EXTERNAL PRESSURE	5
5.1 Linear-Elastic Analysis	5
5.1.1 Introduction	5
5.1.2 Assumptions	7
5.1.3 Analysis of Cross Section	7
5.1.4 Axisymmetric Analysis	9
5.2 Large Displacement Analysis	10
5.2.1 Assumptions	10
5.2.2 Analysis of Using Elastic Model	11
5.2.3 Analysis of Model with Gap Elements	11
5.2.4 Analysis of Bottom Plate	13
5.2.5 Centre Void Analysis	13
5.2.6 Side-Void Analysis	14
5.3 Summary of Results	15
6.0 OVERPRESSURE CONSIDERATION	16
6.1 Top Gap Area	16
6.2 Bottom Head Area	16
7.0 REDUCED SHELL-THICKNESS ANALYSIS	16
7.1 Radial Deflection	17
7.2 Top-Gap Area	17
7.3 Bottom Head Area	17

TABLE OF CONTENTS

	Page
8.0 LONG TERM SETTLEMENT	17
9.0 INTERNAL PRESSURE ANALYSIS	18
10.0 ANALYSIS OF LIFTING LOADS	18
11.0 EFFECT OF CREEP	19
12.0 FUTURE ACTIVITIES	19
13.0 CONCLUSIONS AND RECOMMENDATIONS	20
14.0 ACKNOWLEDGEMENTS	21
REFERENCES	22
APPENDIX A AVERAGE CONTAINER TEMPERATURE	A-1
APPENDIX B PLASTIC ANALYSIS	B-1
APPENDIX C DEFORMATION OF THE PROTOTYPE CONTAINER	C-1
APPENDIX D UNIFORM GAP ESTIMATE	D-1

LIST OF TABLES

TABLE I - Experimental Results from Hydrostatic Test

TABLE II - Mechanical Properties of Titanium

TABLE III - Results of Analysis of Pie-Shaped Model

TABLE IV - Effect of Stiffness Inside Steel Tubes

TABLE V - Strain from Test and Linear-Elastic Analysis

TABLE VI - Stresses Due to Internal Pressure

TABLE VII - Stresses During Lifting

LIST OF FIGURES

FIGURE 1 - Layout of the TWPP Container

FIGURE 2 - Sample of Hydrostatic Test Result

FIGURE 3 - Sample of Hydrostatic Test Results - Test with Rim Void

FIGURE 4 - Mechanical Properties of Particulate

FIGURE 5 - Creep Test Station

FIGURE 6 - Settlement of Particulate

FIGURE 7 - Deformation of Prototype Container

FIGURE 8 - Deformation of Top Lid

FIGURE 9 - Pie-Shaped Model of TWPP Container

FIGURE 10 - Deformation of the Pie Model

FIGURE 11 - Stress Distribution in the Pie Model

FIGURE 12 - Hoop Stress Distribution in the Pie Model

FIGURE 13 - Hoop Strain in Cylindrical Shell

FIGURE 14 - Axisymmetric Finite Element Model

FIGURE 15 - Model of Top and Bottom Areas

FIGURE 16 - Model of Discontinuity Areas

FIGURE 17 - External Loading

FIGURE 18 - Deformations - Isotropic Properties of Particulate

FIGURE 19 - Von Mises Stress Distribution - Isotropic Properties of Particulate

FIGURE 20 - Assumed Plastic Properties of Titanium

FIGURE 21 - Comparison of Results of Top Gap Analyses

FIGURE 22 - Model of Top Area with Gaps

FIGURE 23 - Boundary Conditions

LIST OF FIGURES (continued)

FIGURE 24 - Closing of the Top Gap from Gap Element Model

FIGURE 25 - Radial Strain at Location B

FIGURE 26 - Strain in Top Plate at Full Pressure

FIGURE 27 - Largest Plastic Strains in Titanium Shell

FIGURE 28 - Compressive Force in Cylindrical Shell

FIGURE 29 - Deflection of Unsupported Cylindrical Shell

FIGURE 30 - Compressive Force in Cylindrical Shell, 10 mm Gap

FIGURE 31 - Largest Plastic Strains, 10 mm Gap

FIGURE 32 - Finite Element Model of Bottom Head

FIGURE 33 - Deformations due to External Pressure

FIGURE 34 - Results from Hydrostatic Test with Centre Void

FIGURE 35 - Finite Element Model of Centre Void

FIGURE 36 - Comparison of Results from Tests and Analysis

FIGURE 37 - Strains Measured during Test with Rim Void

FIGURE 38 - Deformations Produced in Tests with Rim Void

FIGURE 39 - Finite Element Model of Rim Void

FIGURE 40 - Analytically Predicted Deformation

FIGURE 41 - Results of Analysis of Side Void

FIGURE 42 - Estimated Compressive Force in Cylindrical Shell

FIGURE 43 - Estimated Strain at Increased Pressure to 13 MPa.

FIGURE 44 - Deformation of Top Head at 13 MPa.

LIST OF FIGURES (continued)

FIGURE 45 - Deformation in the Weld Area

FIGURE 46 - Largest Plastic Strains in 10 mm Gap

FIGURE 47 - Compressive Force in Cylindrical Shell in 10 mm Gap

FIGURE 48 - Result of Gap Analysis for 2-mm-thick Shell

FIGURE 49 - Models for Long Term Settlement Analysis

FIGURE 50 - Model for Analysis of Internal Pressure

FIGURE 51 - Deformations due to Internal Pressure

NOMENCLATURE

AECB	- Atomic Energy Control Board
Back End of Fuel Cycle	- part of the fuel cycle from the removal of the fuel from a reactor to its final disposal
Container	- a receptacle for burying used nuclear waste
Disposal Facility	- a facility used to permanently emplace or discharge waste materials (for example an underground disposal vault and its supporting facilities)
Disposal System	- a disposal facility and the transportation facilities needed to bring the nuclear fuel wastes from the interim storage sites
Ontario Hydro Container	- synonymous with Thin-Walled, Particulate-Packed Container
OHRD	- Ontario Hydro Research Division
Particulate	- Granular material such as glass beads
TWPP Container	- Thin-Walled, Particulate-Packed Container
Used Fuel	- Fuel extracted from a reactor at an end of its useful life.

LAYOUT OF REPORT

A comprehensive report describing: preparation, building and testing of the prototype of the Thin-walled, Particulate-Packed container, and evaluation of the test results is being issued in the following four parts:

Part 1 - Hydrostatic Test - describes the tests conducted in preparation for building of the prototypes; prototype itself; inspection, assembly and instrumentation of the prototype and the hydrostatic test program. (Report No. 84-293-K, dated December 21, 1984.)

Part 2 - Prototype Testing Following the Hydrostatic Tests - describes: handling test; visual inspection following the reopening of the container; and metallographic evaluation. (Report No. 85-313-K, dated November 20, 1985.)

Part 3 - Stress Analysis - describes: testing of titanium, particulate and other materials used in construction of the prototype; detailed stress analysis of the "perfectly" packed container including analytical simulation of the plastic settlement over the postulated 500-year lifespan of the container (this report).

Part 4 - Summary - a brief outline of the work and summary of all results.

Each part of the report has been written to form a separate report and can be read without referring to the previous parts. Some repetition of material between the parts was necessary to facilitate this.

ontario hydro
research division

To Mr. H.N. Isaac
Manager
Nuclear Materials Management Dept.

TEST PROGRAM OF THE PROTOTYPE OF THE TWPP CONTAINER PART 3 - DETAILED STRESS ANALYSIS AND COMPARISON WITH TEST RESULTS

1.0 INTRODUCTION

This paper is the third volume in a comprehensive report on the development, testing and analysis of the Thin-Walled, Particulate-Packed (TWPP) container. The TWPP container was developed for disposal of used fuel bundles from CANDU Nuclear Power Stations in an up-to 1000-m deep underground vault. Each container will hold 72 bundles of used fuel, arranged in a basket in four layers of 18 bundles per layer. The basket has 19 tubes. The centre tube is for handling only. The basket with used fuel is inserted into a corrosion-resistant titanium shell. The container is internally supported by a granular material (particulate) that fills all voids inside the container. Figure 1 shows the layout of the container.

An extensive development program preceded the building of the prototype. Based on the results of this program, we expected the container to perform adequately at all postulated loading conditions, although large (plastic) deformations were anticipated. A full scale prototype of the container was built and tested to show that it would function well. The container was assembled without difficulty. The integrity of the container was not breached during handling and several stages of hydrostatic tests at external pressure of up to 10 MPa. The container did not fail, even though two of the tests were conducted with artificially induced voids. The packing and hydrostatic tests performed on the prototype container were discussed in the first part of this report/1,2/. The handling test, ultrasonic and destructive examination of the container following the test program were described in Part 2/3/. They are summarized here in Sections 2, 3 and 4.

Extensive hydrostatic tests on the prototype showed that the design is adequate for disposal of used-fuel bundles. The results of the tests are presented in Table 1 for comparison with the results of the stress analysis.

The detailed stress analyses, described in this report, have two goals. Firstly, we show that the finite element model may be used to simulate the results of the hydrostatic tests. The comparison of experimental and analytical results is presented in Section 5. In the second part (Sections 6 through 10) of the detailed stress analysis program, the following conditions are considered:

- An external pressure of 10 MPa existing for 500 years. This analysis considers the effect of the long-term settlement of the granular material (particulate) over the postulated lifespan of an immobilization container.

- An internal pressure of 0.05 MPa due to the heating of air from 20°C to 109°C inside the container (see Appendix A), assuming no external pressure.

- Loads during vertical handling of the container.

- The strains and stresses in the titanium shell after 500-year corrosion.

The report shows that the container design is adequate for the above loading conditions, or that the container meets the postulated stress and strain limits.

There are no codes or standards directly applicable to internally supported disposal containers that would provide the guideline for stress or strain limits. The ASME Boiler and Pressure Vessel Code is not applicable to the TWPP container, because its shell is not designed to support an external load. The container is considered to fail if large strain causes it to breach or the shell buckles. A discussion on strains in the titanium shell is presented in Appendix B. Compressive strains are assumed not to contribute to failure and are not limited in magnitude, except where buckling may occur. Container is also considered safe if two mutually perpendicular local tensile strains in the shell's plane meet the condition:

$$e_x + e_y < 5.3\%$$

If one of the strains is zero or compressive, the other strain is limited to 5.3% (see explanation in Appendix B).

2.0 PAST ACTIVITIES

In the preparation for the prototype test, several experimental and analytical programs were run to demonstrate the viability of the concept by showing that:

- the particulate could be compacted adequately,

- the particulate had adequate strength and stiffness,

- titanium has adequate strength and ductility to maintain the integrity of the container under high loads and deformations,

- while plastic deformations of the titanium shell can be anticipated, they will not cause failure.

The prototype container was assembled without difficulty. The container was extensively instrumented with strain gauges and thermocouples in preparation for the hydrostatic test program. The TWPP container development program provided for a single prototype only. The hydrostatic test program was divided into seven steps to obtain as much information as possible.

- Preliminary test where 1 MPa external hydrostatic pressure is applied at ambient temperature

- full pressure test at 10 MPa and at 100°C

- full pressure test at 10 MPa and 125°C

- full pressure test at 150°C

- 16-day test at 10 MPa and 150°C

- test with centre void

- test with side void, as discussed in reference/1/.

During the preliminary low pressure cycle, large strains were detected in the top lid area. These strains were not recorded. The origin of these strains is discussed in Section 5.2.3. Table I shows the measured strains in the prototype at three different temperatures, when the prototype was tested at 10 MPa external pressure. During the first test conducted at 100°C, some additional plastic deformations occurred, resulting in non-linear behaviour of the container. In subsequent tests, the strains varied linearly with pressure, see Figure 2. When artificial voids were created in the particulate, the resulting strains produced by the hydrostatic pressure became non-linear, see Figure 3.

The container survived all tests without a breach of its integrity. Although the hydrostatic tests conducted after artificial voids in the particulate were introduced produced large deformations, the strains in the shell did not exceed 4%.

3.0 PROPERTIES OF PARTICULATE

3.1 Strength of Particulate

Glass beads were used as the particulate in the assembly of the prototype. The mechanical properties of the particulate were determined from uniaxial compression tests. As anticipated, the properties vary with the applied pressure, see Figure 4. The properties at the postulated disposal vault pressure of 10 MPa are:

Young's modulus of elasticity	Ep = 336.6 MPa
Bulk modulus of elasticity	K = 623.3 MPa
Poisson's ratio	ν = 0.41

The value of Young's modulus of the particulate (Ep) is a function of pressure (p), see Appendix A of reference/1/.

$$Ep = 1.044\ [P(E_s)^2]^{0.333}$$

where E_s is the Young's modulus of the solid material of which the particulate is made.

3.2 Creep Properties

Several small-scale tests were conducted to determine the long-term settlement of the particulate. The test temperatures ranged from 20° to 150°C. An external pressure of 10 MPa was used in all tests. The duration of the tests ranged from 15 days to 42 days. The set-up of the test equipment is shown in Figure 5.

Although the tests were conducted for only a few weeks, it was assumed that the pattern of permanent deformation established during the tests would continue for 500 years, the required minimum lifetime of the container. A logarithmic creep law was assumed to be valid to extrapolate the test results, see Figure 6/4/. The settlement can be described by the function:

$$e = A + B \ln t$$

where;

e = strain
A = empirical constant (initial settlement)
B = empirical constant
t = time in years

This equation was used to estimate the volumetric strain in the particulate, for use in the analysis. The experimental program showed that the coefficients for glass were:

$$A = 76 \times 10^{-6} \qquad B = 11 \times 10^{-6}$$

For comparison, these coefficients for sand are:

$$A = 144 \times 10^{-6} \qquad B = 5 \times 10^{-6}$$

Coefficient A shows the initial settlement that occurs due to incomplete packing. Such settlement produced a gap of up to 14.5 mm at the top of the prototype container/4/. After 500 years, the settlement of glass is estimated as:

$$e = 247. \times 10^{-6} \text{ of initial volume (see Figure 6).}$$

About 425 litres of glass beads were used to fill the prototype, which contained 48 simulated fuel bundles. A TWPP disposal container with 72 bundles will have less particulate - about 355 litres. Due to long-term settlement, volume of the particulate will reduce by about 0.06 litres under external pressure.

4.0 PROPERTIES OF TITANIUM

Following the hydrostatic test program, a detailed metallurgical examination was performed on the container. The examination showed that the properties of the titanium used to construct the prototype did not always meet ASTM specifications. The properties of titanium, as specified in the ASME Boiler and Pressure Vessel Code, Section VIII, are listed in Table II. Based on the ASTM Boiler and Pressure Vessel Code specification for titanium at 100°C, the following properties of titanium were used in the finite-element analysis:

- Young's modulus of elasticity	100 GPa
- Post Yield modulus	3.7 GPa
- Yield strength	216 MPa
- Ultimate strength	345 Mpa
- Maximum strain (see Appendix B)	20%

5.0 CONTAINER UNDER EXTERNAL PRESSURE

5.1 Linear-Elastic Analysis

5.1.1 Introduction

The container is intended for the disposal of used fuel in an up to 1000 m deep underground vault. If the vault is resaturated with ground water, the container will have to support an external pressure of at least 10 MPa. Based on the plastic deformation of the top plate and strains measured during the hydrostatic tests, the deformed shape of the container was estimated (see Appendix C and Figure 7).

During assembly of the container, the layer of particulate above the used-fuel basket was monitored. At the end of particulate compaction, after top head was inserted, the layer of particulate was about 25-mm thick. Following the hydrostatic test program, the distance between the top of the basket and top head was measured to be 14.5 mm shorter than it would indicate from the results of packing. The layer of particulate was reduced to about 10 mm. There are several possible explanations for this discrepancy:

- A void formed at the top of the container during its transportation by truck from Ontario Hydro Research Division (where the container was assembled) to the Whiteshell Nuclear Research Establishment (where the hydrostatic tests were performed).

- During transportation by truck, the container saw large vertical accelerations which caused the basket to "float" upwards, supported underneath by particulate.

- During hydrostatic test, two voids in particulate were intentionally introduced following the long-term test. These voids resulted in large settlement near the voids. Small general settlement of the top lid could have also occurred.

- Part of the discrepancy may be due to measurement inaccuracies.

A 14.5-mm gap could have formed by reducing the initial volume of particulate from 420 litres to 415.5 litres - an improvement in packing density by 1.1%. For conservatism, we assumed that a 14.5-mm gap formed at the top and that the top lid deformed inward uniformly by about 14.5 mm, as shown in Figure 8/1/. Only a small deflection would occur if the shell were in contact with particulate. A detailed stress and strain distribution was calculated in the finite element analysis. Four finite element models were used in the analysis:

1. A pie-shaped section of the container, away from the heads, was used to evaluate the non-axisymmetric internal structure of the container.

2. An axisymmetric model of the whole container is used to show that the as measured properties of particulate were adequate to approximate the deformations measured during the hydrostatic tests. These properties will be used in the subsequent analyses. The model was also used to determine the length of cylindrical titanium shell where deformations are affected by heads (length of discontinuity areas).

3. A detailed axisymmetric model of the discontinuity area at the top was analyzed to gain a better understanding of the behaviour of the titanium shell and the top lid near the resistance-welded area.

4. A detailed axisymmetric model of the discontinuity area at the bottom head was analyzed to determine the behaviour of the titanium shell and bottom lid near the welded area.

The results of the hydrostatic tests are shown in Table 1. The difference between results of the three stages of the test is due to different test conditions and plastic deformations which took place during the preliminary and first full pressure cycle tests. Since we are most concerned with the first pressurization of a disposal container, the comparison will be made with the 100°C stage. The analysis of the settlement of the top plate during the preliminary, low pressure cycle is also discussed.

5.1.2 Assumptions

Some simplifying assumptions were required to allow for linear-elastic material properties and efficient analysis:

- The granular material was assumed to perform like a continuous medium having a constant tensile and compressive modulus of elasticity, and constant shear modulus and Poisson's ratio, see Subsection 3.1.

- The properties of glass beads as determined from the preliminary tests/1/ were used in the analysis.

- Unless otherwise stated, all geometry and material properties are assumed to be linear, even beyond yield (see Appendix B for a list of non-linearities considered in analysis discussed in Subsection 5.2).

5.1.3 Analysis of Cross Section

A few centimeters away from the end plates, the cylindrical shell behaves like a uniform continuous cylinder, independently of length. The cross-section of the TWPP container is symmetrical every 30°. Therefore, only one 30° segment need be modelled in the finite element analysis, see Figure 9. The model includes all internal components of the container:

- 4.76-mm thick titanium shell,

- 3.05-mm thick tubes of the steel basket,

- particulate fills the spaces between the titanium shell and the basket tubes and between the fuel bundles and the tubes of the basket,

- fuel bundles and particulate in the space inside the tubes.

The model consisted of 357 plane-strain four-noded and three-noded elements with 768 degrees of freedom. External loading on the model was applied by radial forces acting on the outside surface of the shell. These forces approximated the 10 MPa pressure used in the hydrostatic test.

The analysis indicated that the internal structure of the container behaved in a near axisymmetric manner. The deformed shape of the container is shown in Figure 10 and in Table III. The average radial deformation was 0.544 mm. The largest deviation from axisymmetric deformation was below 5%. The stress distribution inside the container was not axisymmetric and followed the contours of the titanium shell and steel pipes, see Figure 11 and 12.

The largest stress calculated in the titanium shell was in the hoop direction (-217 MPa or 100.5% of yield stress). The steel tubes experienced the highest stress where the tubes were in contact (Location D in Figure 9): -107 MPa or 53% of yield stress in the radial direction. The stresses in particulate are low: a maximum of -7.9 MPa at the steel tube near Location E, see Figure 9.

The maximum total strain in the titanium shell was 0.2%. No yielding of the steel tubes occurred. Particulate settlement was not considered in this stage of analysis (see Section 8.0).

Figure 13a shows the measured strain in the cylindrical shell away from discontinuities. Four finite element runs were made for four different pressures (2.5, 5.0, 7.5 and 10.0 MPa). The stiffness of the particulate was calculated from the equation:

$$Ep = 1.044\ [p(E_s)^2]^{1/3}$$

The strains determined from the analysis were compared with the experimentally evaluated strains (see Figure 13b). The difference between the measured and the calculated strains was less than 6%.

Material properties were assumed for the bundle - particulate mixture inside the steel tubes. In the analysis, it was assumed that the combined modulus of elasticity of the bundles and particulate inside the tubes was the same as the particulate alone. Two additional computer runs were made using this model to determine the effect of the properties of the material inside the steel tubes on the deformation in titanium shell. If the material stiffness were either 6.6 times lower or 3 times higher than the originally used value of 337 MPa, the deformations changed by less than 2%, see Table IV. It was concluded that the shell surface deformations had low sensitivity to this assumed material property.

The comparison of the predicted and experimental results showed good correlation which tends to validate the analytical approach. Further comparisons are presented in the following sections.

5.1.4 Axisymmetric Analysis

The axisymmetric analysis was used to evaluate the behaviour of the titanium shell. The behaviour of the container's internal structure can not be analyzed by this method because it cannot be modelled accurately using axisymmetric assumption.

The axisymmetric model (see Figure 14) consists of 617 nodes and 645 elements. Four-noded, biquadratic stress and strain elements were used to represent the internal structure and two-noded elements were used to model the shell. The model has 1651 degrees of freedom. To simplify the analysis, the following assumptions were made:

a) The titanium shell was represented by 4.76-mm thick shell elements (dark brown color in Figure 14a), except for the 6.35-mm thick bottom plate.

b) The particulate between the shell and the basket was modelled by two layers of elements, having a total uniform thickness of 40 mm. These are shown in Figure 14b by the colour green.

c) The particulate above the basket was represented by four layers of elements 40-mm thick. These elements are shown in brown in Figure 14b. A steel plate, one element thick (10 mm) and three elements wide (46 mm in the radial direction) was used to represent the lifting plate in the central tube of the basket (shown in red in Figure 15).

d) The basket and its contents were modelled as a continuous, axisymmetric, uniform structure. The mechanical properties of the structure were assumed to be isotropic, although the steel tubes would be stronger in the axial direction. The modulus of elasticity was assumed to be 2,800 MPa and Poisson's ratio 0.3. These elements are shown in dark blue.

e) The steel ring and the spoked wheel were modelled as a solid steel plate, shown in light blue in Figure 15.

f) Simplified models of the top and bottom rim areas are shown in Figure 16.

Loading was by a uniform external pressure of 10 MPa, see Figure 17. The light blue circles indicate the nodes that were restrained from vertical displacement.

If the particulate above the basket area (item (c) above) is assumed to be isotropic, with a Young's modulus of 337 MPa and a Poisson's ratio of 0.41, the radial deflection of the cylindrical shell is 0.56 mm (0.54 mm was measured during the tests). However, the calculated vertical displacement of the top plate was only at 2.7 mm, see Figure 18. Following the hydrostatic tests, this deflection was estimated to be 14.5 mm. The Von-Mises stress

distribution inside the container is shown in Figure 19. The highest principal stress derived in this analysis was -637 MPa (ie, significantly above yield), in the rim of the top lid.

A comparison of the analytical and experimental results is shown in Table V. The results for locations C and D differ by up to 33%. Some of the potential sources of error are:

- approximations used in the numerical model,
- strain gauge errors
- fabrication defects and/or out-of-roundness in the shell,
- stress redistributions in the top lid due to plastic deformation,
- the presence of residual stresses due to fabrication
- anisotropy in the rolled titanium plate

The experimental results at locations A and B are inconsistent and therefore are suspect. The strains at a centre of the flat plate (location A) should have the same sign. The axial strain at location B should be tensile (positive) under external pressure.

5.2 Large Settlement Analysis

5.2.1 Assumptions

Several potential loading conditions could produce large deformations requiring non-linear, plastic analysis. The previously discussed deflections resulting from the 14.5-mm gap between the particulate and the top plate could be a source of large deflection. The analysis was done with the ABAQUS code, enhanced by the PATRAN processing code. Some of the common assumptions of the theory of plasticity were assumed to be valid:

- Plastic strains are not caused by the hydrostatic part of the principal stress components. The hydrostatic part is defined as:

$$p = (\sigma_1 + \sigma_2 + \sigma_3)/3$$

- Plastic strain occurs when the deviatioric stress defined as:

$$\sigma_1' = \sigma_1 - p$$

exceeds yield. The amount of plastic strain was determined using the Von-Mises stress criterion.

For example, if the three principal stresses are large but nearly equal, yielding will not occur. On the other hand, material will yield if one principal stress is positive and another is negative, and both exceed 50% of the material yield stress.

A Stress - Strain curve for titanium was obtained from several tensile tests performed at 20°C. The plastic region of the curve was transferred downward to meet the 100°C yield and ultimate strength listed in the ASME Boiler and Pressure Vessel Code (see Table II). The curve is shown in Figure 20.

The titanium shell was modelled as an elastic-plastic material with yield strength of 216 MPa. Strain hardening is assumed to increase the stress to 325 MPa as the strain reaches 2%. A large plastic range is assumed to allow peak strain of 20% at the ultimate strength of 345 MPa. This simplified stress-strain curve is compared with actual in Figure 20. The high strain hardening assumption results in high stresses in the analysis. Stresses will not be used here as the failure criterion, but only strains. We expect that strains of up to 5.3% can be safely tolerated in the shell (see Appendix B).

In any comparison of the analytical and experimental results for the large deflection analysis, sources of errors listed in subsection 5.1.4 also apply. In addition, errors could be introduced by simplifications in:

- the yield criteria
- the strain hardening and flow rule
- the assumption of isotropic behaviour in strain-hardened titanium

5.2.2 Analysis Using Elastic Model

The finite element model used in the axisymmetric, linear-elastic analysis (see Figure 14) was also used here to try to obtain realistic deformations in the region of the top gap. The properties of the particulate were adjusted to be anisotropic and to lead to a deformation of up to 14.64 mm.

The results of this analysis did not match experimental results. The top plate was observed to remain nearly flat during the hydrostatic tests, while the analysis predicts a dished shape (See Figure 21).

5.2.3 Analysis of Model with Gap Elements

This analysis is based on a partial model that included only the top area of the container. The model is shown in Figure 22. The space above the top surface of the particulate was modelled using gap elements, shown by black lines. The red-coloured elements indicate the steel plate covering the central tube. The boundary conditions and external loads are shown in Figure 23. The final deformation pattern resembles the results observed in the tests, see Figure 24.

During testing of the prototype, and following the preliminary, low pressure tests (up to 1 MPa) it was observed that some of the strain gauges on the top lid indicated strains that were beyond their range of accurate measurement. At that time, and because the prototype could not be directly observed during testing, there was uncertainty as to whether these indications were real or

the result of instrument malfunction. The subsequent, higher-pressure tests indicated lower additional strains in this region. Following completion of the test series and subsequent detailed measurement, a significant permanent deformation of the top head was observed to have occurred, confirming that the original strain gauge data was not an artifact of faulty instrumentation. Figure 24 shows the settlement of the top plate as a function of pressure, as predicted by the model. Clearly, most of the deformation of the top head could have occurred during the preliminary test. As pressure was raised further in the subsequent tests, only a small additional plastic deformation was recorded. Such behaviour was confirmed by the analysis.

A complete comparison of the strains measured in the hydrostatic tests and those derived analytically for the top plate area is not possible because the predicted strains vary considerably with radius and only several strain gauges could be accommodated at discrete locations on the head of the test container. From the analysis, between a radius of 270 and 280 mm, the strain ranges from tensile 0.006 to compressive -0.004. The variation in strain as a function of pressure is shown in Figure 25. A comparison of radial strain at two locations, as measured during the test, with those predicted by the analysis is shown in Figure 26, as a function of radius.

The largest compressive strain (6.2%), was predicted to occur in the cylindrical shell, just below the top lid-to-shell weld. The largest tensile strain (4.4%), was predicted to occur in the top head, just below the radius of the dished area, see Figure 27. These strains are within the allowable tensile strain of 5.3% (see Appendix B).

In the analysis, the cylindrical shell was unsupported for about 40 mm (14.5 mm gap plus 25 mm radius). This unsupported cylindrical shell buckled. The load supported by the cylindrical shell began to decrease as the pressure increased above 8.8 MPa (see Figure 28). The radial deflection of the cylindrical shell increased significantly towards the end of pressurization (see Figure 29), due to the plastic collapse.

The analysis was repeated assuming a 10 mm gap between the top head and the particulate. Buckling no longer occured. Figure 30 shows that the force supported by the shell always increase with pressure, although the rate of increase levels off. The predicted strains for the three locations in Figure 22 are smaller, as shown in Figure 31. The largest strain is less than 2.6%.

The partial model of the top area is considered conservative because the assumption of a 14.5-mm gap is likely an overestimate (the origins of this gap were discussed in Section 5.1.1).

5.2.4 Analysis of Bottom Plate

In the analysis conducted in 5.1.4, the bottom plate was constrained against vertical deformations. This assumption is, however, inaccurate. A more detailed finite element model was assembled to evaluate the effect of the components of the bottom of the basket on the titanium shell, under 10 MPa external pressure. The model is shown in Figure 32. The steel support ring at the bottom of the basket (see Figure 1) is represented by the red-coloured elements in the model. The bars of the spoked wheel are spaced 30° apart and the space between the bars is filled by particulate. For conservatism, the spoked-wheel region was modelled as a layer of particulate (green-coloured elements). The basket (blue elements) was modelled as a uniform, isotropic component.

In the stress analysis, three regions are of interest:

1. That area of concentration where steel ring and particulate meet (location 2 in Figure 32)

2. The unsupported length of titanium shell adjacent to the steel ring (location 1) which could collapse inward. It was assumed that this region might be void of particulate because of the close tolerances between the steel ring and the shell.

3. The titanium head near the centre (location 3).

The plot of the deformed model (Figure 33) shows that no collapse occured. Although the shell yielded at location 1, plastic strain was below 0.02%. The stress concentration area (location 2) produced stress levels of only 50% yield. The stresses at the centre of the bottom head are were near 25% yield.

5.2.5 Centre Void Analysis

During the hydrostatic test program for the TWPP prototype, two additional tests were conducted following the creation of artificial particulate - packing voids in the container. The results of these tests were discussed in reference/1/. The strains measured in the top head during the test which included central void are shown in Figure 34. The axisymmetric finite element model (Figure 35) was used in the analysis. The analysis considered the non-linear deformation behaviour and material non-linearity of the structure, including gap elements. The test and analytical results are compared in Figure 36. In the analysis, the closing of the void produced higher predicted strains than were measured in the tests. Initially, the predicted strains at positions removed from the void increased faster with increasing load than strains measured in the test. After the void was fully closed, the predicted strains were similar, see Figure 36a. At the edge of the void, the predicted strains generally exceeded the measured strains

(Figure 36b). After the void closed, the calculated and measured strains began to converge.

5.2.6 Side-Void Analysis

A void near the shell was produced by removing about 0.8 L of particulate from beneath the top lid, near the rim. During pressurization of the container, shell and head strains near the void were measured. The largest strain was 1.2%, in the cylindrical shell near the top head. In the top head, strains in excess of 0.6% were detected. Some typical test results are shown in Figure 37. Figure 38 shows the post-test condition of the head and shell. Two dents formed in the cylindrical shell because spacer ring of the basket partially supported the shell (see Figure 38b). The depth of the top buckle was about 6 mm and bottom buckle about 4.0 mm. The top head deformed downward by about 12 mm (Figure 38a). The dents in the shell spanned about 30% of the circumference.

A simplified finite element model was used to attempt to simulate the experimental results. The void was assumed to be axisymmetric (see Figure 39). The axisymmetric approximation is acceptable because the thin titanium shell will closely follow the shape of the backing material (basket or particulate). Edges of the void do not effect general deformations of the titanium shell. The model was coarse to allow for a non-linear analysis. Both deformation behaviour (geometric) and material non-linearities were modelled. Material non-linearities were required for the large plastic strains. Geometric non-linearities were handled using gap elements. Thesize of the void below the support ring was adjusted to best simulate the experimentally observed deformation. The analytically obtained deformation is shown in Figure 40. The largest deflection in the cylindrical shell was 10 mm, and in the top head was 15 mm. The deformations were 3 mm in the bottom dent of the cylindrical shell.

In the cylindrical shell, the largest strain calculated was in the axial direction at -7.0%. It occurred near the top head (node 61 in Figure 39). In the monitored area, the axial strain was -3.0%. The strain in the top plate was below 4.0%.

The general analytically and experimentally determined deformation patterns are similar, as seen from Figures 38 and 40. However, the calculated deformations and strains were higher than those measured. This may be because the axial length of the voids assumed in analysis may have been slightly larger than those which were created for the tests. Figure 41 shows that the predicted deformations increased more rapidly as the pressure approached 10 MPa.

In general, good correlation between the analytical and the test results was obtained.

5.3 Summary of Results

The objective of the analysis of the effects of external pressure on the prototype container was to demonstrate the adequacy of the analytical procedure by comparing it with the experimental results. Although there were discrepancies in several areas, we feel that the finite element technique is a useful tool for predicting the behaviour of the disposal container. Discrepancies can result from many factors such as:

- Simplifications in the analytical models,
- Strain gauge inaccuracies,
- Limited volume of results from tests,
- Localized pertubations such as welds, ovality, or small material defects,
- The use of ASME Code material properties in the analysis whereas the actual materials used in tests may have different properties,
- Errors introduced into the analysis by the use of simplified yield criteria (eg, von Mises), a simplified uniaxial yield curve, or a simplified strain-hardening and flow rule.

Comparison of strains from linear-elastic analysis (Figure 13) in the top head (Figure 26) was good. However, these potential sources of errors make a a comparison of local strain effects particularly difficult. Consequently, a comparison of deformations and changes over large areas is viewed as being more appropriate. The general deformation pattern obtained from the tests agrees well with the predicted deformations. The measured radial deformations agree well with the deformations calculated for the pie-shaped model. The deformation of the top plate, as determined from the model with gap elements agrees well with the test results. The comparison of deformations for cases with artificially introduced defects were also in reasonable agreement. The agreement between the measured and calculated strains for the top head was less well defined. In Table V, good agreement was obtained at locations C, D and E. The measured strains at the centre of the top plate are much lower and of an opposite sign to the predicted results. The experimentally determined strains do not appear to be realistic for a flat plate under uniform loading. From the theory of plates and shells/7/, hoop and axial strains at locations A and G should be equal. This was the result obtained from the analysis for strain gauge locations. Potential sources of errors in the measured values include an overestimate of the top gap, and strain gauge averaging effects when the large Ailtech gauges were used.

6.0 OVERPRESSURE CONSIDERATION

The buffer material that will be used to surround the container in the disposal vault could, when saturated, swell and exert an additional hydrostatic pressure of up to 3 MPa on the container. The effect of this additional pressure is evaluated here.

6.1 Top Gap Area

The finite element analysis discussed in Subsection 5.2.3 was conducted for an external pressure of 13 MPa, using model in Figure 22. The unsupported cylindrical shell collapsed below 10 MPa (see Node 61 in Figure 41) - it could only support a load of 8.8 MPa. Strain in the cylindrical shell increased rapidly as pressure increased above 8.8 MPa. At 10 MPa, the cylindrical shell touched the deformed top head. In the cylindrical shell, strain increased slowly at constant rate, above 10 MPa. The deformations in the top head increased only slightly between 10 and 13 MPa, largely because of contact between the shells. The largest strain in the titanium shell was over 15% and it occurred at location 3 in the axial direction (see Figure 43). The top head and the cylindrical shell were in contact for a distance of about 20 mm below the head-to-shell weld, as shown in Figures 44 and 45.

A 14.5 mm gap caused buckling of unsupported shell at 13 MPa pressure. The 10-mm gap analysis was extended to 13 MPa hydrostatic pressure. The results of analysis plotted in Figures 46 and 47 show that the strains in the gap region may be acceptable: the largest value calculated was below 2.7%. As pressure was increased, the force supported by the cylindrical shell continued to increase, although quite slowly. This was due to the increasing area of contact between top head and particulate. At 13 MPa, about 70% of the top head was in contact with particulate. In this area, the pressure is balanced by particulate.

6.2 Bottom Head Area

The finite element model shown in Figure 32 was used to determine the effect of 13 MPa pressure on the bottom head. At 13 MPa, the unsupported area of the shell did not collapse, although the plastic strain increased to 0.11% (from 0.02% at 10 MPa). The stress at the discontinuity between the steel ring and particulate increased to yield (210 MPa), or twice that calculated at 10 MPa. The 6.35 mm thickness of the shell appears adequate for an external pressure of 13 MPa.

7.0 REDUCED SHELL THICKNESS

A reduced shell-thickness of 2 mm was analyzed to determine the structural durability of container following an extended period of uniform general

corrosion. Finite element models of the container including the axisymmetric model of the full container (see Figure 14), top gap area (Figure 22) and bottom head (Figure 32) were used again, and the shell thickness was reduced to 2 mm.

7.1 Radial Deflection

The finite element model in Figure 14 was modified to have a 2-mm thick shell. The deformation pattern obtained from the analysis was similar to that described in Subsection 5.2.2, but the calculated displacements were larger. The radial deflection of the cylindrical shell, at locations removed from any discontinuity, increased from 0.56 mm to 0.70 mm. The hoop stress in the shell, at locations removed from any discontinuity, increased to 233 MPa or 15% above yield. The corresponding strain was 0.3%.

7.2 Top-Gap Area

The analysis of the top gap area, with a 2-mm thick titanium shell, was initiated with a 10-mm void. The analysis showed that the shell would become unstable at 2.5 MPa pressure. The analyses were repeated for top-gap thicknesses of 5-mm and 2-mm with similar results as shown in Figure 48. The results indicate that strains in excess of 8% may be anticipated.

The large deflections of a 2-mm thick shell indicate that thorough packing of the particulate to avoid head-to-shell gaps would be needed to ensure continued container structural integrity, if the shell thickness is reduced to 2 mm because of a uniform corrosion.

7.3 Bottom Head Area

The model in Figure 32 was modified to have a shell thickness of 2 mm. The results of the analysis showed only a slight increase in the predicted stresses. The largest von Mises stresses in the shell exceeded yield: 245 MPa adjacent to the steel ring and 240 MPa adjacent to the void. The void (see Subsection 5.2.4) did not cause the shell to collapse, but the total strain increased to 0.4% (from 0.02% for the 6.35-mm thick shell).

8.0 LONG-TERM SETTLEMENT

The long term settlement of the particulate within a container could result in a uniform gap over the entire container surface, except for the region adjacent to the bottom support ring which was assumed to remain in contact with the shell. Calculation of gap sizes is shown in Appendix D. The differential thermal expansion between titanium and particulate can be simulated by a uniform gap of 0.01 mm. The long-term creep of the particulate can be simulated by a gap of 0.04 mm. The postulated 14.5-mm gap used in all previous analyses was assumed to form over an extended period of time. This gap was simulated by a 1.0 mm gap spread over the entire

container surface. The total gap could reach 1.05 mm. The shell would, over time, deform to absorb this gap.

The consequences of this gap were calculated using two finite element models - one for each of the top and bottom areas of the container, see Figure 49.

- red indicates the 4.76-mm thick titanium shell,
- black indicates the 6.35-mm thick titanium shell,
- green indicates the particulate, and
- gray is the basket containing the fuel bundles and particulate.

The analyses were conducted twice. In the first run, shell thicknesses of 4.76 mm and 6.35 mm were assumed. In the next run, the thickness was reduced to 2 mm. The strains and deflections obtained from the two analyses were within 5% of each other. Some plastic deformations may occur in the shell. The largest anticipated strains are: 0.86% at the rim of the top lid, and 1.4% in the cylindrical shell at the steel support ring.

9.0 INTERNAL PRESSURE ANALYSIS

An increase in the temperature of the container from 20°C (293K) (during assembly) to its average temperature of about 109°C in the vault (to 382K) (see Appendix A) will result in an internal pressure increased of 0.04 MPa. When the external pressure is atmospheric only in the vault (ie, during the operation phase), tensile stresses will be produced in the shell.

In the analysis, the bottom plate was assumed to be supported on a flat and undeformable surface. The particulate weight applies a uniform pressure of up to 0.02 MPa, to the bottom of the container.

The finite element model used in this analysis is shown in Figure 50. Stresses were calculated for all locations listed in Table I and are shown in Table VI. The calculated stresses in the container were acceptably low. Near the discontinuities, the highest calculated stress is below 110 MPa, or below 60% yield. Highly amplified deformations in the shell resulting from internal pressure are shown in Figure 51.

It can be concluded that the internal pressure in the container will not cause a failure of the shell.

10.0 ANALYSIS OF LIFTING LOADS

The stresses in the shell due to lifting of the container had been experimentally determined for several locations, see Table VII/3/. An initial attempt to simulate the results of the tests using finite element analysis, assuming the particulate acted as a fluid imposing an internal hydrostatic

pressure, failed because, it is believed, the particulate forms bridge-like structures between tubes of the basket. Bridging forms as a result of shear stresses in a particulate and it tends to form a 45° angle with a vertical constraining structure. Variation from the 45° angle is common and depends on pouring friction in the particulate, shape of column and so on. From the analysis, it appears that only a small fraction of the particulate exerts a force on the bottom lid. Almost the full weight of the particulate is transferred through the basket to the bottom support ring. The total load on the support ring was assumed to be 19,200 N, which is the combined weight of the particulate, the simulated used fuel bundles and the basket. The pressure applied on the bottom head was equivalent to the weight of the head plus a 325-mm height of particulate. The radial pressure on the cylindrical shell was taken to be equal to a 50-mm column of particulate equal to the average distance between the tubes and the shell. The weight of the top head was included in the analysis. The 325-mm and 50-mm thick layers of particulate were chosen to best simulate the experimental results. Of the 325-mm thickness, 58-mm represents the layer in the support ring and the spoke wheel areas, and 267-mm is inside the basket (about twice the basket tube diameter of 115 mm). A comparison of the experimental and analytical results is shown in Table VII. Good correlation was established for most locations, particularly where higher stresses are anticipated.

Some discrepancies between the experimental and analytical results exist (see Table VII). These differences has been seen before and their reasons have been discussed.

11.0 EFFECT OF CREEP

Based on the above analysis, we anticipate stresses in the titanium shell at or above yield. Based on our experience with creep tests in steel, we expect that titanium may exhibit creep at stresses above 67% yield for tensile stress and 100% yield for bending. The extent and effect of creep in the titanium sheli has not been evaluated yet. We expect that creep will result in significantly lower stresses due to material relaxation. This is highly advantageous. However, long term strains in the shell will be much higher. Creep induced high strains are not likely to produce failure because of the high ductility of titanium.

Testing and analysis of creep in titanium will be started shortly and will be presented in future reports.

12.0 FUTURE ACTIVITIES

Much work has already been done to show that the TWPP container is acceptable for used fuel disposal. However, the tests and analysis are still incomplete.

Tests to determine creep properties of titanium at low temperature are planned. The analyses presented above will be repeated to include the effect of creep on the container performance.

The above analysis considered only axisymmetric loading. Several sources of non-axisymmetric loading conditions can be postulated. For example, if bentonite does not absorb water uniformly, the 3 MPa overpressure may not be uniform. Some handling accidents may be tolerated under moderate impacts. The effects of such loadings should be analysed.

The shell material and the welds are likely to contain flaws. Fracture mechanics techniques should be employed to determine an acceptable flaw size and frequency. Such fracture analyses are planned.

Alternative container materials are also under consideration. High purity, oxygen-free electrolytic copper is one alternative under consideration. Creep tests on copper and finite element analyses of a conceptual copper container design are being planned.

13.0 CONCLUSIONS AND RECOMMENDATIONS

The Thin-Walled, Particulate-Packed Container fabricated of ASTM Grade 2 titanium has been tested and analyzed in significant detail. The container is not expected to fail under any of the considered loading conditions if good packing of the particulate is achieved, although in some areas, plastic deformation can be anticipated. The shell will be at the compressive yield stress throughout, except for the rim of the top and bottom heads where tensile stresses are anticipated.

The analysis was shown to closely approximate the strain results obtained from the hydrostatic tests, at locations removed from discontinuities. At discontinuities, the comparison was shown to be adequate for purely elastic conditions. Where large plastic deformations occur, a comparison of strains is difficult, but the comparison of the total deformation pattern is good.

An ability to perform a detailed predictive analysis of the structural behaviour of the conceptual container design has been demonstrated.

Based on the tests and analysis performed to date, the container design appears to be acceptable for long term disposal of used fuel bundles from the structural viewpoint.

14.0 ACKNOWLEDGEMENTS

WNRE personnel conducted a critical review of the manuscript. The author acknowledges and thanks them for their input.

Recommended by:

J.A. Chadha
Area Co-Ordinator
Containment and Immobilization Studies

Submitted by:

B. Teper
Engineer
Applied Mechanics Section

Approved by:

G.J. Clarke
Manager
Mechanical Research Dept

Reviewed by:

J.D. Tulk
Unit Head - Special Projects
and Computing
Applied Mechanics Section

BT:11g

REFERENCES

1. B. Teper, "Test Program of the Prototype of the TWPP Container, Part 1 - Hydrostatic Tests", Ontario Hydro Research Division Report 84-316-K, December 29, 1984.

2. B. Teper, "Feasibility Assessment of the Particulate-Packed, Thin-Walled Container", The 19th Information Meeting of the Canadian Nuclear Fuel Waste Management Program, Toronto, Ontario, May 14-16, 1985.

3. B. Teper, "Test Program of the Prototype of the TWPP Container, Part 2 - Post Hydrostatic Tests", Ontario Hydro Research Division Report 87-313-K, November 20, 1985.

4. B. Teper, "Test Program of Granular Materials for the Thin-Walled, Particulate-Packed Container", Ontario Hydro Research Division Report 87-154-K, dated August 27, 1987.

5. B. Teper, "Preliminary Evaluation of Stress-Strain Distribution in Particulate-Packed Container", Ontario Hydro Research Division Report 81-316-K, dated October 29, 1981.

6. D.A. Dixon, M.N. Gray, P. Baumgartner and G.L. Rigby, "Pressures Acting on Waste Containers in Bentonite - Based Materials", 2nd International Conference on Radioactive Waste Management, September 7-11, 1986, Winnipeg, Manitoba, Canada.

7. S. Timoshenko, S. Woinowsky-Kreiger, Theory of Plates and Shells, McGraw-Hill Book Company, Toronto, 1959.

8. D. Taralis, "Determination of an Equivalent Thermal Conductivity of Sand Packed Thin Wall Container for Irradiated Fuel," Ontario Hydro Research Division Report 81-151-K, dated, May 22, 1981.

TABLE I

EXPERIMENTAL RESULTS FROM HYDROSTATIC TEST

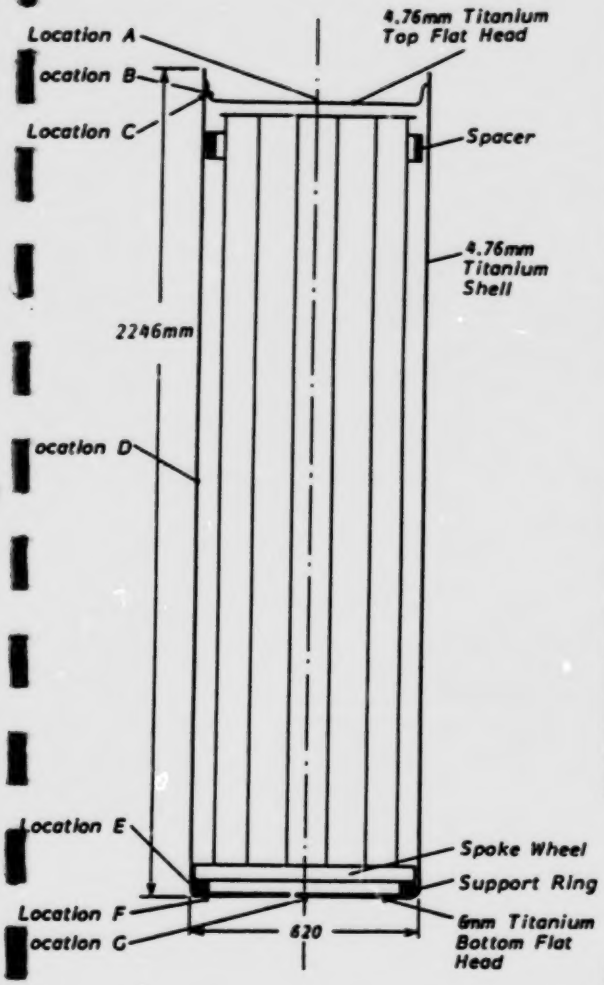

(a) Locations used in analysis

Notes:

* Represents radial direction on lids

** Location was not monitored

Location	Measured Strain (μm/m)		Stresses (MPa)		
	Axial*	Hoop	Axial	Hoop	Radial
A	230	-250	33	-38	-5
B	-2100	-110	-432	-146	-5
C	-2200	-3020	-630	-750	-5
D	-500	-1230	-222	-447	-5
E	230	-1700	-52	-336	-5
F	**	**			
G	**	**			

b) Results of 100°C, 10 MPa Test

Location	Measured Strain (μm/m)		Stresses (MPa)		
	Axial*	Hoop	Axial	Hoop	Radial
A	200	-220	28	-34	-5
B	-950	60	-192	-44	-5
C	-1460	-2210	-432	-543	-5
D	-30	-1500	-95	-312	-5
E	40	-1150	-60	-235	-5
F	**	**			
G	**	**			

c) Results of 125°C Test Strains at 9.5 MPa

Location	Measured Strain (μm/m)		Stresses (MPa)		
	Axial*	Hoop	Axial	Hoop	Radial
A	**	**			
B	**	-350			
C	**	**			
D	**	-80			
E	**	-350			
F	**	**			
G	**	**			

d) Results of 150°C, 10 MPa Test

TABLE II

MECHANICAL PROPERTIES OF TITANIUM

Material	Temperature °C	E MPa	ν	Sy MPa	Su MPa	Sm MPa	α μm/m °C
Titanium	*30*	*107,000*	*0.34*	*275*	*345*	*115*	-
Titanium	*100*	*103,000*		*216*	*345*	*115*	*8.46*
Titanium	*150*	*99,000*		*173*	*252*	*84*	*8.55*
Titanium	*200*	*95,000*		*130*	*198*	*66*	*8.64*

Notes:

1. *Thermal expansion coefficient is given as an average value from 30°C to the specified temperature.*

TABLE III

RESULTS OF ANALYSIS OF PIE-SHAPED MODEL

Property	Locations			
	A	B	C	D
Radial Deformation (mm)	*-0.562*	*-0.510*	*-0.586*	*-0.200*
Average Radial Def. (mm)	*-0.544*			
Hoop Stress (MPa)	*-217.*	*-171.*	*-184.*	*-26.*
Radial Stress (MPa)	*-15.*	*-11.*	*-54.*	*-107.*

All stresses are for the outside surface and include bending moments.

See Figure 9 for locations

TABLE IV

EFFECT OF STIFFNESS INSIDE STEEL TUBES

Stiffness Inside Steel Tubes (MPa)	Deflection		
	location A	location B	location C
50	*-0.565*	*-0.523*	*-0.595*
337	*-0.562*	*-0.510*	*-0.586*
1000	*-0.553*	*-0.487*	*-0.570*

TABLE V
STRAIN FROM TEST AND LINEAR-ELASTIC ANALYSIS

Location (1)	Strains (μm/m)			
	Test Results (2)		Analytical Results	
	Axial or Radial	Hoop	Axial or Radial	Hoop
A	200	-220	1,400	1,300
B	-950	60	1,011	-400
C	-1460	-2210	-997	-1,636
D	-30	-1500	-650	-1,814
E	40	-1150	-84	-1,702
F	(3)	(3)	-70	-860
G	(3)	(3)	-45	-45

Notes:

1. *See Table I for locations.*
2. *Test results are obtained from the 125°C test shown in Table I.*
3. *These strains were not monitored during the test.*

TABLE VI
STRESSES DUE TO INTERNAL PRESSURE

Location (1)	Stresses (MPa)	
	Axial or Radial	Hoop
A	183.0	184.0
B	159.0	56.9
C	7.71	22.50
D	2.78	5.67
E	-1.00	14.80
F	8.30	20.60
G	1.34	1.34

TABLE VII

STRESSES DURING LIFTING

LOCATION	PRINCIPAL STRESSES (MPa)			
	EXPERIMENTAL		ANALYTICAL	
	AXIAL	HOOP	AXIAL	HOOP
1	-0.3	-0.3	-0.1	-0.1
2	1.2	-3.9	0.2	-0.3
3	1.7	-1.4	2.2	-0.1
4	2.3	-0.4	2.6	-0.4
5	20.8	-0.2	22.2	-7.5
6	10.3	3.9	11.4	11.5

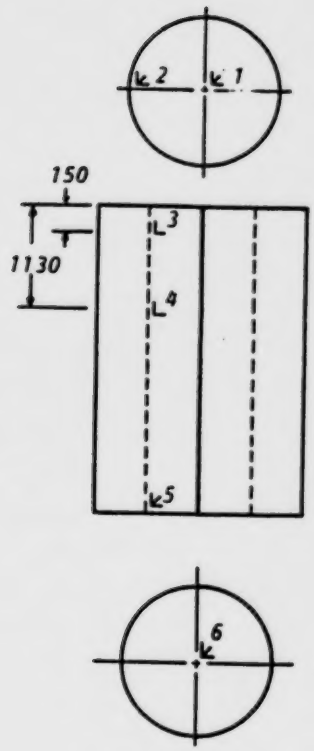

LOCATIONS IN THE TABLE

87-296
175926-RD

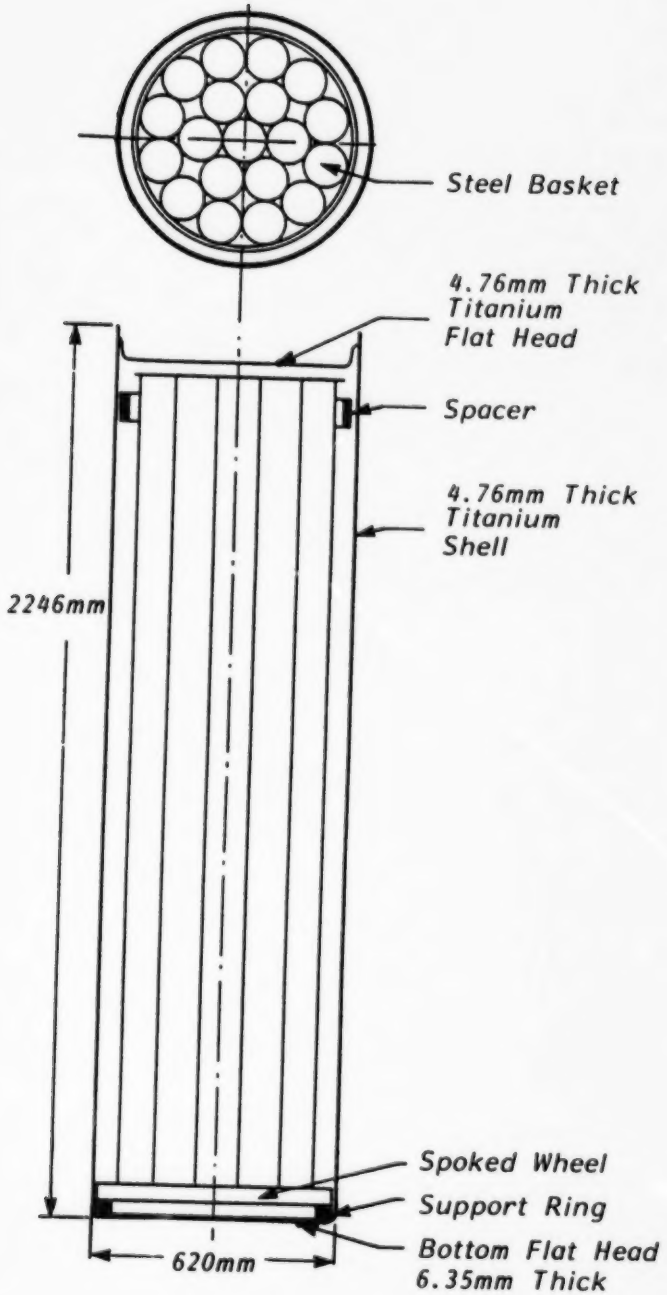

FIGURE 1

LAYOUT OF THIN-WALLED
PARTICULATE-PACKED CONTAINER

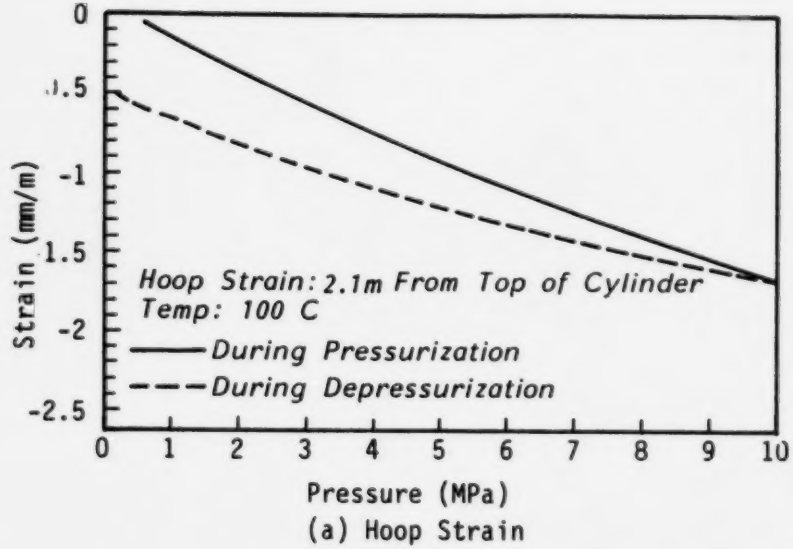

(a) Hoop Strain

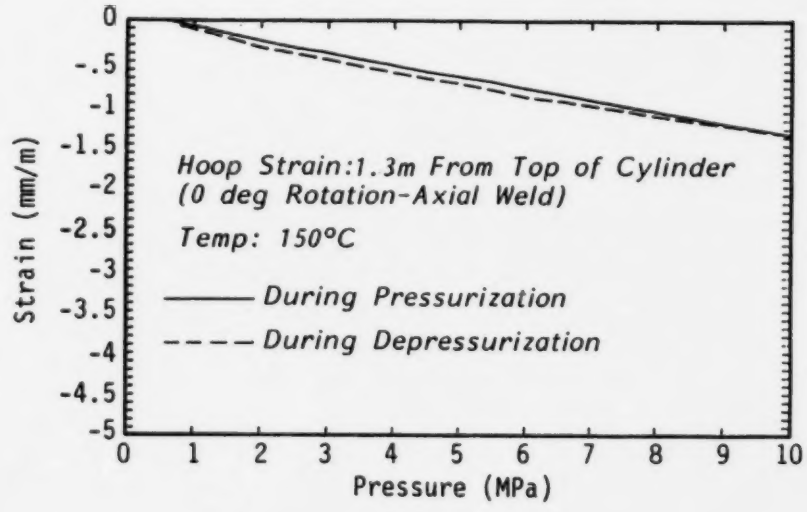

(b)

FIGURE 2

SAMPLE OF HYDROSTATIC TEST RESULT

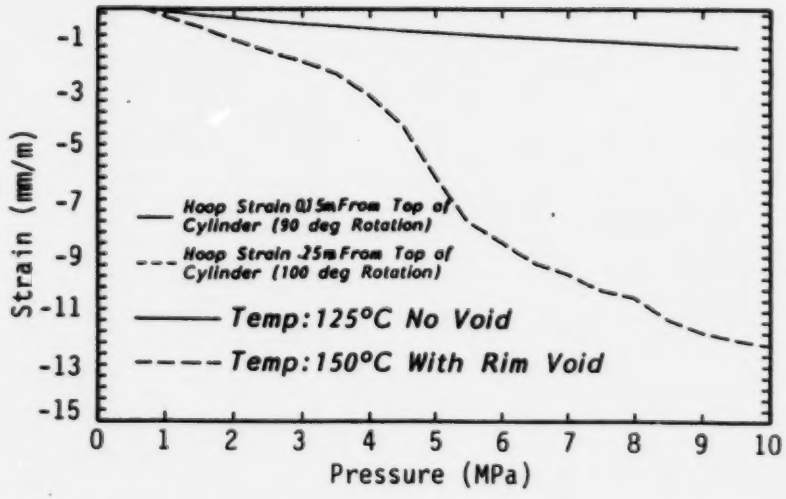
Strain (mm/m)
Pressure (MPa)
Hoop Strain 0.15m From Top of Cylinder (90 deg Rotation)
Hoop Strain .25m From Top of Cylinder (100 deg Rotation)
Temp:125°C No Void
Temp:150°C With Rim Void

(a) Near Rim Void

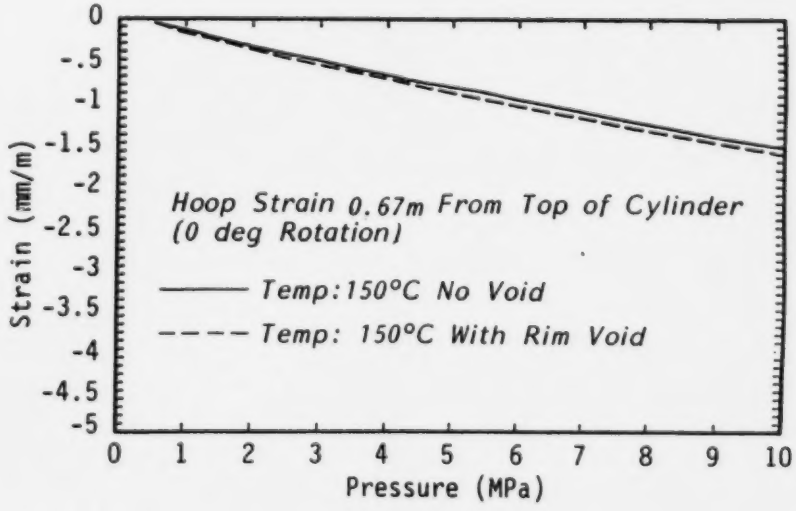

(b) Away From Rim Void

FIGURE 3

SAMPLE OF HYDROSTATIC TEST RESULT
TEST WITH VOID

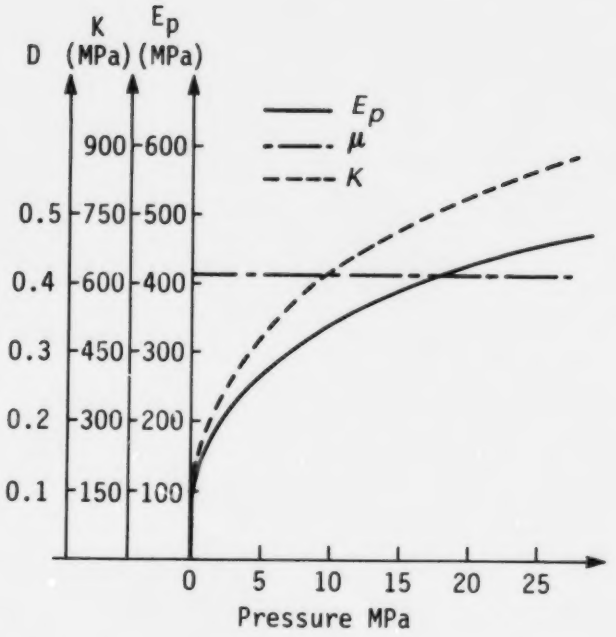

FIGURE 4
MECHANICAL PROPERTIES OF PARTICULATE

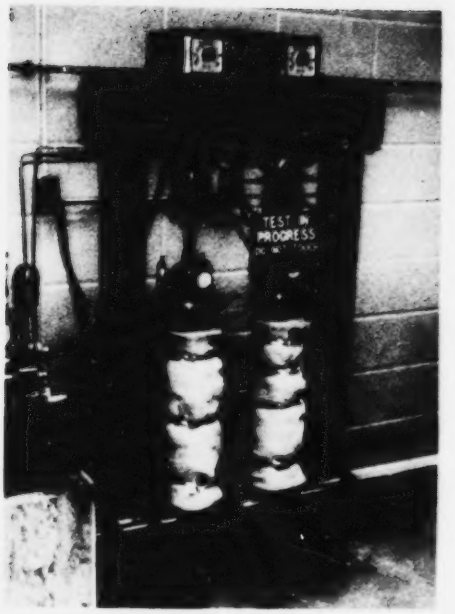

FIGURE 5
CREEP TEST STATION

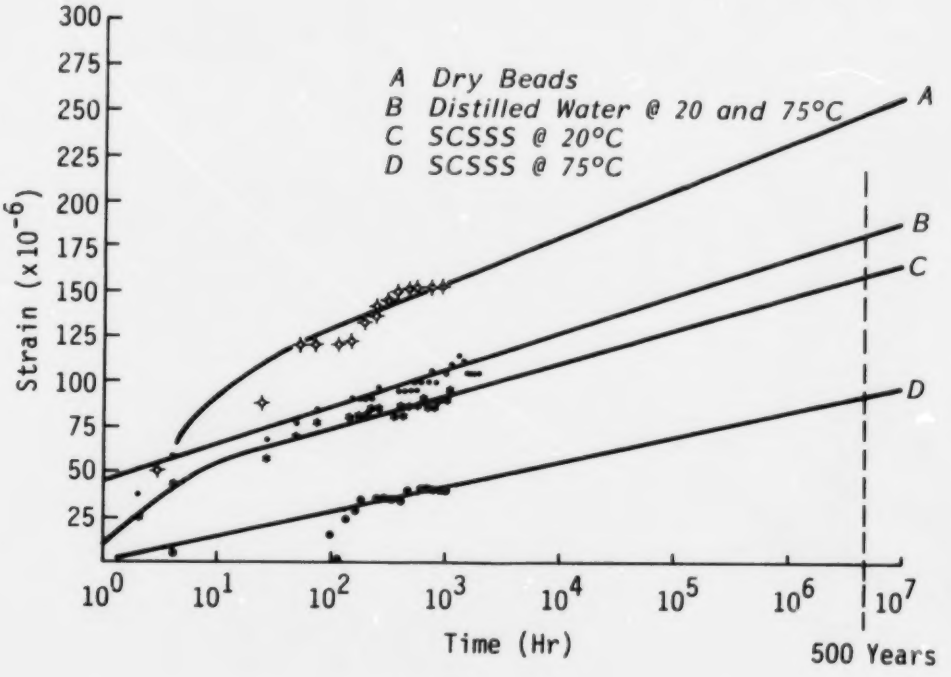

FIGURE 6
SETTLEMENT OF PARTICULATE (GLASS BEADS)

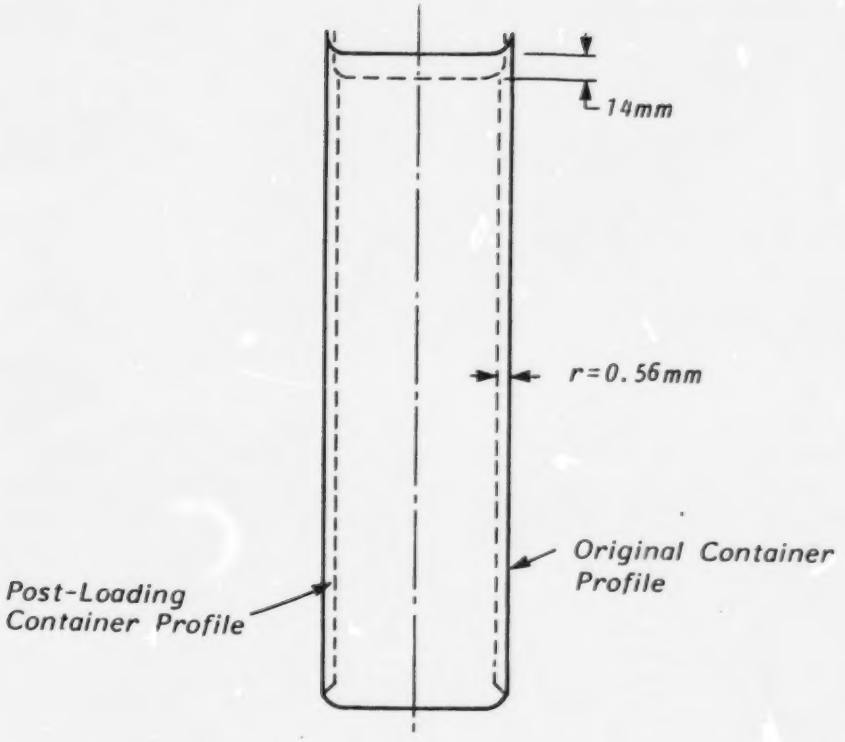

FIGURE 7
DEFORMATION OF PROTOTYPE CONTAINER

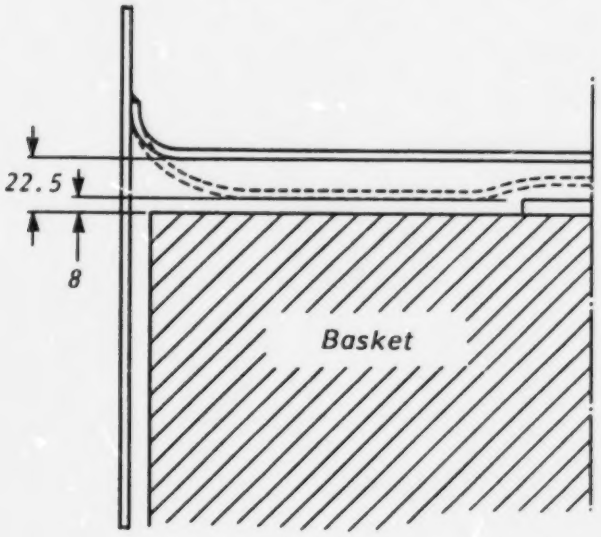

All Dimensions are in Millimeters
Not to Scale

FIGURE 8
DEFORMATION OF TOP LID

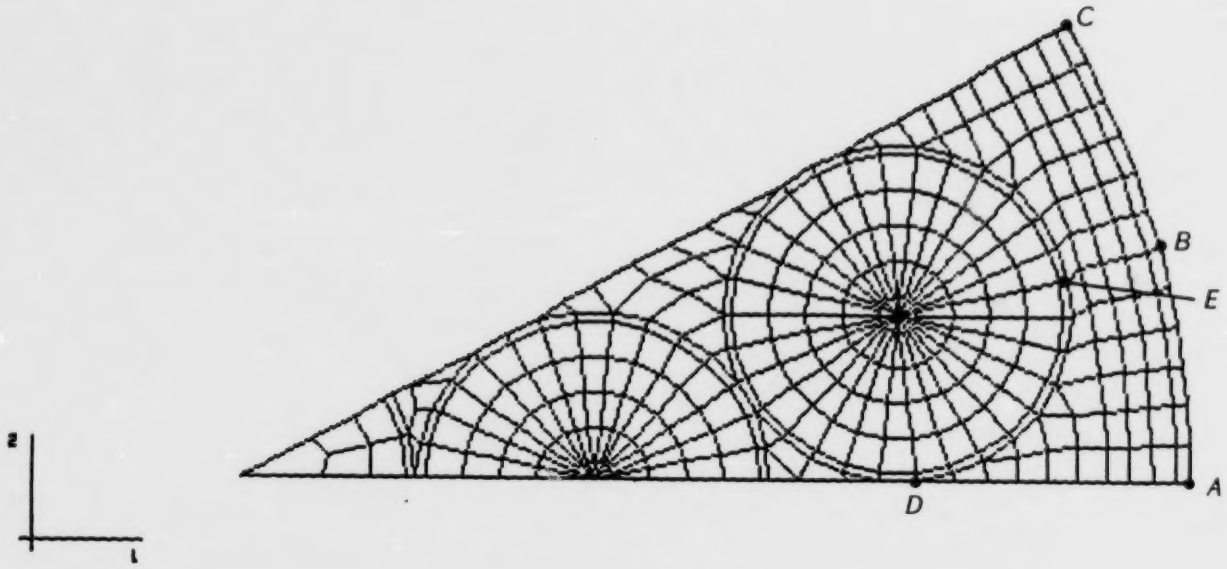

FIGURE 9
PIE-SHAPED MODEL OF TWPP CONTAINER

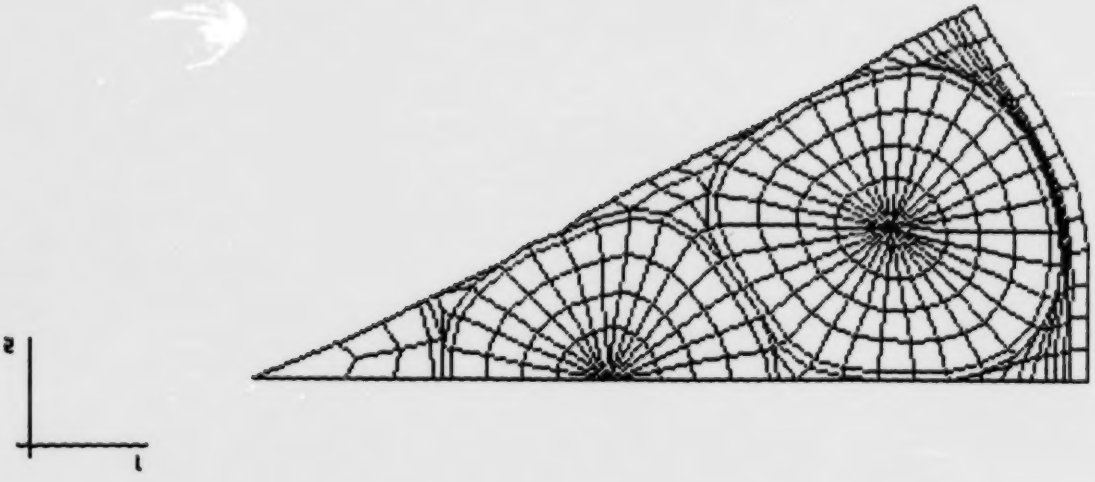

FIGURE 10
DEFORMATION OF THE PIE MODEL

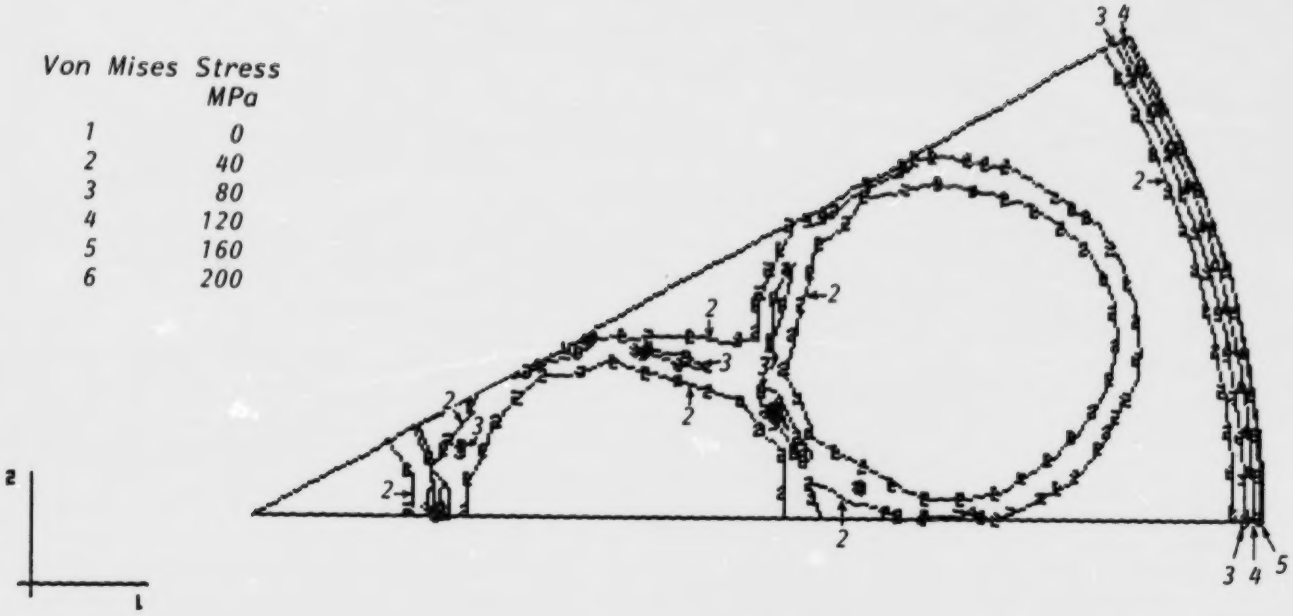

FIGURE 11
STRESS DISTRIBUTION IN THE PIE MODEL

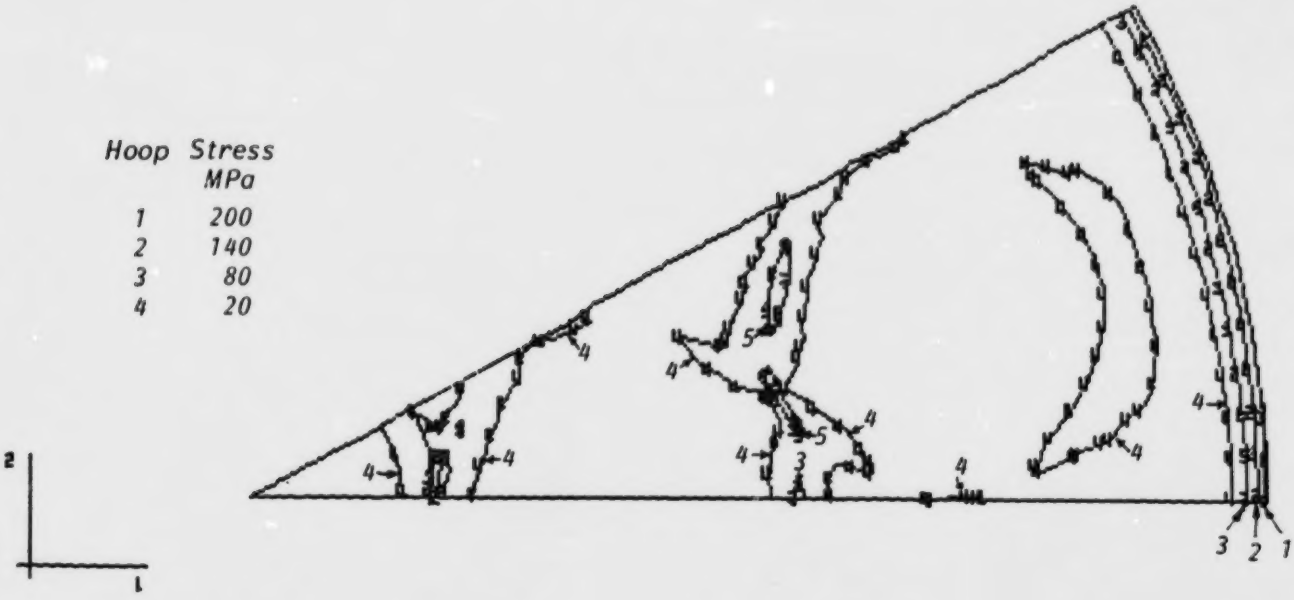

FIGURE 12
HOOP STRESS DISTRIBUTION IN THE PIE MODEL

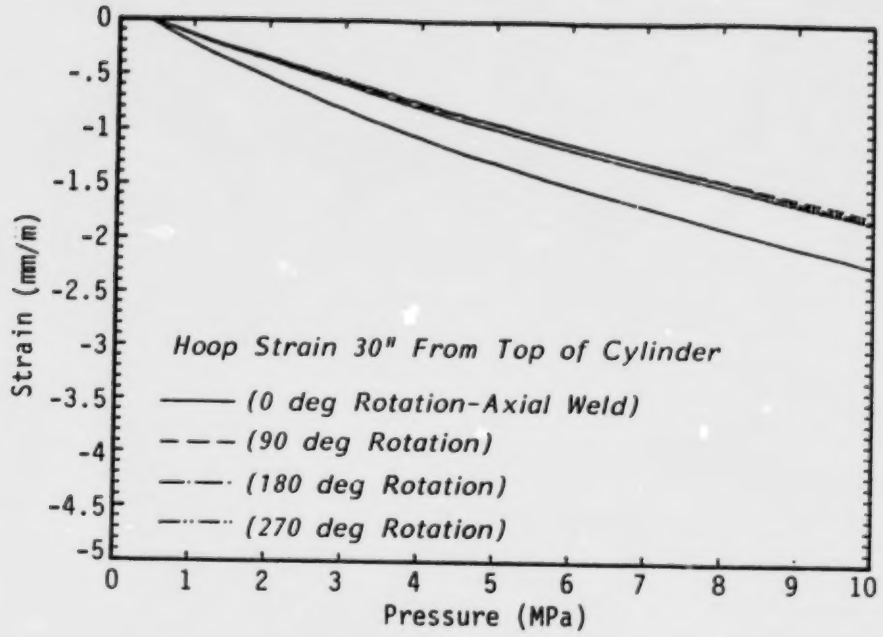

(a) Hoop Strain Experimentally Obtained

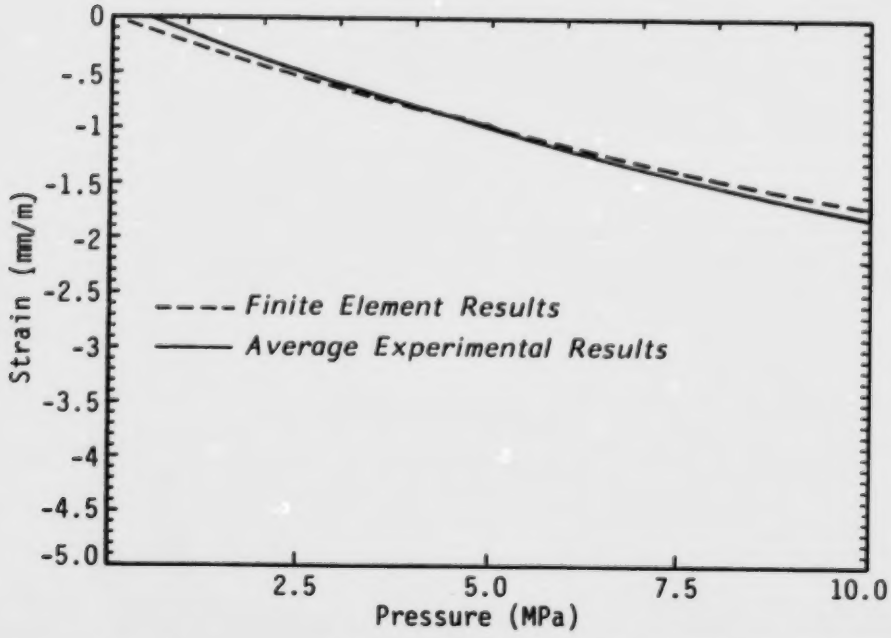

(b) Comparison of Experimental and Analytical Results

FIGURE 13
HOOP STRAINS IN CYLINDRICAL SHELL

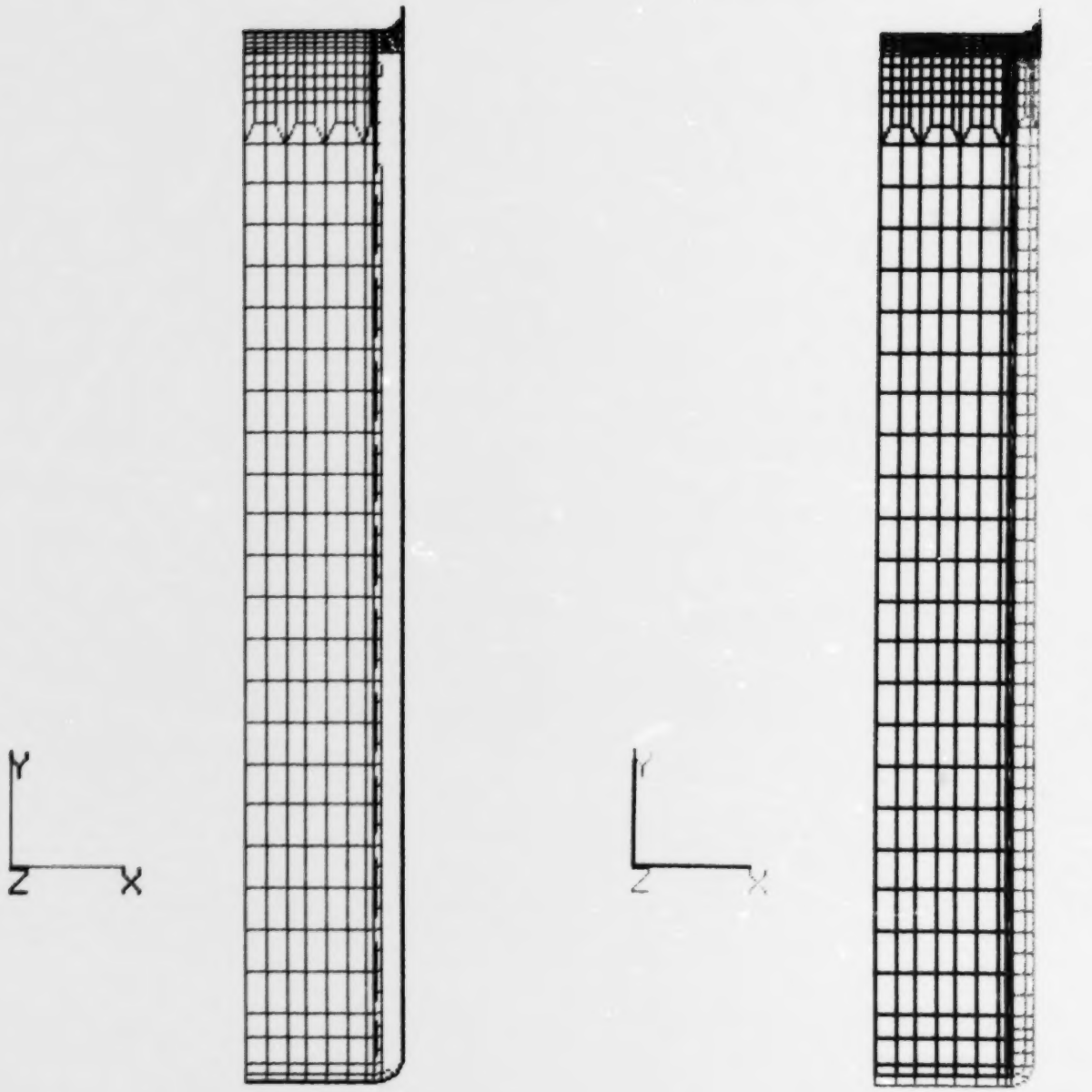

(a) Titanium Shell *(b) Internal Structure*

FIGURE 14
AXISYMMETRIC FINITE ELEMENT MODEL

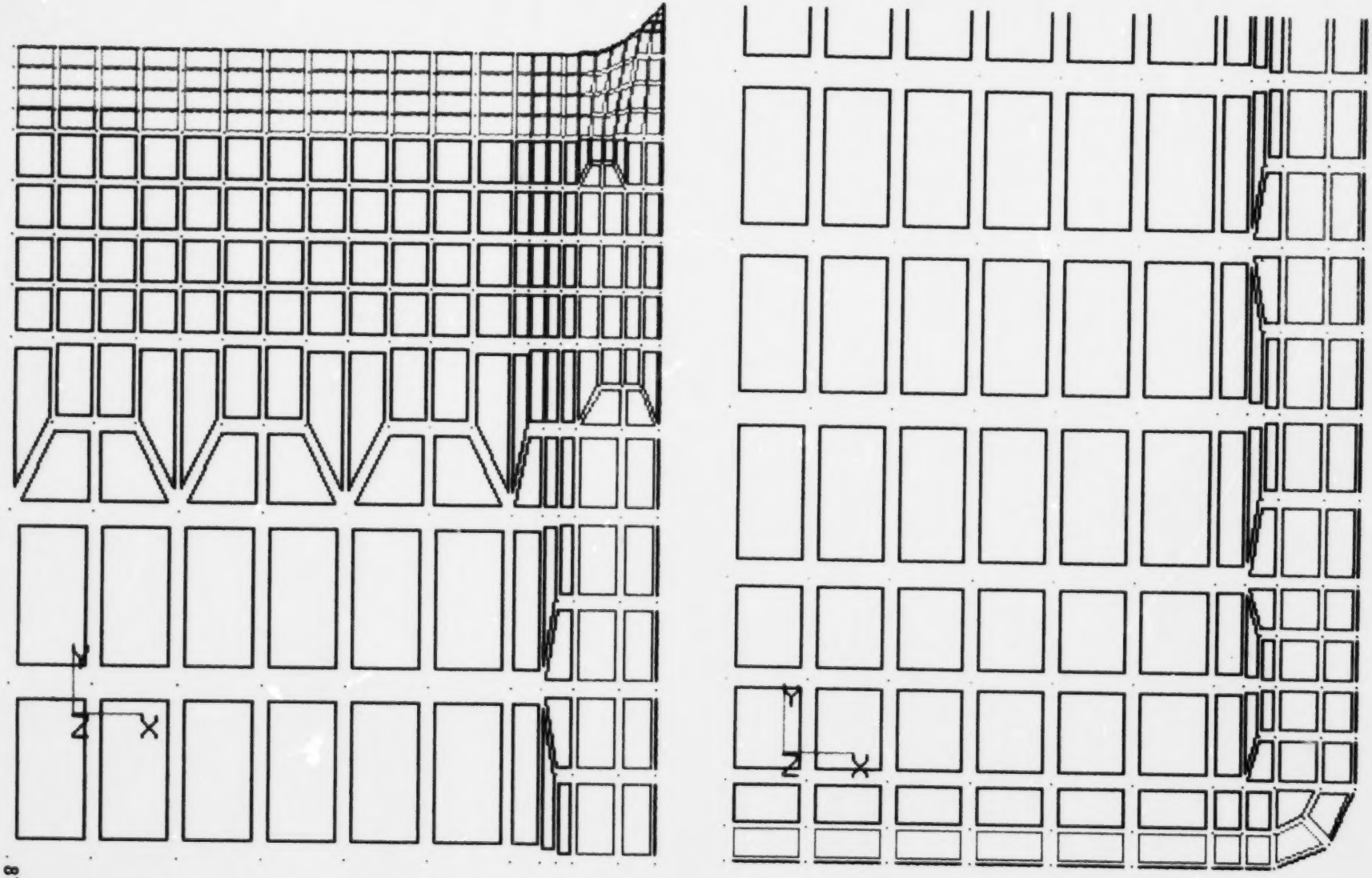

FIGURE 15
MODEL OF TOP AND BOTTOM AREAS

87-296
173162 RD

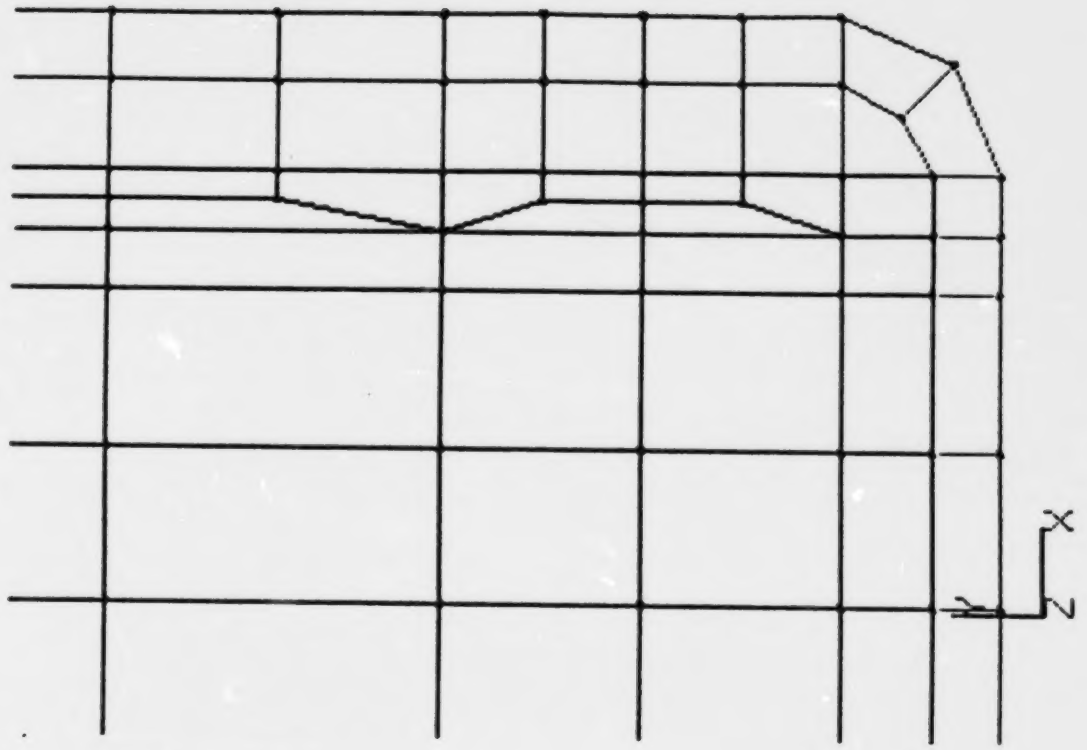

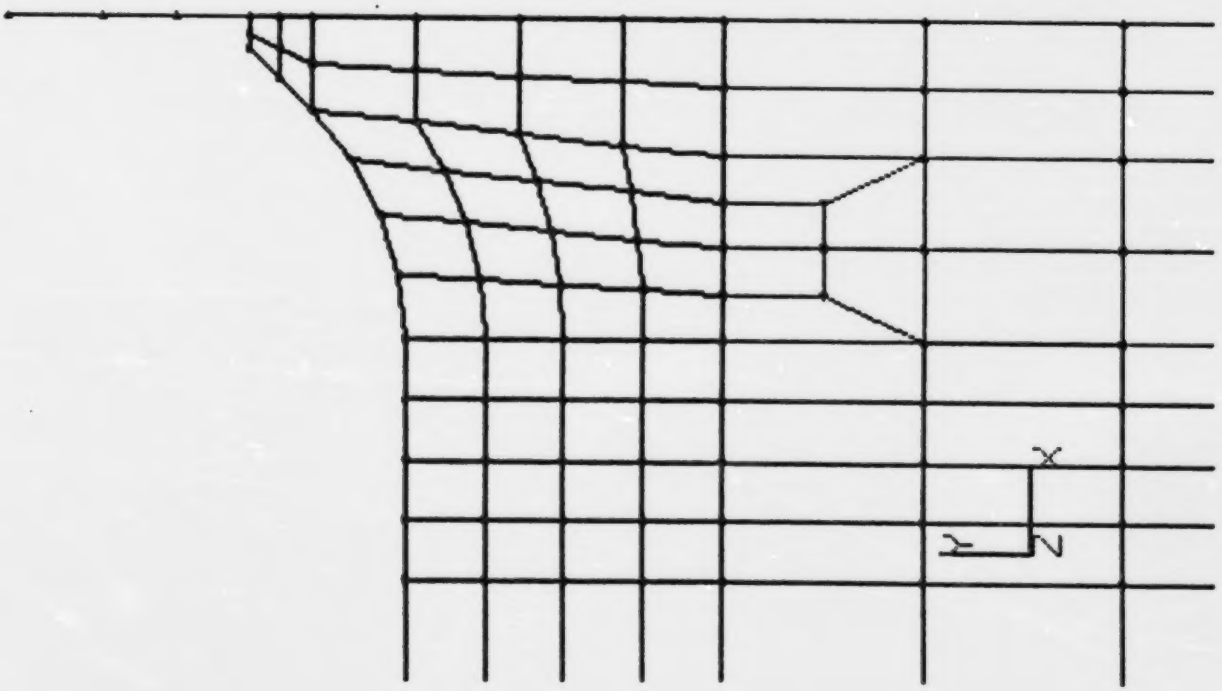

FIGURE 16
MODEL OF DISCONTINUITY AREAS

87-296
172190-RD

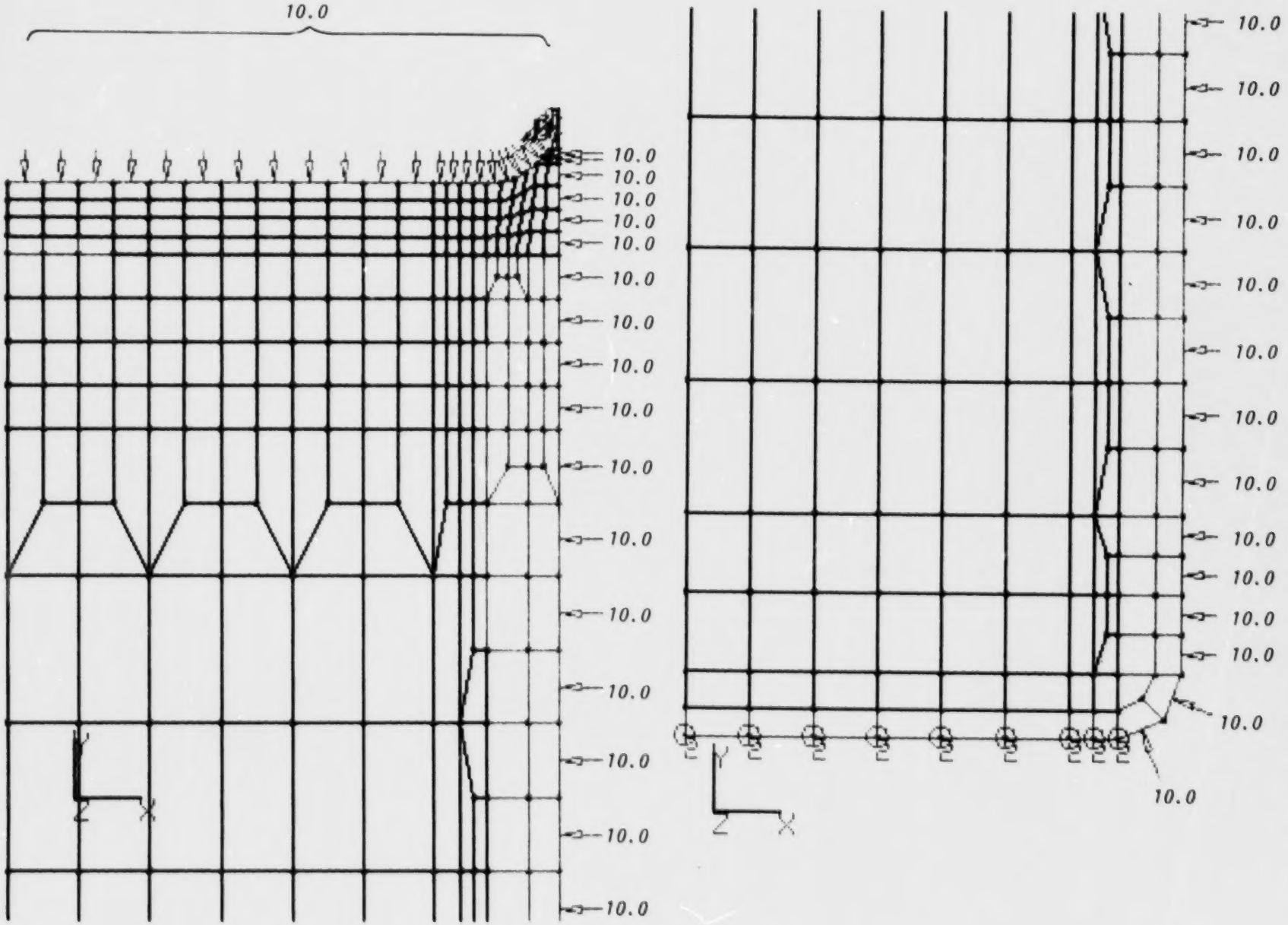
10.0
10.0
10.0

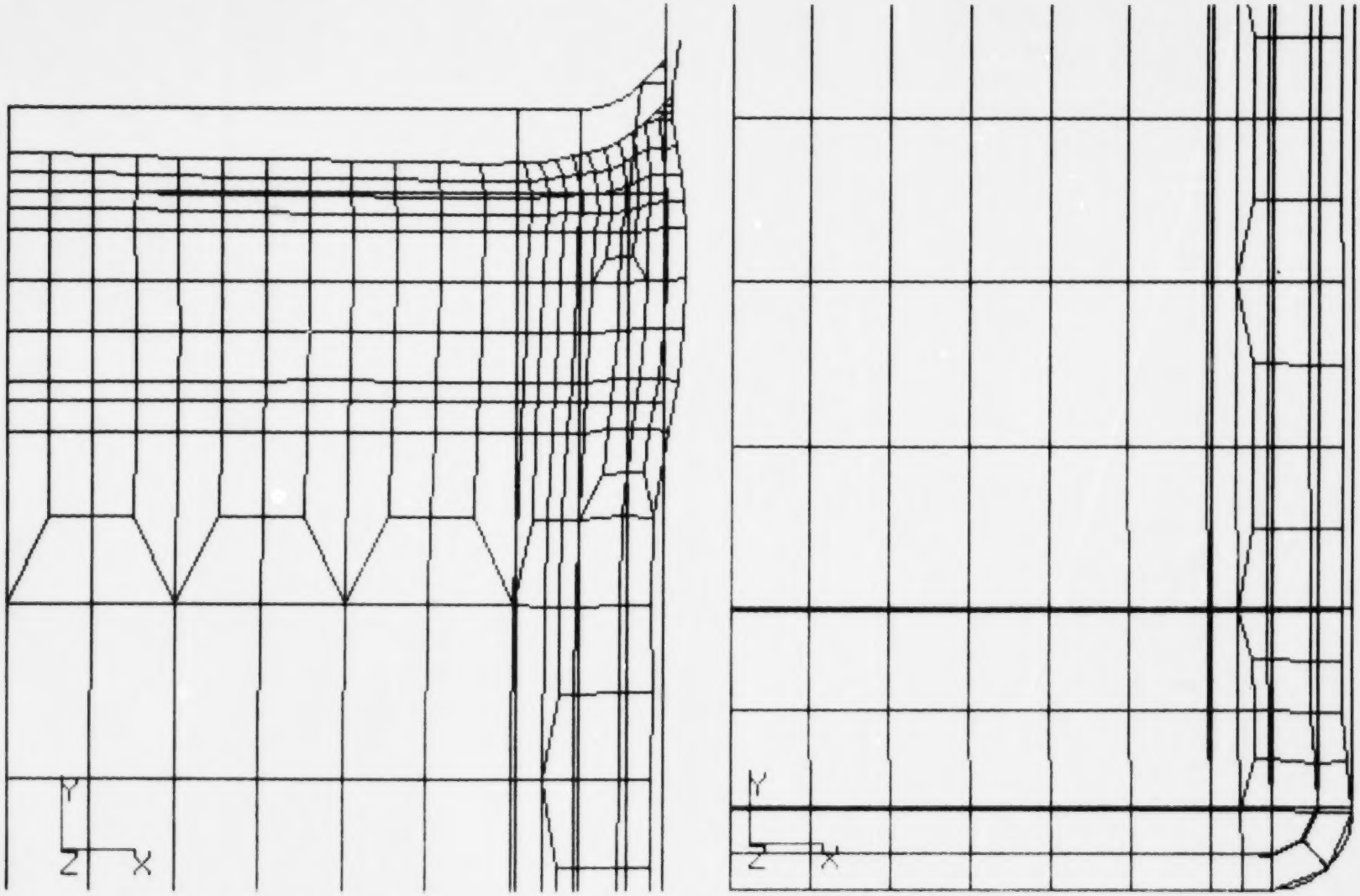

Note: Deformations amplified 10 times

FIGURE 18

DEFORMATIONS - ISOTROPIC PROPERTIES OF PARTICULATE

87-296
173164 RD

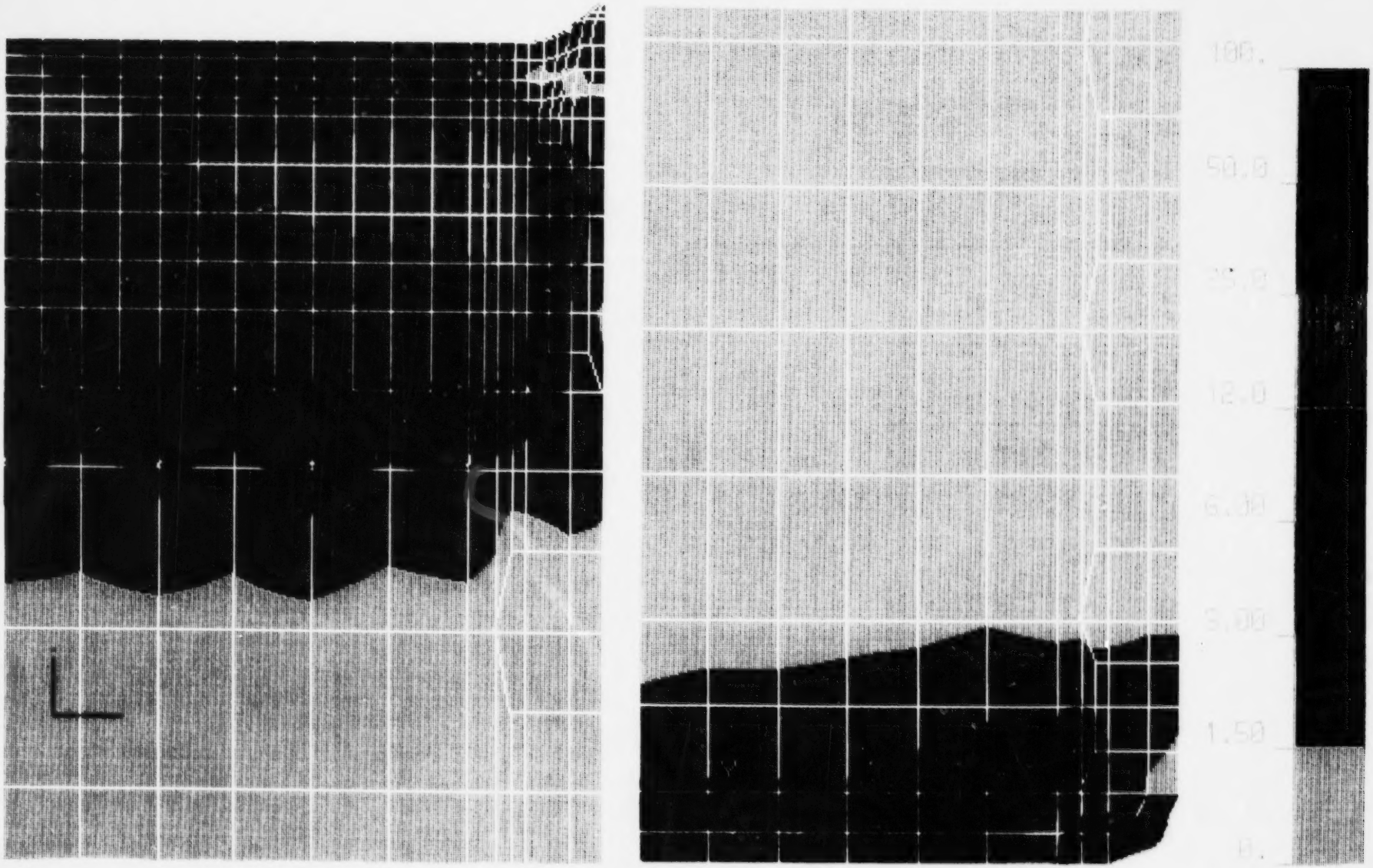

Von Mises Stress Distribution inside the Container

FIGURE 19

VON MISES STRESS DISTRIBUTION - ISOTROPIC PROPERTIES OF PARTICULATE

87-291
173165 RD

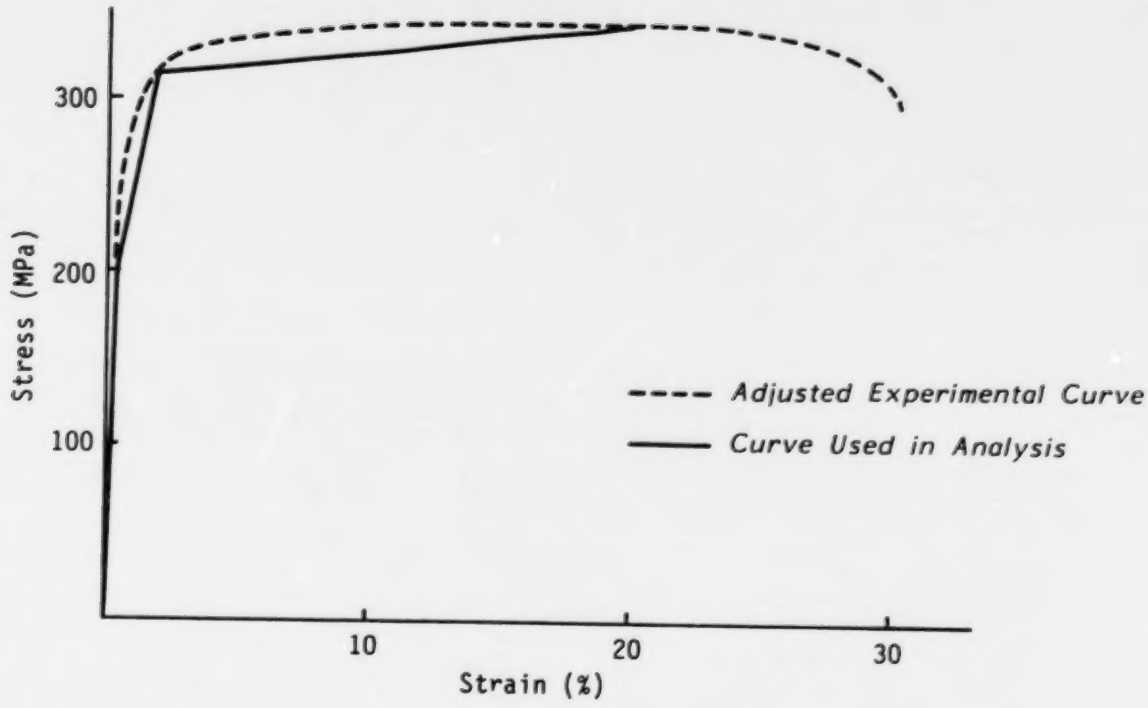

FIGURE 20
ASSUMED PLASTIC PROPERTIES OF TITANIUM

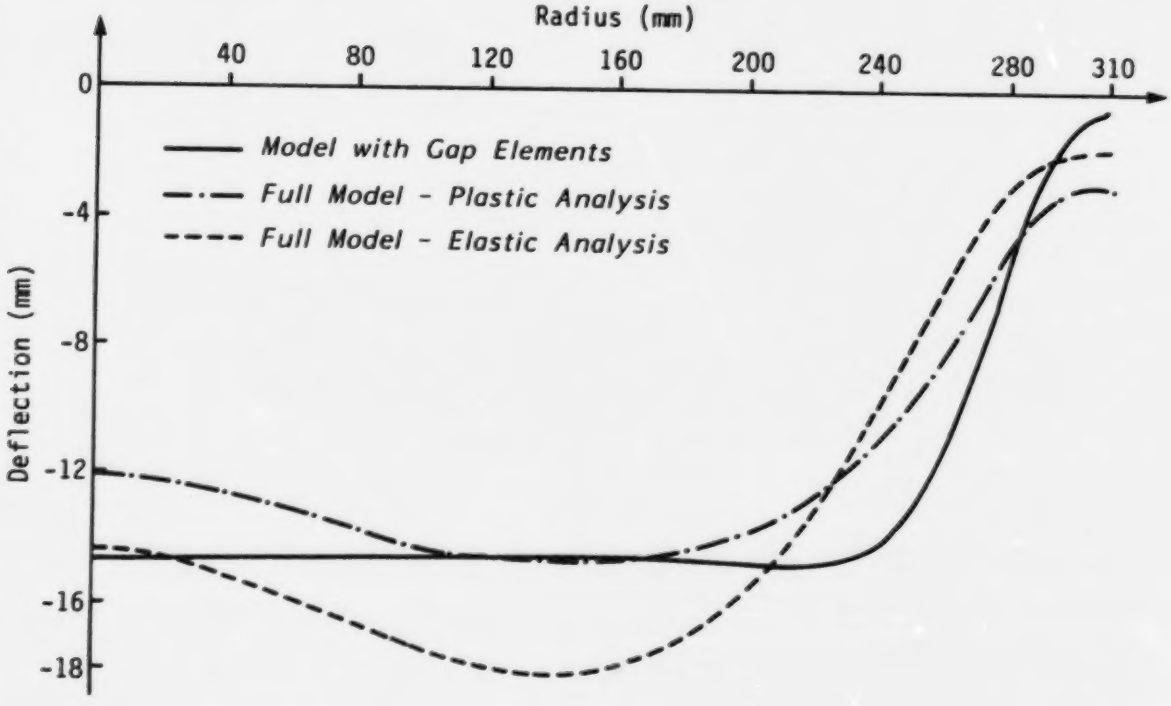

FIGURE 21
COMPARISON OF RESULTS
OF TOP GAP ANALYSES

87-296

173170 RD

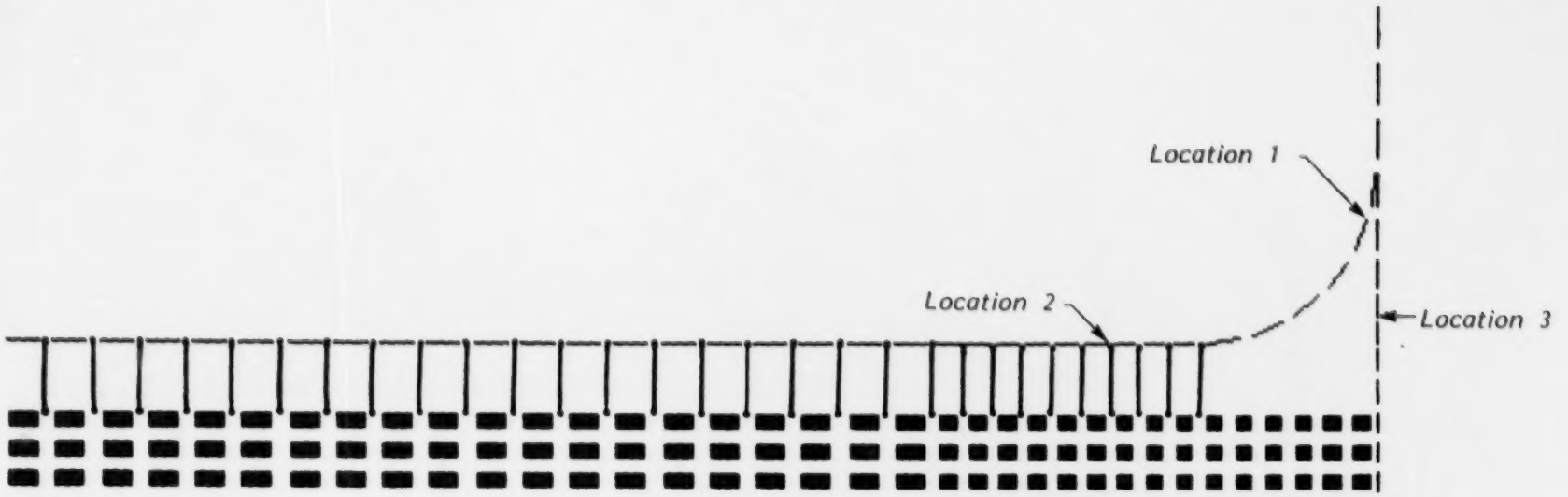

FIGURE 22
MODEL OF TOP AREA WITH GAPS

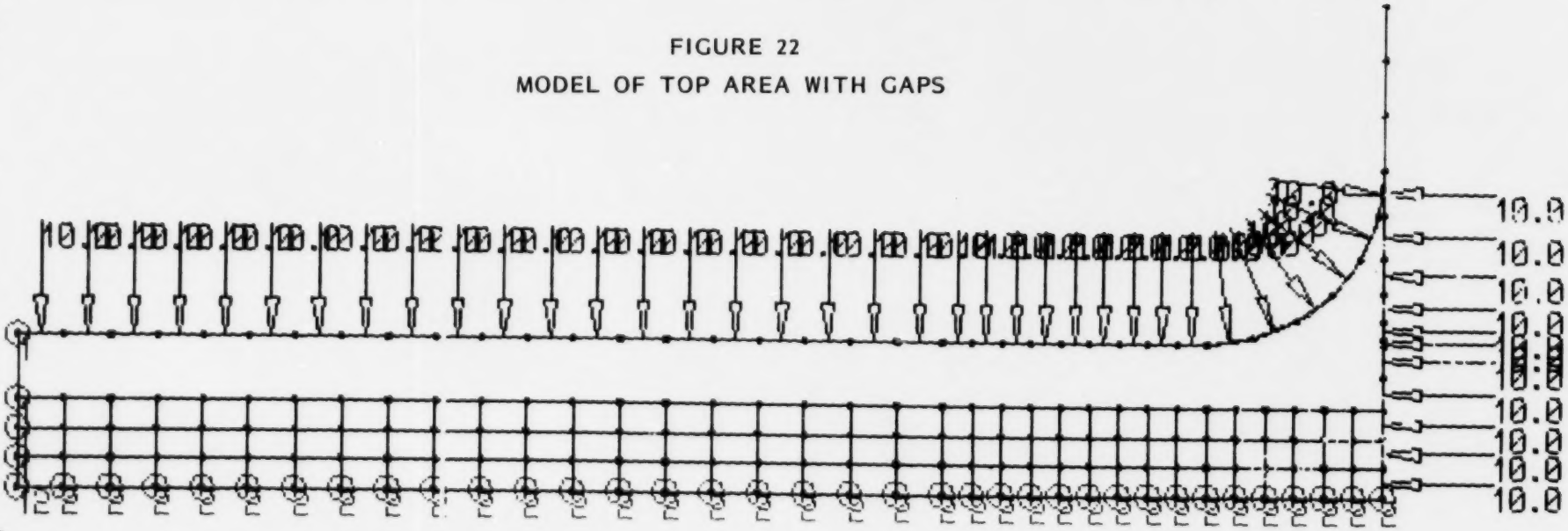

FIGURE 23
BOUNDARY CONDITIONS

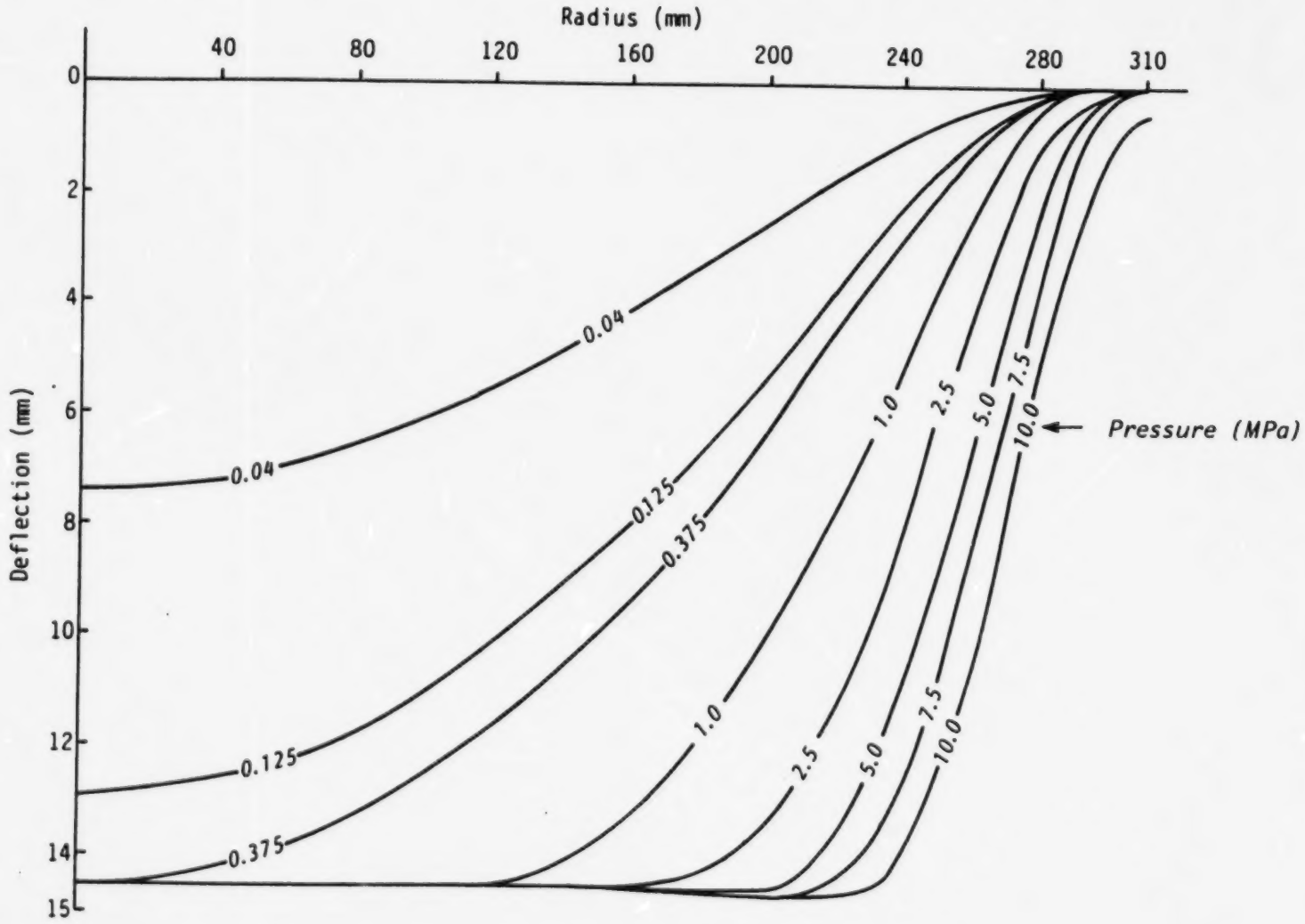

FIGURE 24

CLOSING OF TOP GAP FROM
GAP-ELEMENT MODEL

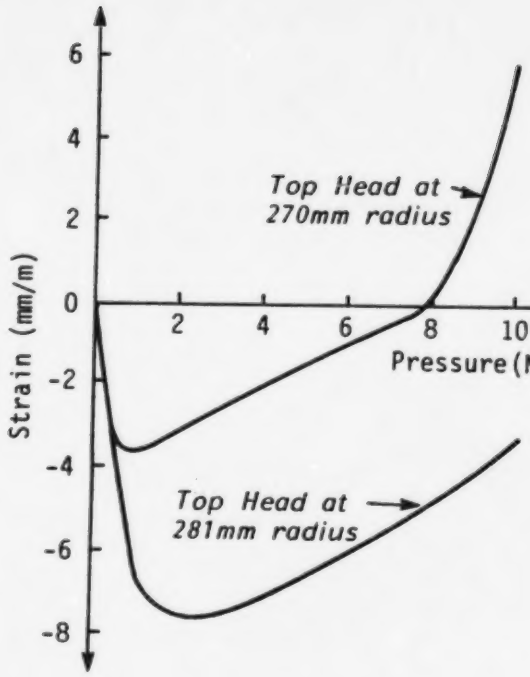

FIGURE 25

RADIAL STRAIN AT LOCATION B

(See Table I for Location B)

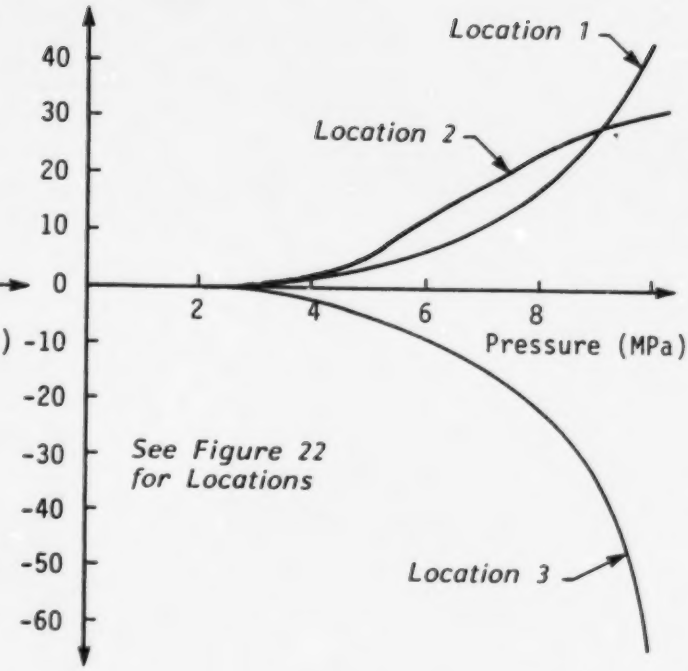

FIGURE 27

LARGEST PLASTIC STRAINS IN TITANIUM SHELL

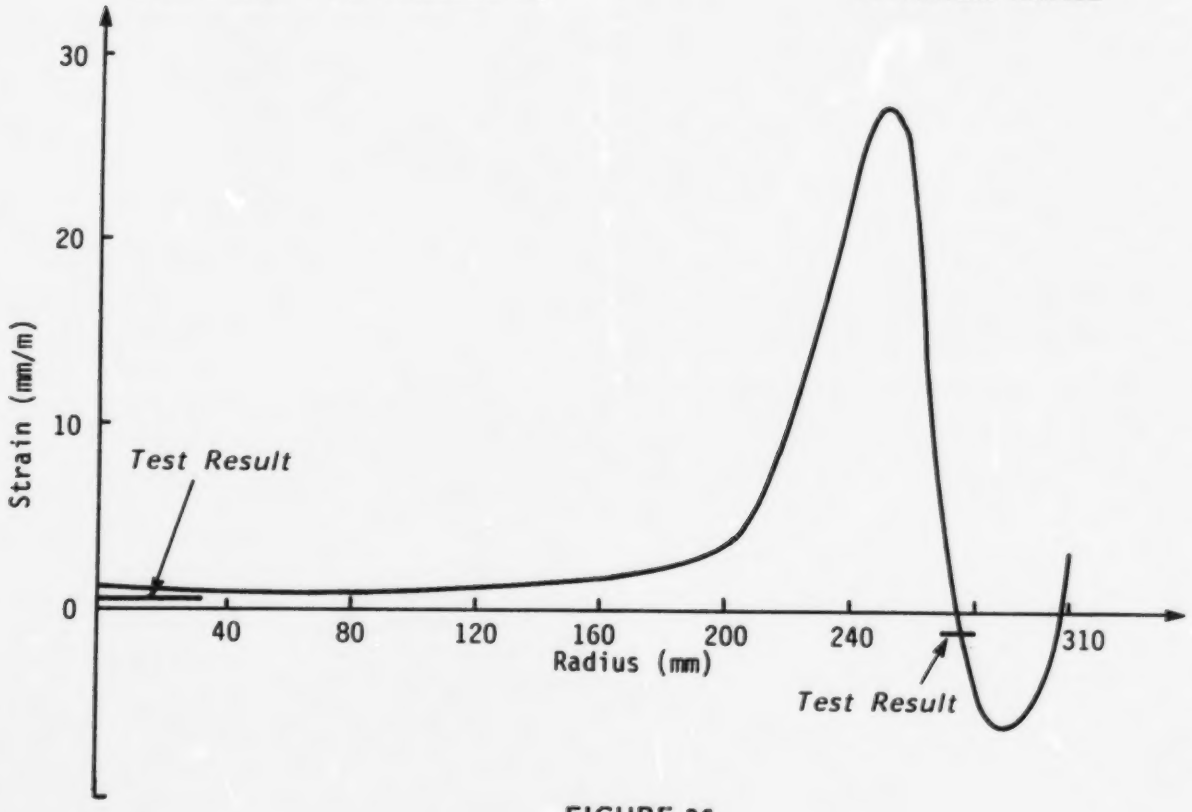

FIGURE 26

STRAIN IN TOP PLATE AT FULL PRESSURE

87-296
173173 RD

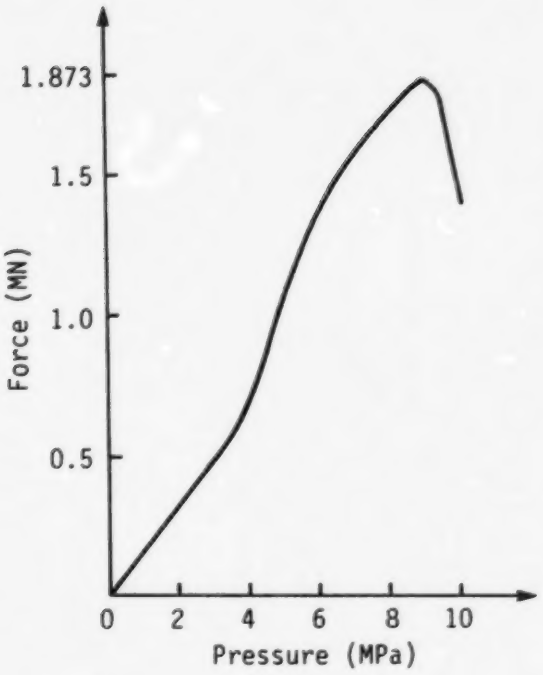

FIGURE 28

COMPRESSIVE FORCE IN THE CYLINDRICAL SHELL

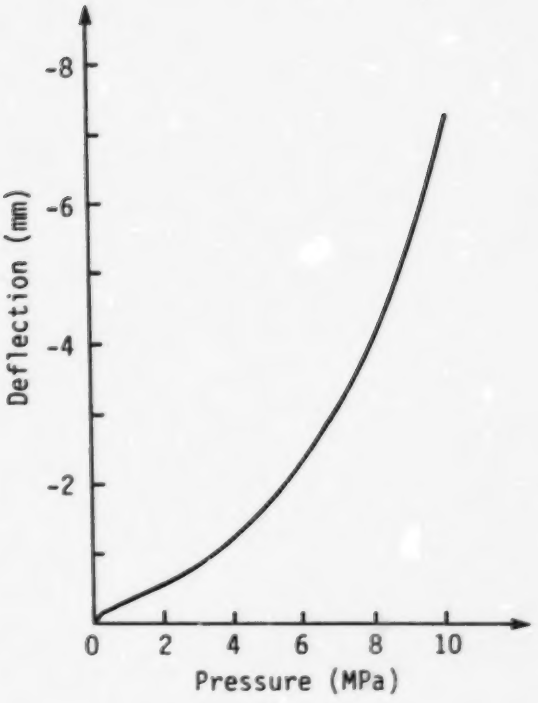

FIGURE 29

DEFLECTION OF UNSUPPORTED CYLINDRICAL SHELL

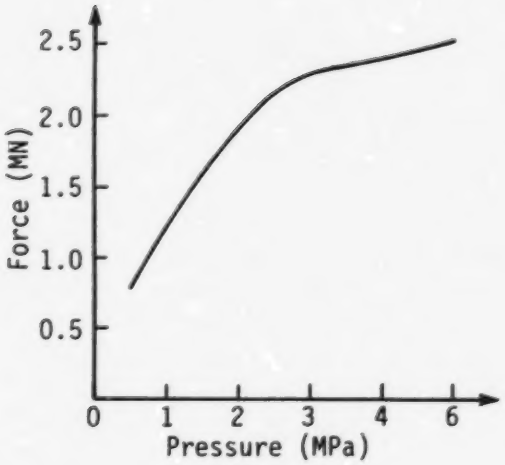

FIGURE 30

COMPRESSIVE FORCE IN CYLINDRICAL SHELL
10mm GAP

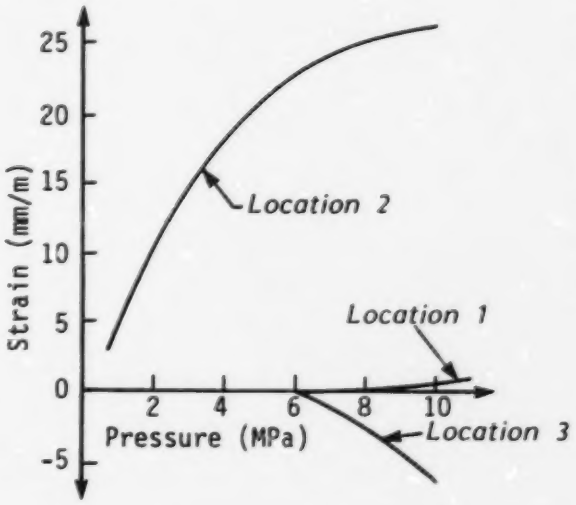

FIGURE 31

LARGEST PLASTIC STRAINS
10mm GAP

87-296

173174-RD

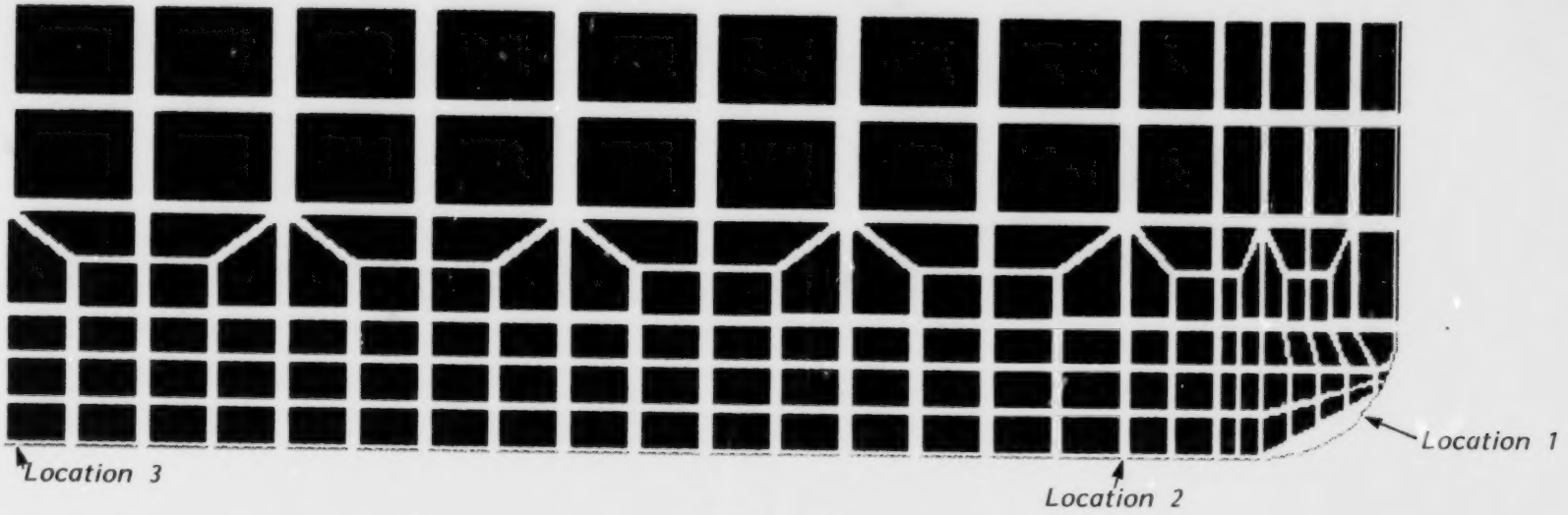

FIGURE 32
FINITE ELEMENT MODEL OF BOTTOM HEAD

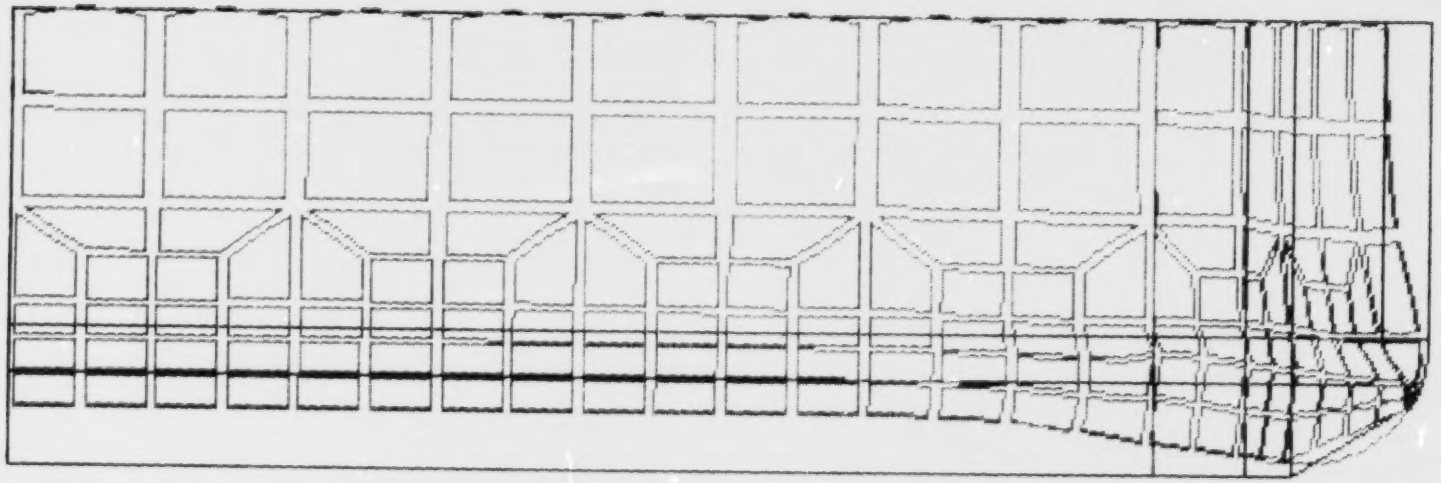

FIGURE 33
DEFORMATIONS DUE TO EXTERNAL PRESSURE (AMPLIFIED 20 TIMES)

87-296
175927-RD

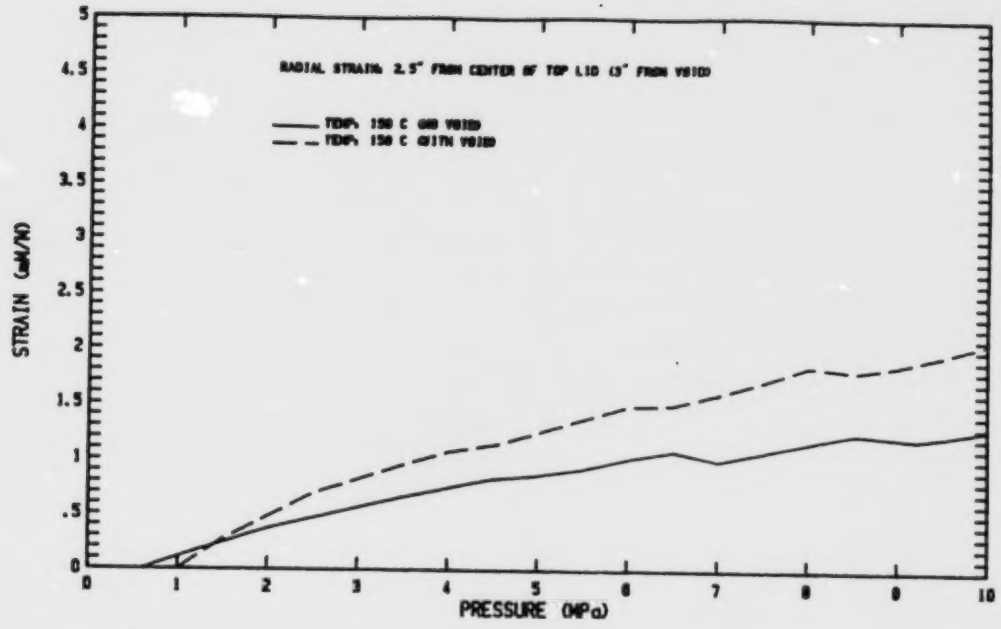

a) STRAIN AT THE CENTRE VOID

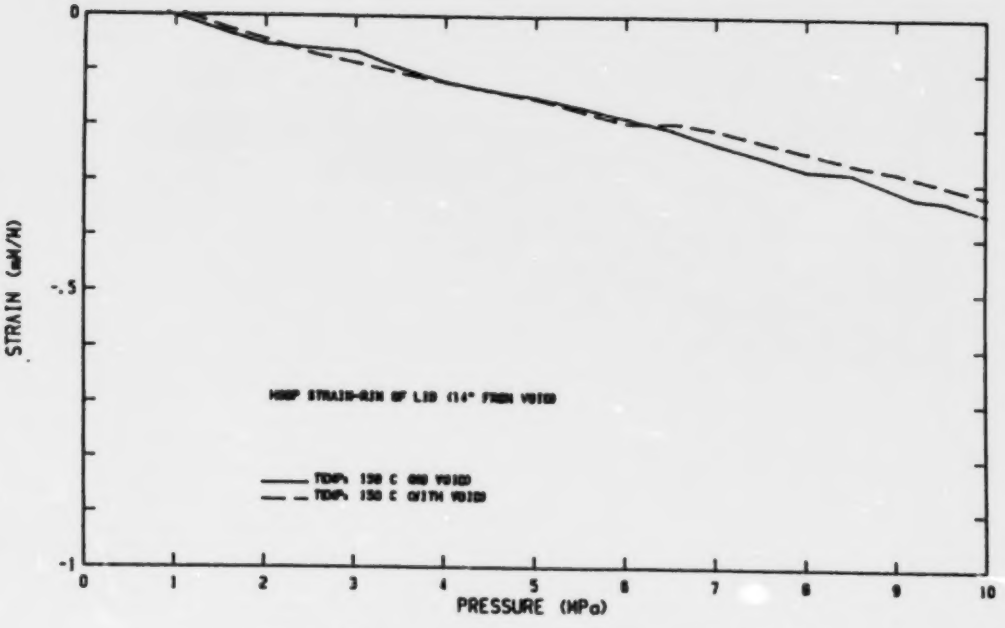

b) STRAIN AWAY FROM CENTRE VOID

FIGURE 34

RESULTS FROM HYDROSTATIC TEST
WITH CENTRE VOID

87-296

175928-RD

FIGURE 35
FINITE ELEMENT MODEL OF CENTRE VOID

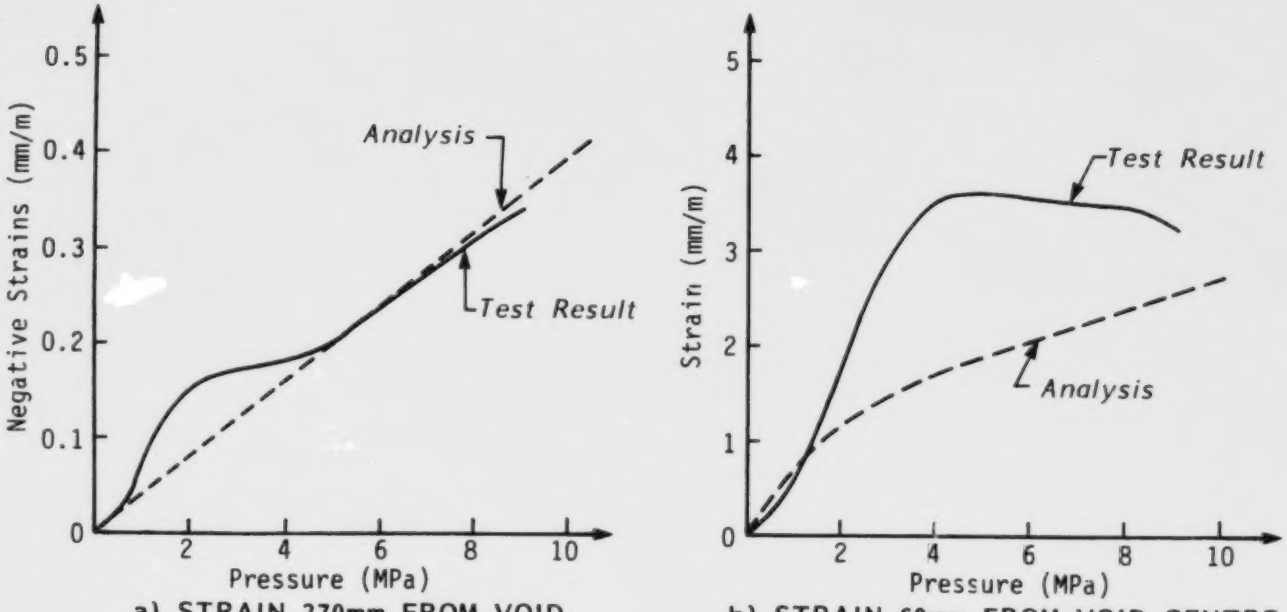

a) STRAIN 270mm FROM VOID

b) STRAIN 60mm FROM VOID-CENTRE

FIGURE 36
COMPARISON OF RESULTS FROM CENTRE-VOID
TEST AND ANALYSIS

87-296
175929-RD

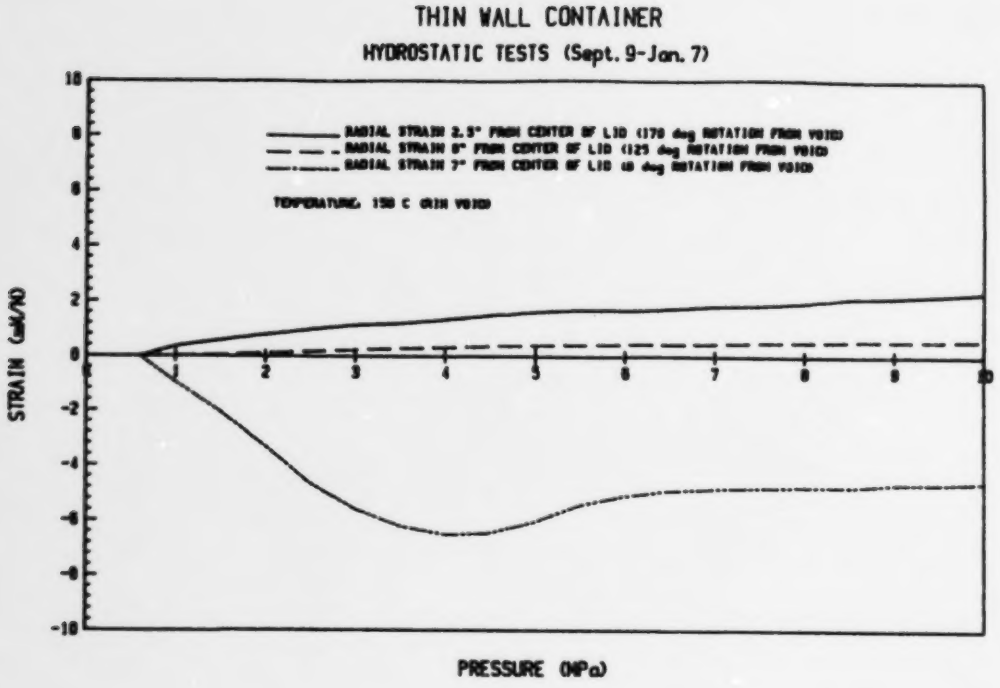

(a) STRAIN PATTERN IN TOP LID

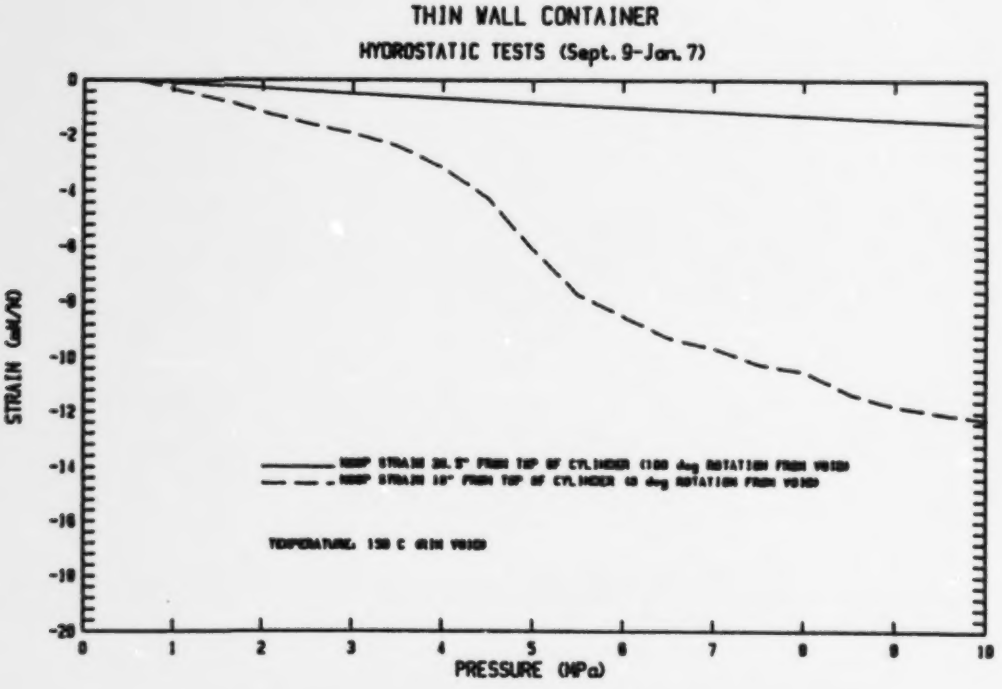

(b) STRAIN PATTERNS IN CYLINDRICAL SHELL

FIGURE 37

STRAINS MEASURED DURING TEST WITH RIM VOID

87-296
175930-RD

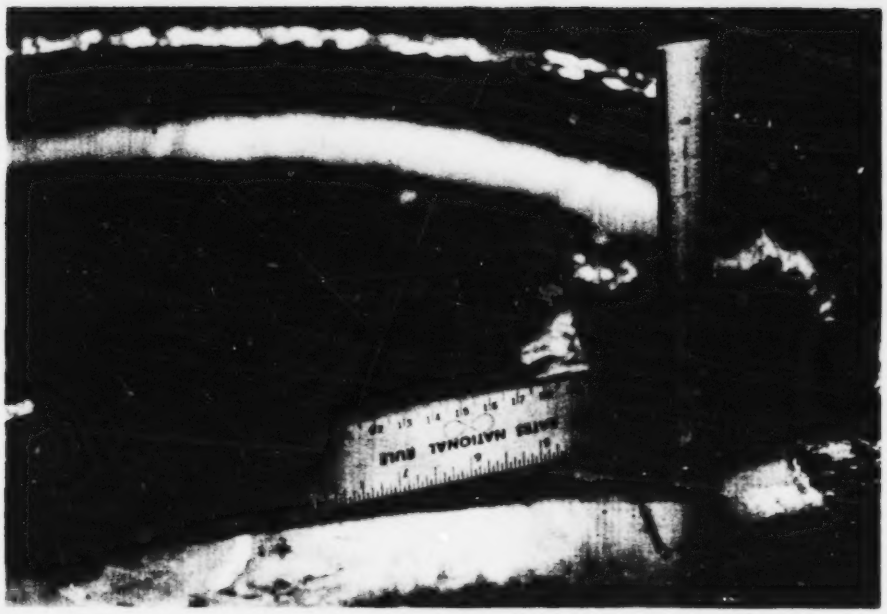

a) DEFORMATION IN TOP HEAD

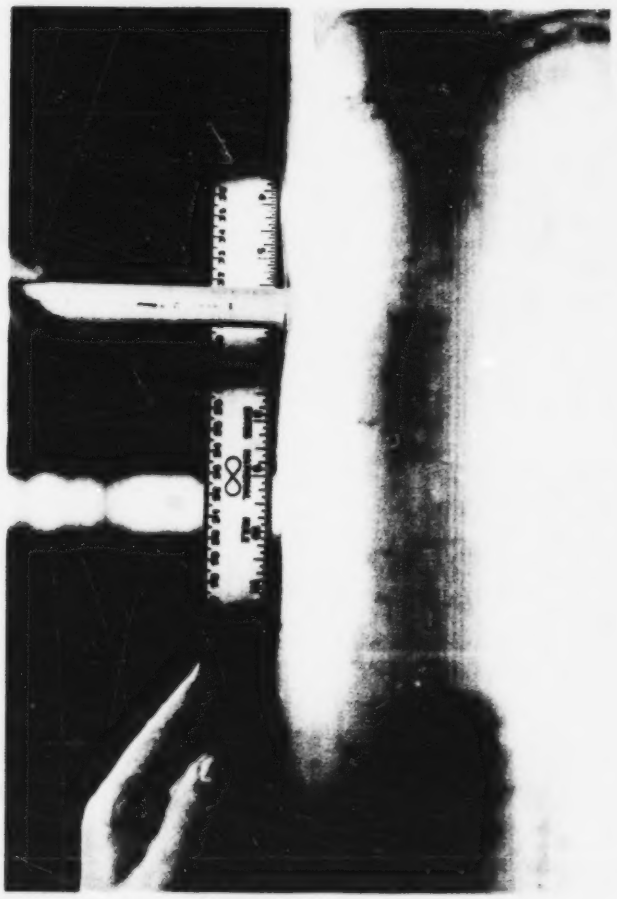

b) DEFORMATION IN CYLINDRICAL SHELL

87-296

175931-RD

FIGURE 38

DEFORMATIONS PRODUCED IN TEST WITH RIM VOID

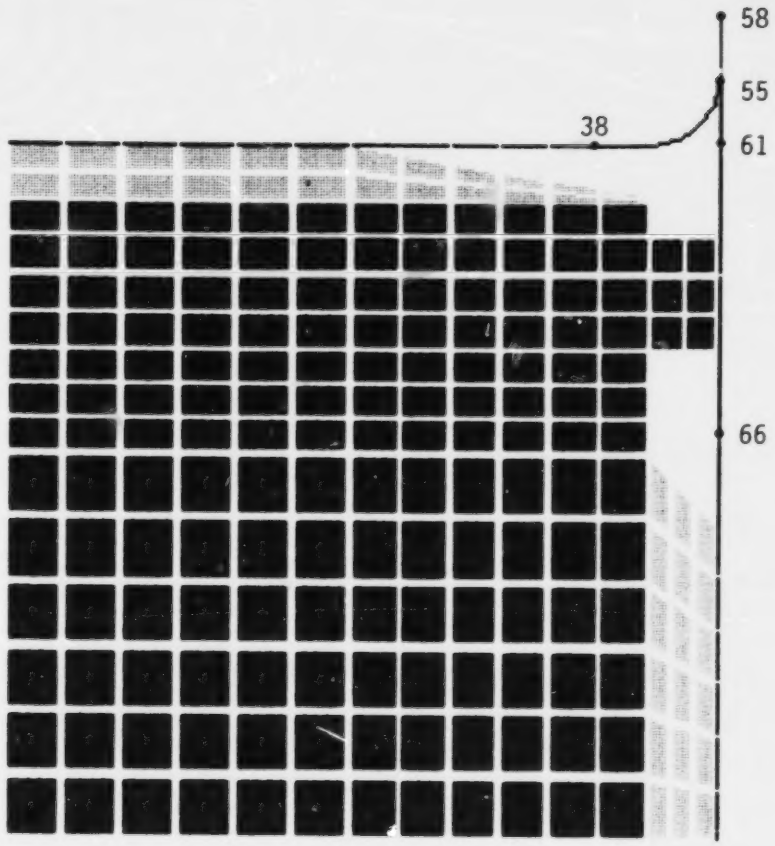

FIGURE 39

FINITE ELEMENT MODEL
OF SIDE VOID

•*n - node number*

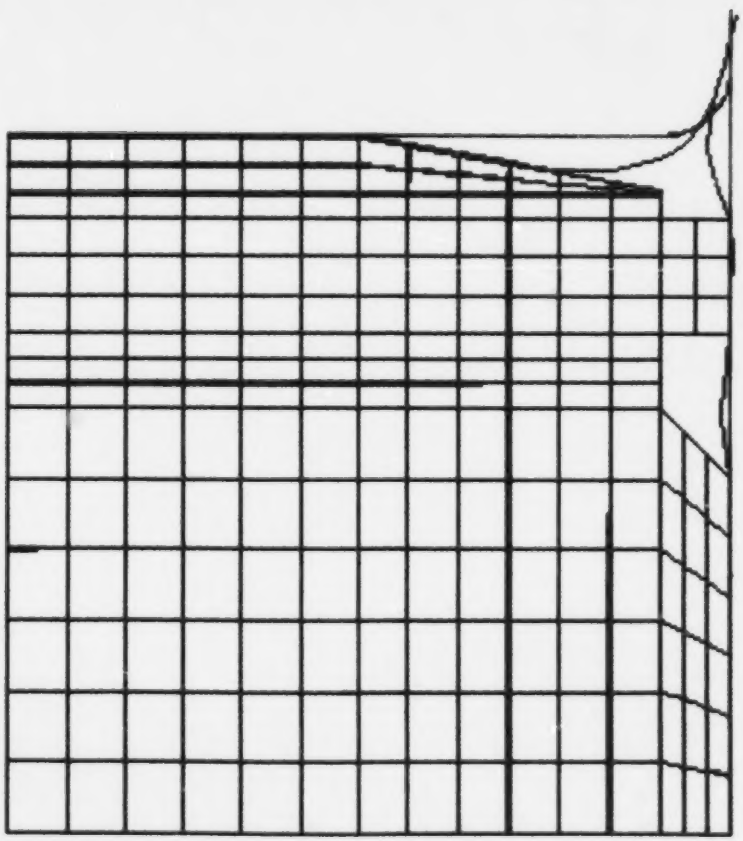

FIGURE 40

ANALYTICALLY PREDICTED
DEFORMATION

87-296

175932-RD

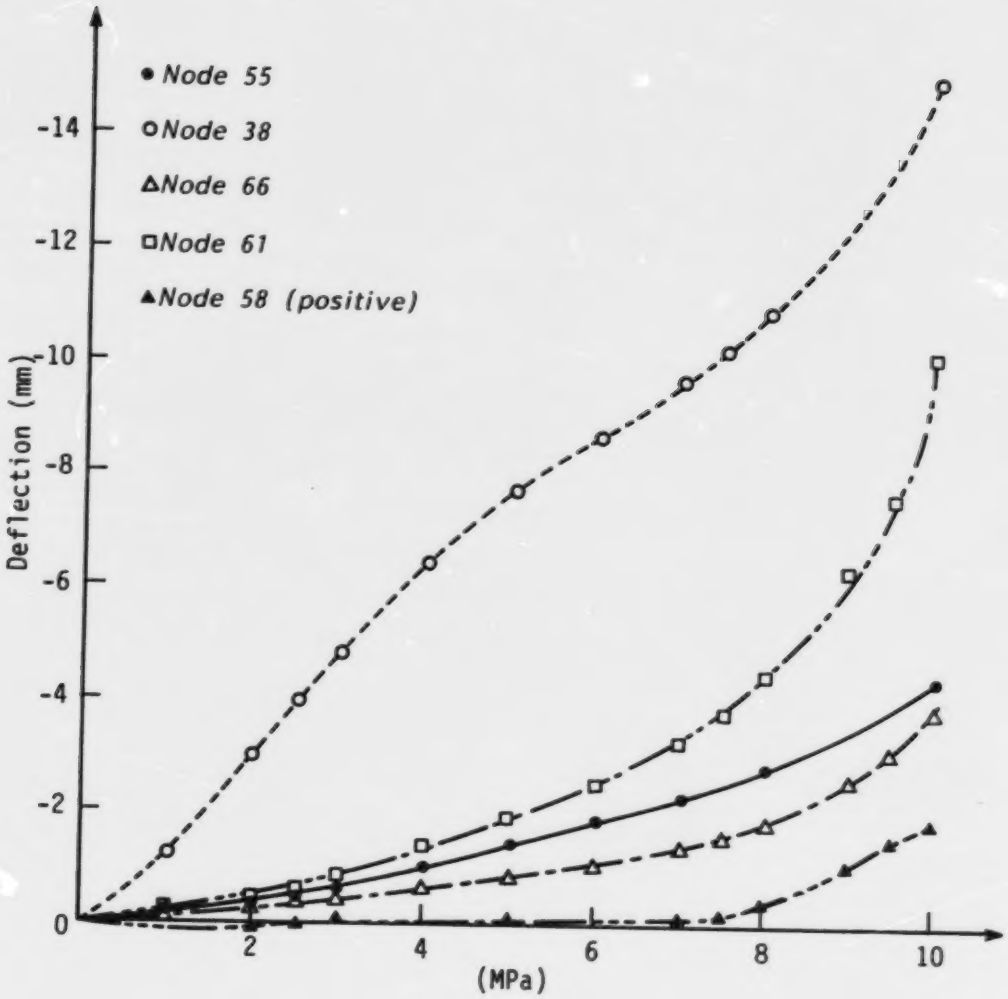

Note: See Figure 39 for Node Locations

FIGURE 41
RESULTS OF ANALYSIS OF SIDE VOID

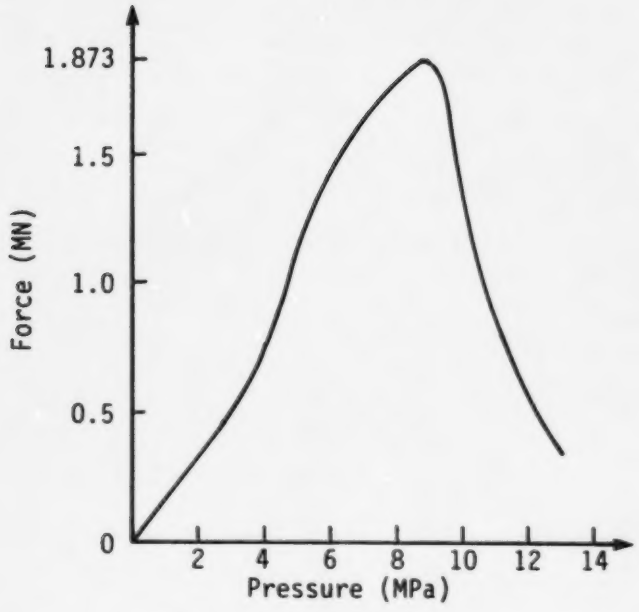

FIGURE 42
ESTIMATED COMPRESSIVE FORCE IN THE CYLINDRICAL SHELL

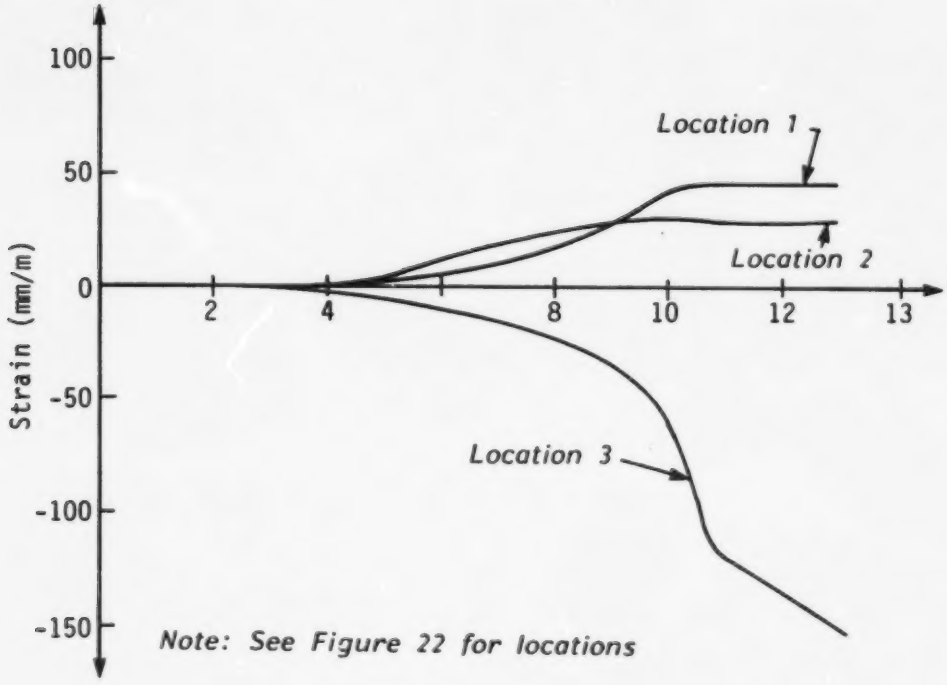

FIGURE 43
ESTIMATED STRAIN AT INCREASED PRESSURE TO 13 MPa

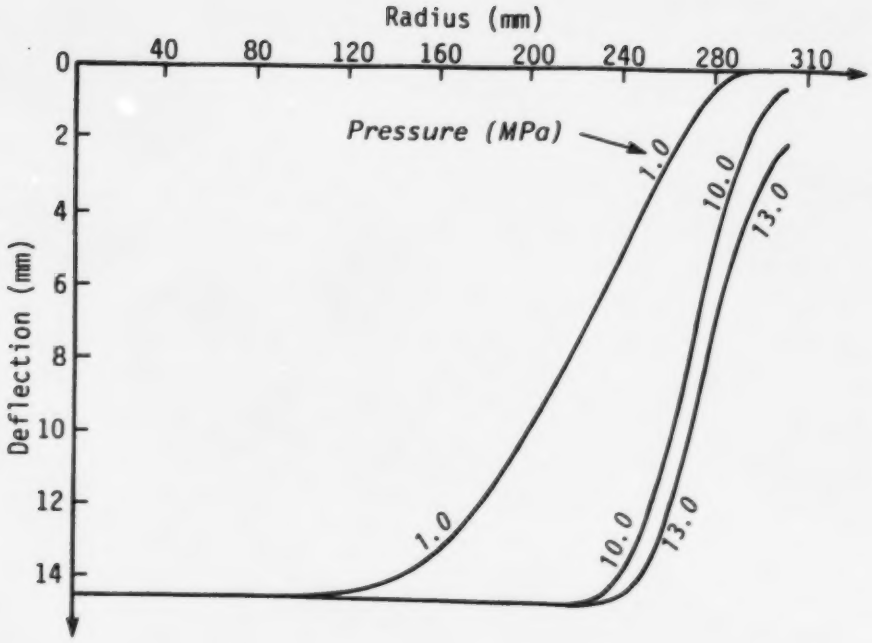

FIGURE 44
DEFORMATION OF TOP HEAD AT 13 MPa

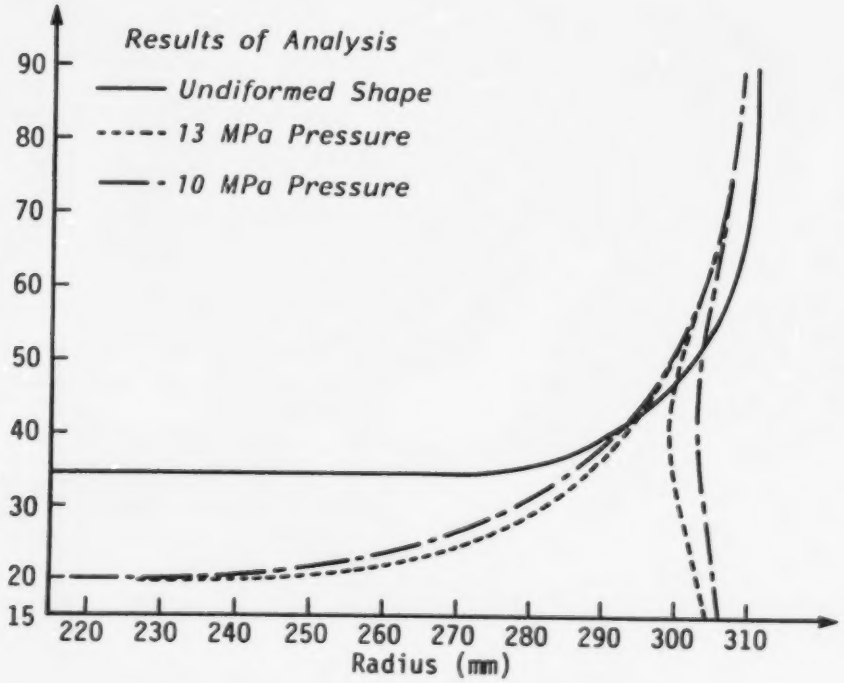

FIGURE 45
DEFORMATION IN THE WELD AREA

87-296
175935-RD

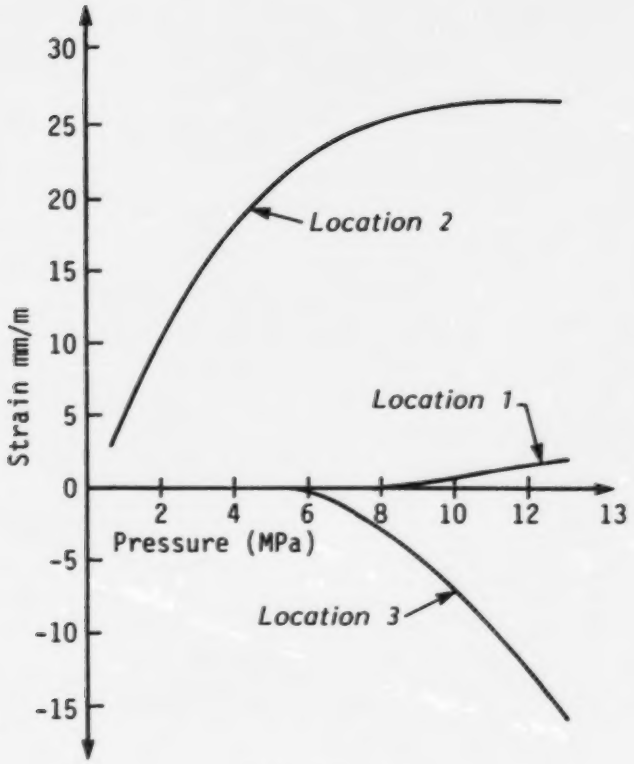

FIGURE 46
LARGEST PLASTIC STRAINS
IN 10 mm GAP

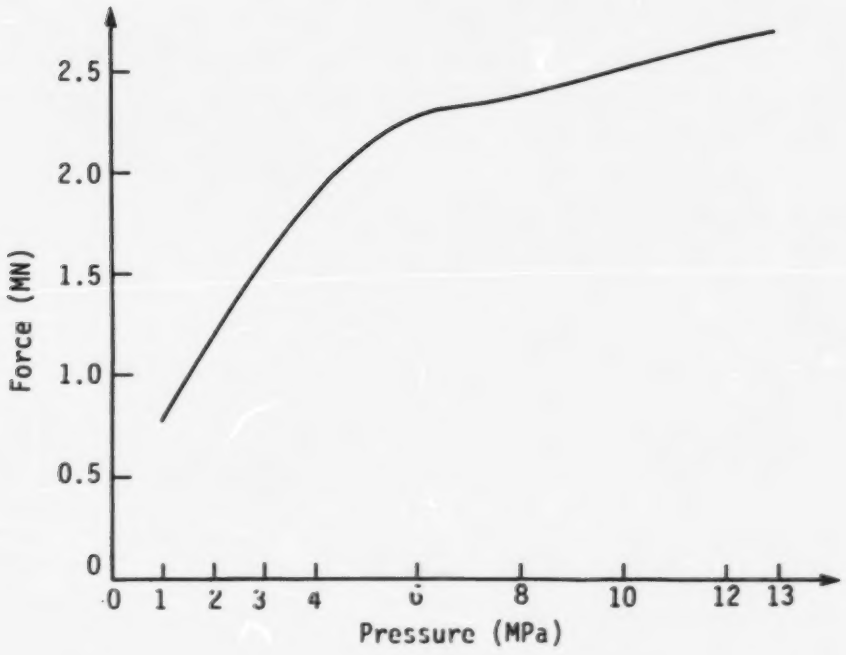

FIGURE 47
COMPRESSIVE FORCE IN CYLINDRICAL SHELL
10 mm GAP

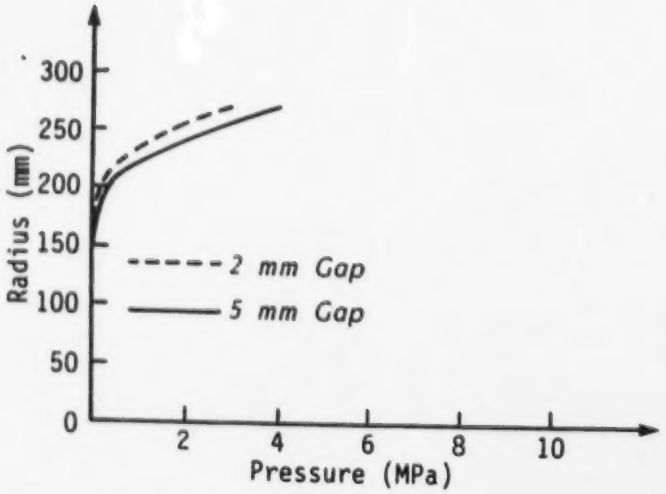

a) CLOSING OF 5 mm GAP

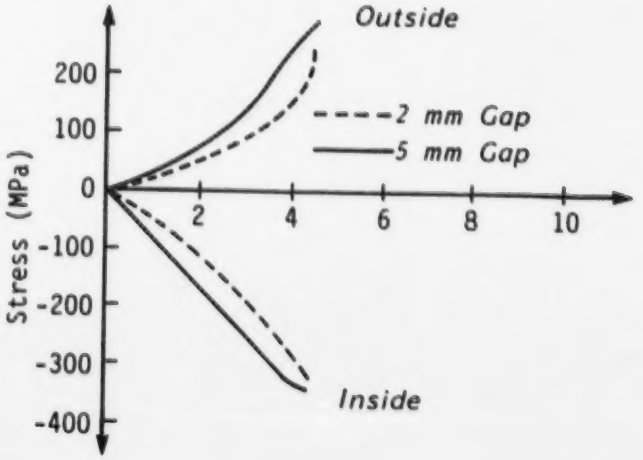

b) AXIAL STRESS IN CYLINDRICAL SHELL

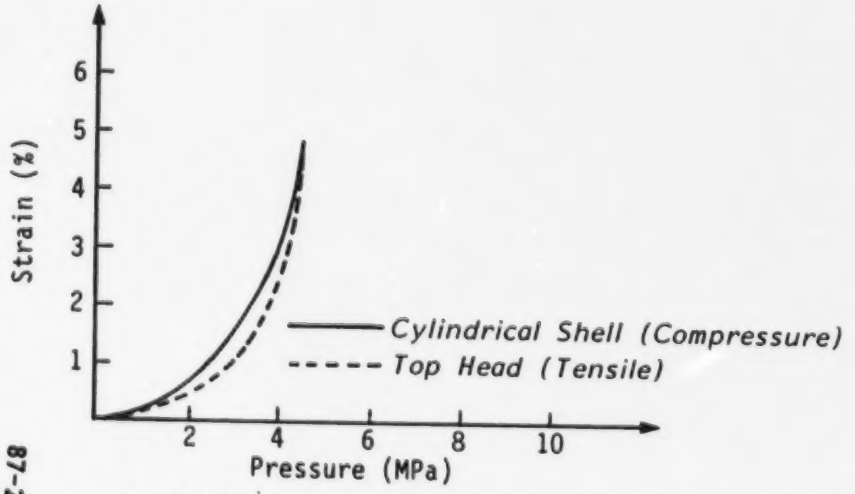

c) LARGEST STRAINS FOR 5 mm GAP

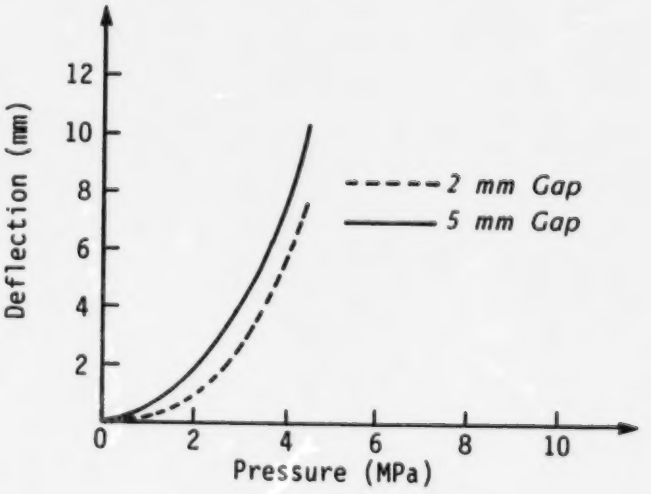

d) RADIAL DEFLECTION OF CYLINDRICAL SHELL

FIGURE 48

RESULTS OF GAP ANALYSIS FOR 2 mm THICK SHELL

87-296
175937-RD

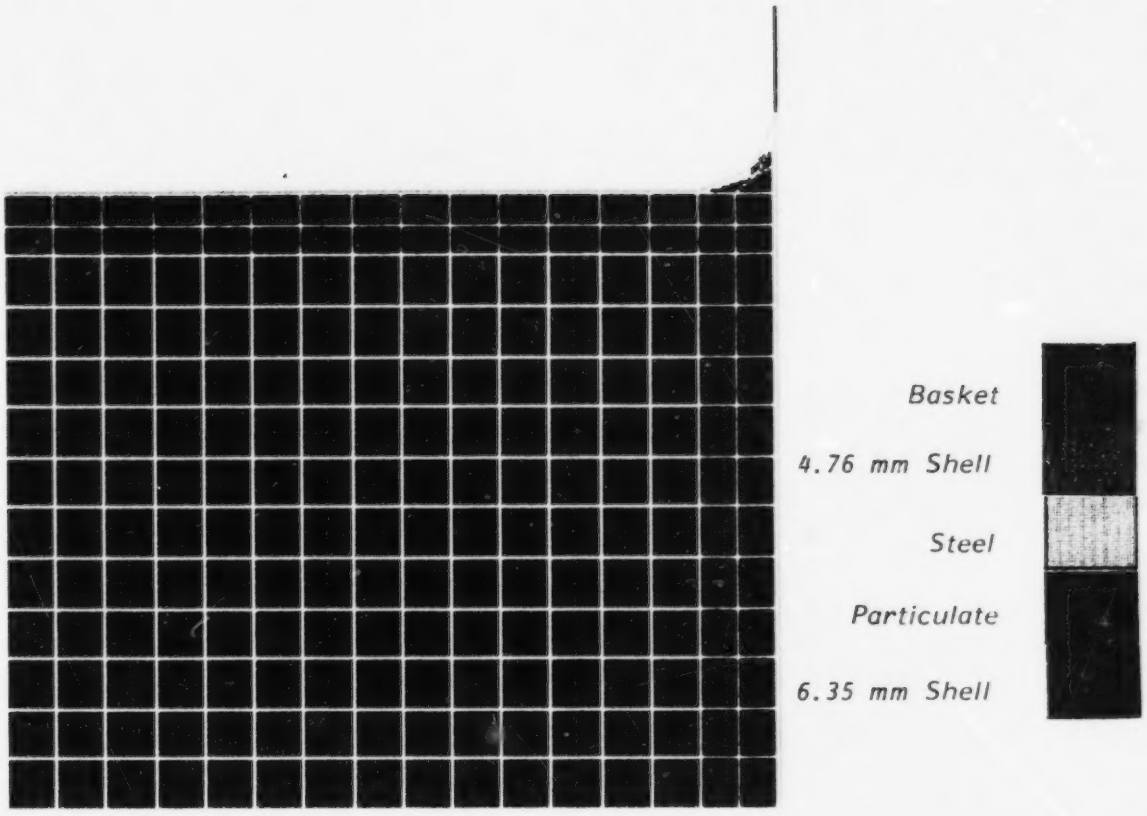

a) TOP AREA

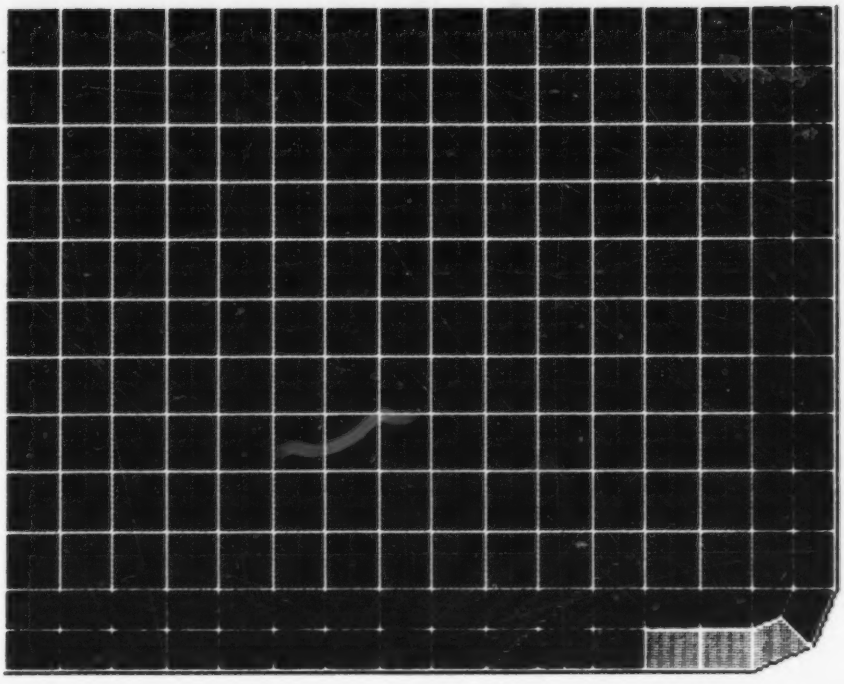

b) BOTTOM AREA

FIGURE 49
MODEL FOR LONG-TERM SETTLEMENT ANALYSIS

87-296
175938-RD

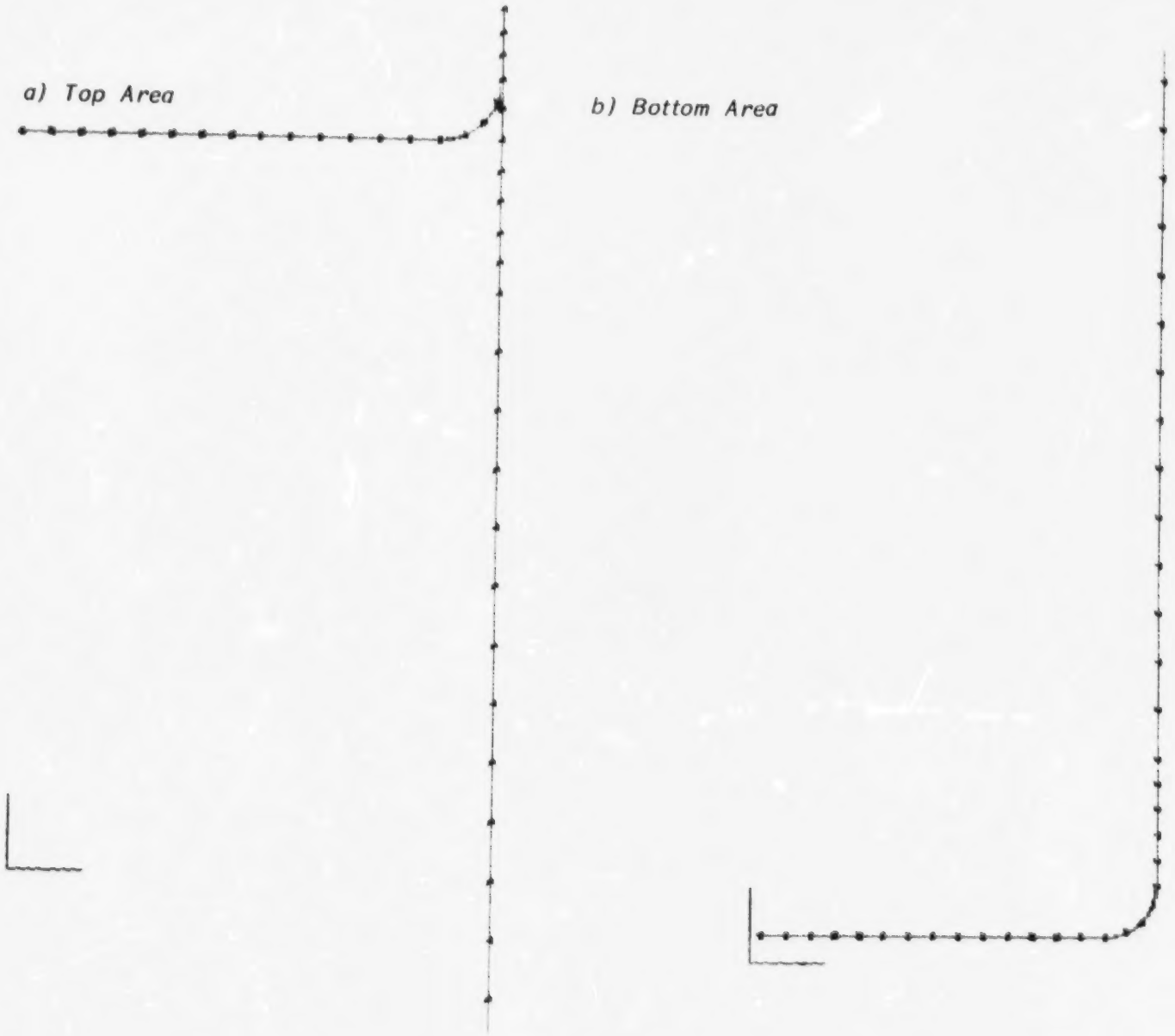

FIGURE 50
MODEL FOR ANALYSIS OF INTERNAL PRESSURE

87-296
173175 RD

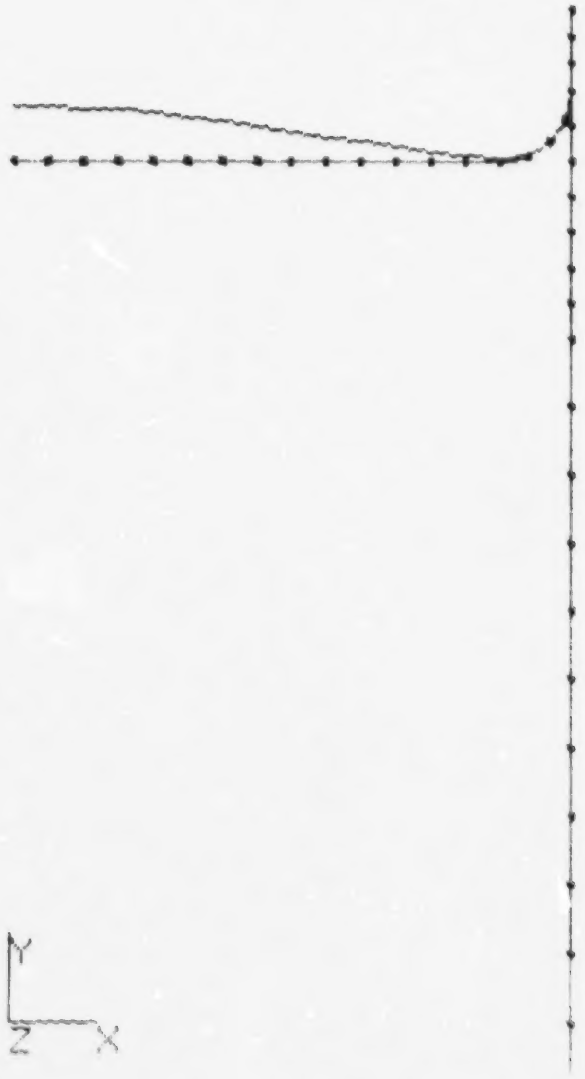

a) Top Area - Amplified 5 times

b) Bottom Area - Amplified 750 times

FIGURE 51
DEFORMATIONS DUE TO INTERNAL PRESSURE

87-296
173176 RD

APPENDIX A

AVERAGE CONTAINER TEMPERATURE

Contents

A.1 Nomenclature

A.2 Assumptions

A.3 Axial Heat Transfer

A.4 Radial Heat Transfer

A.5 Average Container Temperature

A.1 Nomenclature

d - Partial derivative

K - thermal conductivity (W/m K)

Ka - thermal conductivity in axial direction

Kr - thermal conductivity in radial direction

r - radial distance

r - radius of the container(305 mm)

t - time (hour)

T - temperature

To - temperature at the container surface, assumed to be 100°C

Tc - temperature at the centre of the container

Ta - average temperature in the container

z - distance from mid-height of the container

Figure A.1 illustrates some of the above nomenclature.

A.2 Assumptions

The fuel to be disposed will be at least 10 years out of reactor. The decay heat generation rate will be below 6.50 W per bundle for over 99% of fuel (conservative - average heat output is 4.13 W/bundle). A container with 72 bundles will generate heat at the rate of 468 W. A uniform, volumetric heat generation in a container is assumed to be:

$$W = 745 \text{ W/m}^3$$

This heat is transmitted into the vault in both axial and radial directions. The average heat transfer coefficients for the two directions have been estimated/8/ to be:

$$Ka = 33.57 \text{ W/m °C}$$
$$Kr = 0.47 \text{ W/m °C}$$

The radial heat transfer coefficient is low because the glass beads form a good insulator. The steel tubes of the basket improved heat conduction in the axial direction.

The container was assumed to be in a steady state ($dT/dt = 0$). Heat transfer and temperature are axisymmetric ($dT/d\theta = 0$). The temperature distribution in the container is given by the general equation:

$$(dT/dr)/r + (d^2T/dr^2) + (d^2T/dz^2) + W/K = 0.0$$

where

a - axial direction (subscript)

c - container centre (subscript)

d - derivative

K - thermal conductivity coefficient

r - radius

- radial direction (if used as subscript)

T - temperature

W - volumetric heat generation (watt) (if used as a unit)

To simplify the analysis of this equation, two cases are considered: heat transfer only in the radial, or only in the axial directions.

A.3 Axial Heat Transfer

If we assume that the container is insulated in the radial direction or $dT/dr = 0$, then the above equation has a solution of the form:

$$T = Tc = (W/2Kz)z^2$$

The largest temperature at the mid-height of the container is expected to be:

$$Tc = 113°C$$

and the axial temperature distribution is:

$$T = 113 - 11.1\ z$$

A.4 Radial Temperature Distribution

If we assume that the container is insulated in the axial direction or $dT/d_z = 0$, the equation has a solution in form:

$$T = Tc - (Wr/4Kr)$$

The largest temperature occurs at the centre of the container and would be equal to:

$$Tc = 137°C$$

The axial temperature distribution would be:

$$T = 137 - 398\ r^2$$

A.5 Average Container Temperature

The heat transfer in the radial direction will be low and is therefore neglected in the analysis of the average container temperature. The average container temperature is then given by:

$$Ta = \int_0^r (113 - 11.1\ z^2)\ dz/z$$

The average temperature is:

$$Ta = 109°C$$

This result is conservative and may be valid for the statistically hottest container in the vault.

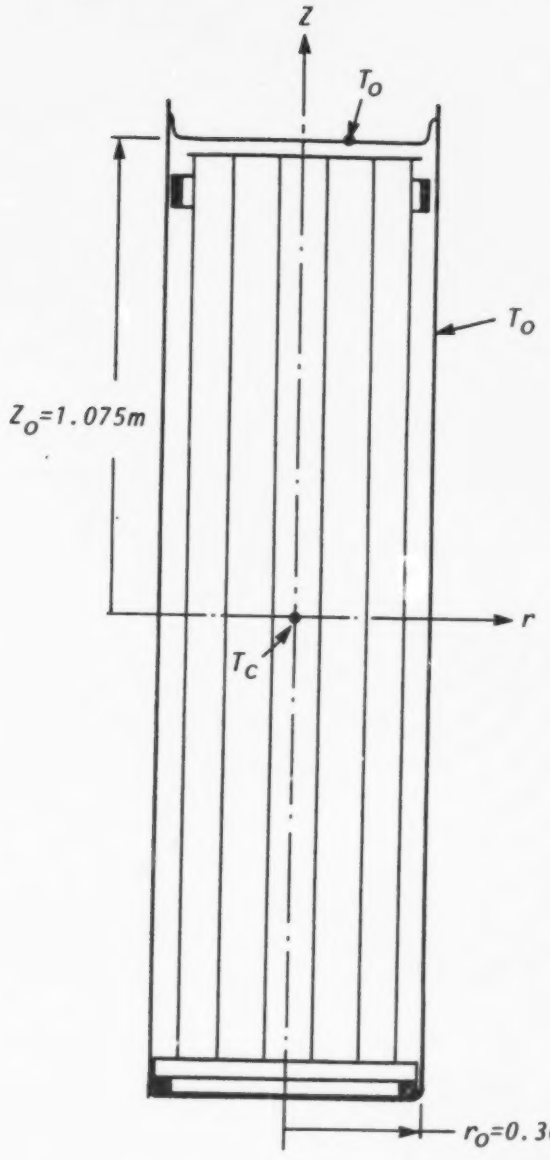

See section A.1 for nomenclature

FIGURE A-1
SELECTED NOMENCLATURE

APPENDIX B

STRAINS IN TITANIUM SHELL

Contents

B.1 Non-Linear Behaviour

B.2 Constant Volume Consideration

B.3 Failure Consideration

B.4 Uniaxial Tensile Strain

B.5 Biaxial Tensile Strain

B.6 Summary

B.1 Non-Linear Behaviour

Large deformations and strains were measured during the hydrostatic test program and predicted in the finite element analysis. Large deformations are necessary to transfer the external pressure through the shell onto a much softer (having lower modulus of elasticity than titanium) particulate. The shell will deform plastically. This should be acceptable, provided that the shell does not buckle or stretch until it tears. These deformations either cause or are a result of two types of non-linearities.

Material non-linearity originates in the change of material behaviour beyond the yield point. It includes the strain hardening properties.

Geometrical non-linearities are caused by titanium shell sliding over particulate and by presence of gaps (limiting deformation):

- 14.5 mm gap at the top head,
- gap between bottom head and support ring (in Figure 32),
- intentionally induced gaps in the last two hydrostatic tests, and
- gap formed by long term settlement.

B.2 Constant Volume Consideration

We will assume here that as a material deforms plastically, its volume remains constant and only its shape changes. Let us look at a cube having each side one unit long (see Figure B-1). Under tensile load, the cube elongates in the direction of tension by distance D. To preserve constant volume requirement, the other two sides will be shortened by d_x and d_y respectively. Volume of the cube is:

$$V = 1^3 = (1 + D)(1 - d_x)(1 - d_y)$$
$$= 1 + D - d_x - d_z - Dd_x - Dd_z + d_xd_z + Dd_xd_z$$

Neglecting second and third order terms (error committed here will be discussed below) we obtain:

$$D - d_x - d_z = 0$$

The tensile strain due to a unaxial tensile load is equal to the sum of the two orthogonal compressive strains:

$$D = d_x + d_z$$

If the compressive strains are equal ($d_x = d_y = d$)

$$D = 2d$$

Neglecting of higher terms for the largest strain of D = 8% produces a small error:

$$-2dD + d^2 + Dd^2$$

$$= -3d^2 + 2d^3$$

$$= -0.5\%$$

Similarly, if the cube is in biaxial tension with largest tensile strains of D_x and D_y and compressive strain d, we have:

$$V = 1 = (1 + D_x)\ (1 + D_y)\ (1 - d)$$

or

$$D_x + D_y = d$$

If tensile strains are equal

$$2D = d$$

B.3 Failure Consideration

Titanium is a ductile material with a 20% minimum required elongation in a 2-inch tensile specimen. This elongation results in thinning of the specimen. In the case of titanium container, the shell is assumed to fail if a rapid thinning occurs for a small increase in load.

If d and d_z denote through thickness strain (subsection B.1), the shell "thinning" strain in a case of uniaxial tension is one-half of the tensile strain (d = 0.5D). In the biaxial tension, the "thinning" strain is twice the tensile strain (d = 2D). To obtain the same through-thickness strain, the biaxial strain should be one-quarter of the uniaxial strain.

B.4 Uniaxial Tensile Strain

To gain a better understanding of the strains in titanium shell, a square region of the shell is analyzed using finite element method. A model of the shell region is shown in Figure B-2.

Since large deformations are considered, use of engineering stress-strain curve is inappropriate. The engineering curve in Figure B-3 is recalculated to true curve using relationships:

True strain	$e = \ln (1 + e')$
True stress	$s = (1 + e')S'$

where (') designates engineering values of stress and strain. Figure B-3 shows the true stress-strain curve. This curve is further liniarized in Figure B-4 for input to the finite element analysis.

Strains obtained from the uniaxial run confirms the strain ratios proposed in B.1 (see Figure B-5). Both compressive strains reach about 8% as stress approaches ultimate. Reduction of the shell thickness approaches 8% as stress approaches ultimate (see Figure B-6).

B.4 Biaxial Tensile Strain

The same finite element model was used to study the effect of uniform biaxial tension. The through-thickness strain increases faster here than in uniaxial case and reaches 8% at about 90% ultimate strength (see Figure B-5). Thickness of the plate reduced by the same amount (8%) at 90% ultimate strength. At 90% strength, both inplane strains are the same and equal 4%, or $d_x + d_z = 8\%$. Strains increase too rapidly above 90% ultimate load to consider them acceptable.

B.5 Summary

The titanium shell is not intended to support external loads. Stress levels in the shell are of secondary importance. Based on the above analysis of a flat plate, titanium shell is not expected to fail by tearing until its thickness is reduced by over 8%. This thickness reduction occurs when in-plane tensile strains total 8%:

$$d_x + d_z \leq 8\% \quad \text{(failure condition)}$$

Strains are considered acceptable if $d_x + d_z \leq (2/3)$ of 8% or 5.3% by analogy to the ASME Boiler and Pressure Vessel Code, which frequently limits the loads to two-thirds of the limiting (failure) value (eg, paragraph NB-3228.3 of Section III).

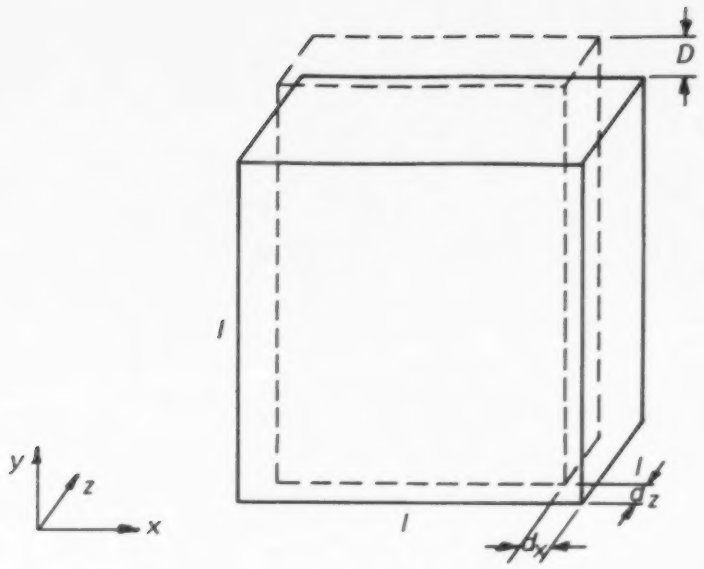

FIGURE B-1
DEFORMATION OF A CUBE

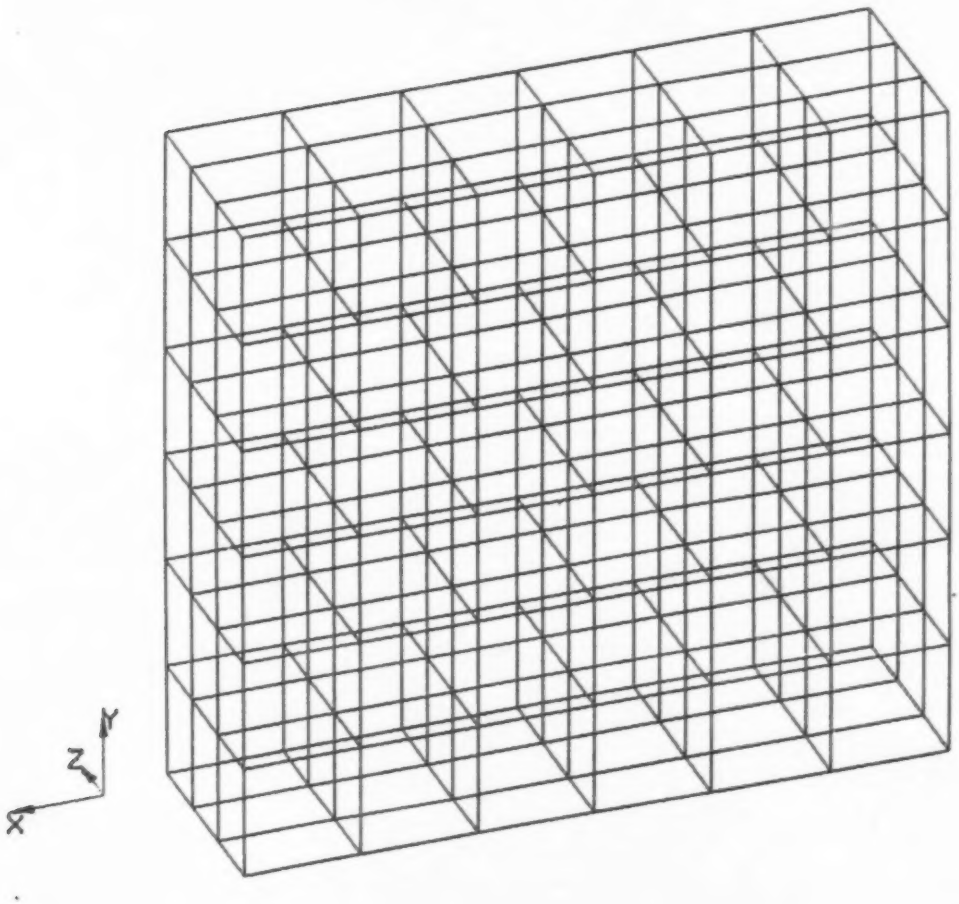

FIGURE B-2
FINITE ELEMENT MODEL OF SHELL

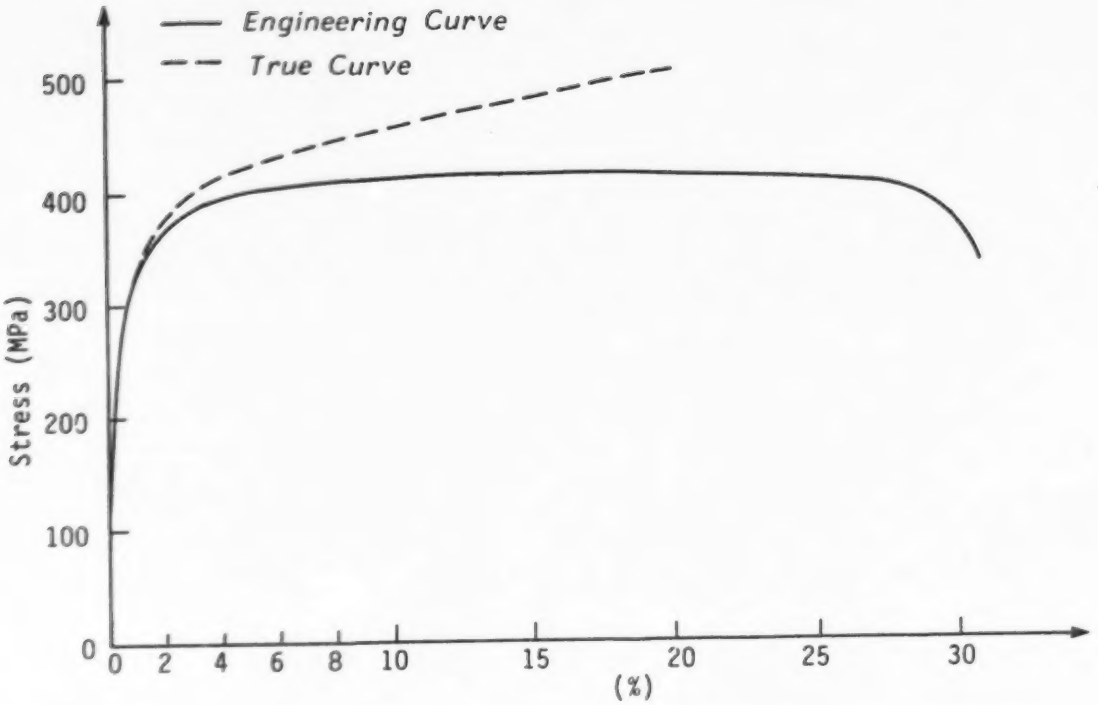

FIGURE B-3
ENGINEERING AND TRUE STRESS-STRAIN CURVES

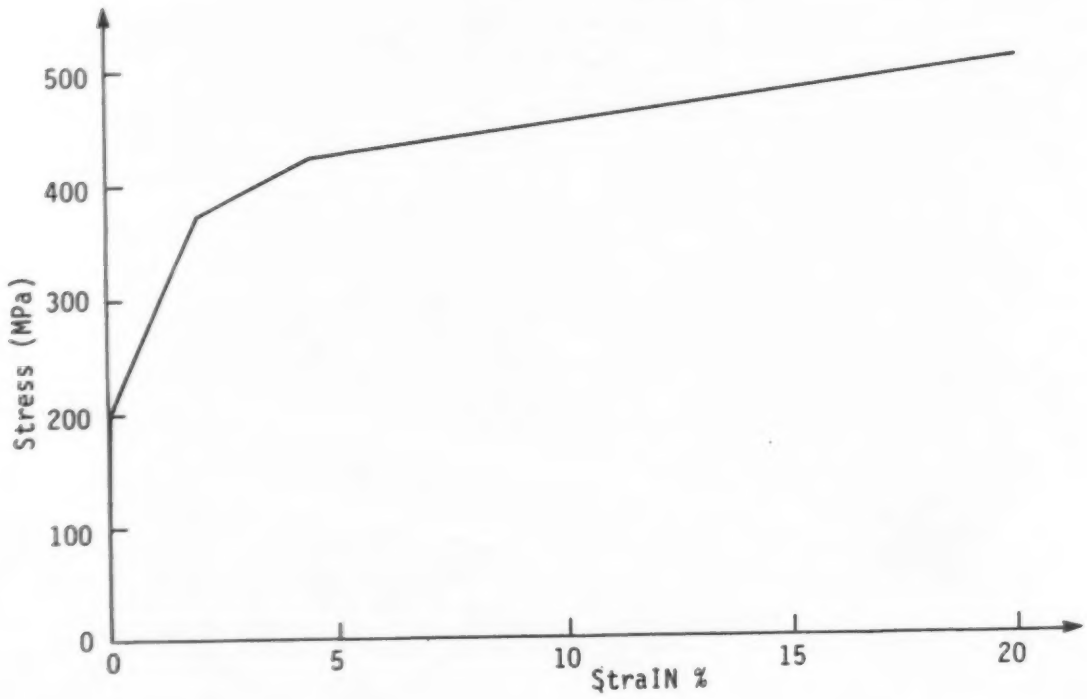

FIGURE B-4
STRESS-STRAIN CURVE USED IN ANALYSIS

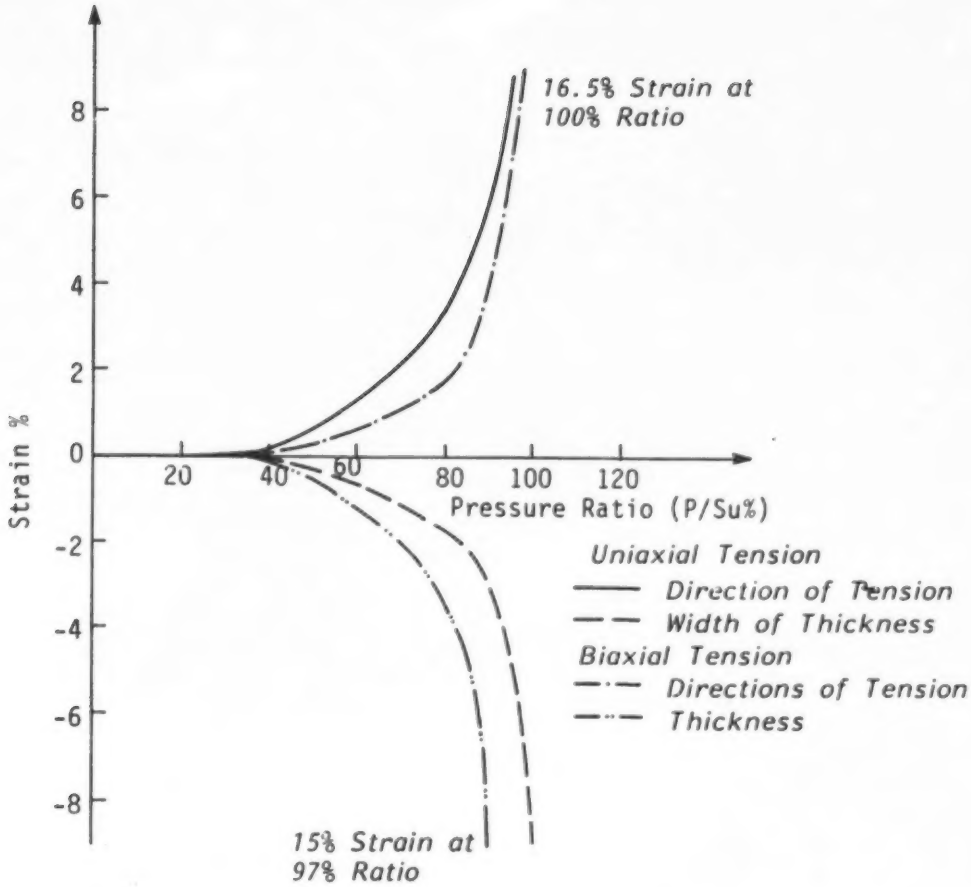

FIGURE B-5
STRAINS AT PLATE CENTRE

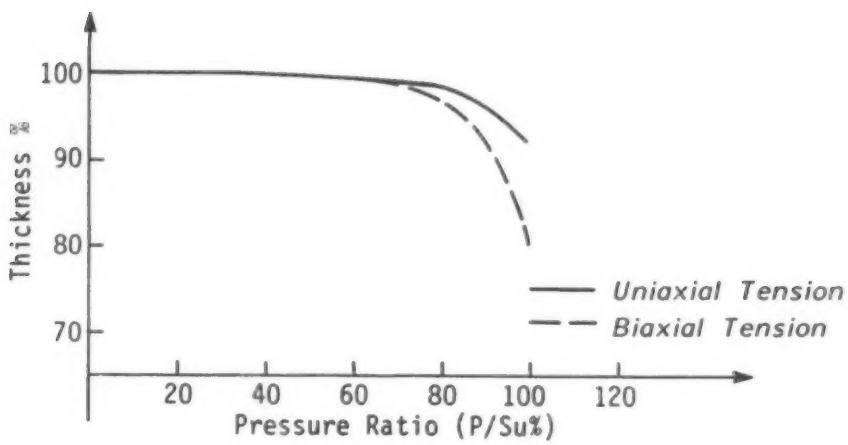

FIGURE B-6
PLATE THICKNESS REDUCTION

APPENDIX C

DEFORMATION IN PROTOTYPE CONTAINER

The results of the hydrostatic test program have provided a good indication of the deformation pattern in the container. Deformations of the cylindrical shell can be calculated from the hoop strain (e) as:

$$\Delta r = er$$

where r is cylinder radius.

For example, the cylindrical shell away from discontinuity deformed by:

$$\Delta r = (-0.00183)\ (310)$$
$$= 0.567 \text{ mm}$$

In the top plate, curvature is a function of strain. Elastically, the top plate deformed into a segment of a sphere of a radius R (see Figure C-1). If we select a length of the sphere segment to be small, such that:

$$\sin(\alpha/2) = \alpha/2$$

(see Figure C-1 for meaning of characters)

then,
$$\sin(\alpha/2) = Le/t$$
$$= L/2\ R$$

or,
$$R = t/2e$$
$$= 12.7 \text{ m}$$

The anticipated deflection in the top plate would be negligibly small at:

$$y = R - \sqrt{R^2 - r^2}$$
$$= 0.0038 \text{ m}$$

in comparison with the parallel settlement of the top plate.

Following the hydrostatic test program, several holes were drilled in the top plate and the distance between the top plate and the inner basket measured at several locations showed on overall settlement of the top plate to be about 14 mm, as shown in Figure 8.

The estimated deformed shape of the container is shown in Figure 7.

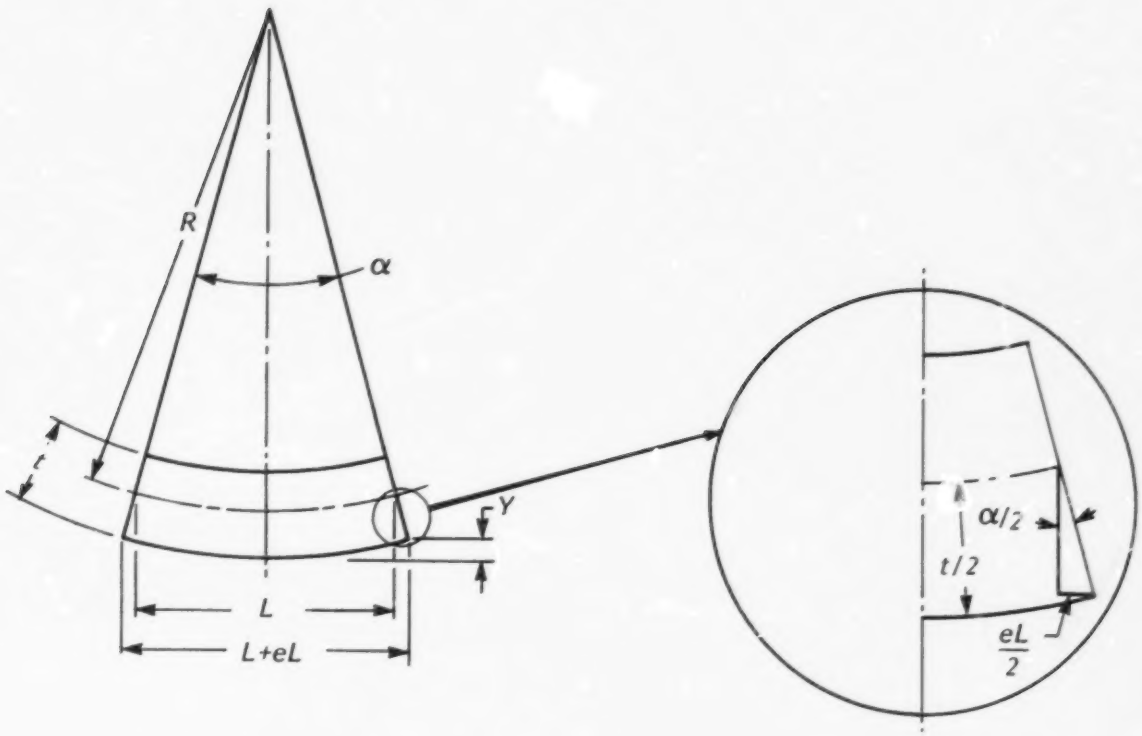

FIGURE C-1
DEFORMATION OF TOP PLATE

APPENDIX D

UNIFORM GAP ESTIMATE

Contents

C.1 Reasons for "gap"

C.2 Effect of temperature

C.3 Effect of creep in particulate

C.4 Uniform settlement

C.5 External pressure

C.6 Summary

D.1 Reason for "Gap"

The disposal container is designed to support at least 10 MPa external pressure for an extended period of time (up to 500 years). During this time, some reduction in the volume of particulate could occur, causing deformation (settlement) of titanium shell. The settlement is expected to form uniformly on the surface of the container except for areas near the corners between the end plates and the cylindrical shell. The total surface of the container is

$$A = 4.416 \text{ m}^2$$

In the finite element analysis, the settlement is introduced by using gap elements. Several sources of the "gap" have been postulated. They are discussed below.

D.2 Effect of Temperature

The container will be assembled at a temperature of about 20°C. After it is placed in the vault, it will heat up to about 109°C, due to the heat generated by the bundles. The thermal expansion coefficients (d) of the materials are:

steel	$\alpha_s = 12.37$ μm/m°C
titanium	$\alpha_t = 8.55$ μm/m°C
glass	$\alpha_g = 8.47$ μm/m°C

Though the thermal expansion of steel is higher than that of titanium, a sufficient space is provided inside the container to allow for the thermal expansion of the steel without affecting the titanium shell. The thermal expansion of glass is slightly less than that of titanium, thus creating a small uniform void of:

$$\Delta V = \pi r^2 l \ (\alpha_t - \alpha_g) \Delta T$$
$$= 0.046 \text{ l}$$

The resulting gap thickness will therefore be:

$$g_t = \Delta V / A = 0.011 \text{ mm}$$

D.3 Effect of Creep in Particulate

The possibility of uniform, long-term settlement of the particulate was discussed in Subsection 3.2. The total volume reduction in particulate should not exceed 0.06 l (400 litres of particulate undergo volumetric creep strain of 0.000160/4/). This volume reduction is expected to increase the size of the uniform gap by

$$g_c = 0.014 \text{ mm}$$

D.4 Uniform Settlement

Because disposal containers will be assembled at the disposal site the 14.5 mm settlement of particulate at the top of a container will not form. For conservatism, we assumed that this void will form over a long period of time creating a uniform volume loss of:

$$\Delta V_u = \pi(310)^2 (14.5)10^{-6} = 4.38 \text{ l}$$

The thickness of a uniform gap due to this void would be:

$$g_u = 1.000 \text{ mm}$$

D.5 External Pressure

The 10 MPa external pressure will result in the same compression of the particulate. The bulk modulus defines the volume reduction as a function of pressure P:

$$\Delta V = PV/K$$

The volume of particulate would reduce by up to 5.216 liters if all particulate were under 10 MPa pressure. The increase in the gap size due to the external pressure would then be:

$$g_e = 1.134 \text{ mm}$$

D.6 Summary

The effect of the uniform gap at the top and bottom discontinuity areas will be evaluated using the finite element techniques assuming presence of geometric and material non-linearities. The total gap introduced in these models will be equal to:

$$g_1 = g_t + g_c + g_u = 1.025 \text{ mm}$$

because the deformation due to the 10 MPa pressure will be considered in the computer analysis. The largest deflection of the cylindrical shell due to the long term settlement of particulate is expected to be up to

$$g_2 = 2.16 \text{ mm}$$

if the stiffness of the cylindrical titanium shell is neglected.

This deflection causes a hoop strain of 0.7%. This largely plastic strain will produce an uniaxial stress of 245 MPa.

DISTRIBUTION

Mr. H.N. Isaac	Design and Development-Gen, H11G27
Mr. J.L. Crosthwaite (3)	WNRE
Mr. P.D. Stevens-Guille	Design and Development-Gen, H11A27
Dr. S.J. Naqvi	Design and Development-Gen, H11A25
Mr. J. Freire-Canosa	Design and Development-Gen, H11A26
Mr. A.Y. Cheung	Design and Development-Gen, H14G25
Mr. M. Mikasinovic	Design and Development-Gen, H14G25
Mr. J.A. Chadha	Mechanical Research
Dr. J.D. Tulk	Mechanical Research
Mr. B. Teper (3)	Mechanical Research

Public Reference Centre
Editorial Section (2)
Office Copies (3)
Extra Copies (3)